Acknowledgement

I would like to express my deep and sincere gratitude to my supervisor, Prof. K.M Purohit, Head of the Department Life Science, National Institute of Technology, Rourkela for giving precious advice and excellent guidance in minimum words for completion of my Ph.D.

I owe my most sincere gratitude to Prof. Sunil Sarangi, Director of National Institute of Technology, Rourkela who gave me the opportunity to work leading to successful completion of my Ph.D work.

I wish to express my sincere thanks to Prof. Sukumar Adak**,** VP (Technology), Tata Refractories Ltd, Belpahad, Orissa for his valuable support throughout my research work. His wide knowledge and his logical way of thinking have been of great value for me. I would like to mention that even being over flooded with works he takes care of small things very well.

I wish to express my warm and sincere thanks to Prof. R.K Patel, Department of Chemistry, National Institute of Technology, Rourkela for his understanding, encouraging and personal guidance that provided a good basis for the present thesis.

I wish to express my sincere thanks to Dr. V.K Shrivastav, Department of Biochemistry, I.G.H, Rourkela, Miss. Neetu Shrivastav and their family members for their support and encouragement during my Ph.D work.

I warmly thanks to Dr. Mahua Das Gupta Adak for her valuable advice. Her kind support and guidance have been of great value in my study.

I wish to thank my labmates and friends Yugojyoti, Ramesh, Firoz, Parnashree, Jyoti Prakash and Maimudur Islam for their valuable guidance in my study. I am very much thankful for their essential assistance they have given me during my Ph.D work.

I wish to extend my warmest thanks to all those who have helped me with my work in the Department of Ceramic Engineering and, in the Department of Chemistry, National Institute of Technology, Rourkela.

Last but not least, no words are enough to express my heartful gratitude to my parents, my wife and lovable child and my uncle (Badkababuji) for being a source of inexhaustible encouragement and inspiration and for always being there whenever I needed. Without their encouragement and understanding it would not have been possible for me to finish up my work.

Date: **ANJUVAN SINGH**

P R E F A C E

Chapter – I introduces the topic and background of the existing field.

Chapter – II deals with detailed literature review. Attempts have been made to systematically classify the available information under different sections. This chapter incorporates background information to assist in understanding the aims and results of this investigation, and also reviews recent reports by other investigators with which these results can be compared. The review finds unresolved questions in the literature that can't be answered by a single research work.

Chapter – III deals with the objectives of the present investigation. **Chapter – IV** deals with the detail experimental process related to this research work. **Chapter – V** deals with the results and discussion systematically with respect to powder synthesis, characterization, densification study, development of porous hydroxyapatite, *in vitro* assessment and dissolution behavior of the material for study of its bioactivity. **Chapter – V**I summarizes the conclusions, whereas, the **Chapter – VII** illustrates the possibility of Future Works.

A complete list of references has been given towards the end of the thesis.

CONTENTS

List of Figures

Page No.

List of Tables

Page No

List of Symbols

HAP	Hydroxyapatite
N	Naphthalene
SBF	Synthetic Body Fluid
TCP	Tricalcium Phosphate
T.D	Theoretical Density
Wt	Weight
A.P	Apparent Porosity
B.D	Bulk Density
FTIR	Fourier Transformed Infrared Spectroscopy
XRD	X-Ray Diffraction
SEM	Scanning Electron Microscope
TG	Thermo gravimetric
DTA	Differential Thermal Analysis
SS	Snail shell
$MgCO_3$	Magnesium carbonate
$CaCO_3$	Calcium carbonate
CaO	Calcium oxide
KBr	Potassium bromide
Hr	Hour
OH^-	Hydroxyl ions
µm	Micrometer
Al_2O_3	Alumina
$(NH_4)_2HPO_4$	Diammonium hydrogen phosphate
$Ca(NO_3)2$	Calcium Nitrate
CSD	Critical Size Defect
TGFβ	Transforming growth factor beta
Tris HCL	Hydroxy methyl amino methane

ABSTRACT

A novel attempt is made to convert the calcium carbonate skeleton of widely available garden snail shell to hydroxyapatite based bioceramics. The snail shell was found to decompose within 850^0C to all the carbonate phases. The calcined snail shells were then treated with acids followed by different chemicals in ammoniacal media maintaining proper stoichemetry to produce fine Hydroxyapatite (HAP) as filter cake with Ca/P molar ratio of 1.67. The dried HAP powder was extremely pure with specific surface area of $15m^2/g$.

The different characterization techniques were adopted both for calcined snail shell and HAP synthesized like X-ray Diffraction (XRD), Thermal Analysis (DTA/TGA), Fourier Transform Infra red Spectroscopy (FTIR) and Scanning Electron Microscopy (SEM). The surface area and the particle size, of the HAP powder prepared by chemical precipitation route, were also determined by BET and Malvern particle size analyzer respectively.

It was found that beyond 750MPa compaction pressure there is no significant enhance in green density. The graph of sintered density exhibited a sigmoidal shape with an inflexion point at 1250^OC where maximum density took place. There was increase in density (gm/cc) with increase in temperature (^{O}C), but at high temperature there was no further enhancement in density because of decomposition in HAP to other phosphate taking place.

The volume shrinkage (%) was studied for the green samples and the samples fired at high temperature. It was observed that maximum volume shrinkage took place for the samples fired at high temperature with high concentration of naphthalene (wt%).

The development and control of porosity is an important parameter in the implant in order to make material light as well as to facilitate rapid vascularization. Naphthalene as a porogen has negative effect on the sintering behavior of HAP. Naphthalene being volatile in nature, it escapes at low temperature leaving macropores in the material. The Bulk density,

apparent porosity was also studied with respect to increase in temperature, time and concentration of naphthalene.

The synthesized powder was soaked in synthetic body fluid (SBF) medium for various periods of time in order to evaluate its bioactivity. The changes of the pH of SBF medium were measured. High bioactivity of prepared HAP powder due to the formation of apatite on its surface was observed. The material proved to be non-toxic and compatible for the proposed work.

Key words: Snail shell, Hydroxyapatite, Calcination, Naphthalene, Microstructure, Synthetic Body Fluid, Bioactivity**,** Bioceramics.

Dedicated to my

Son: Hemkesh

CHAPTER 1

1.1 INTRODUCTION

Biomaterials are class of engineering materials, which can be used in animal body, tissue replacement, reconstruction, and regeneration without any long-term adverse effects. Among the different classes of biomaterials, bioceramics is one of the important classes of available material used as human- body implants[1]. Hydroxyapatite [$Ca_{10}(PO_4)_6$ $(OH)_2$] based bioceramics is a potential implant material due to its excellent osteoconductive properties[2].

Over the last several decades, bioceramics have helped improve the quality of life for millions of people. These specially designed materials—polycrystalline aluminum oxide, hydroxyapatite (a mineral of calcium phosphate that is also the major component of vertebrate bone), partially stabilized zirconium oxide, bioactive glass or glass-ceramics, and polyethylene-hydroxyapatite composites—have been successfully used for the repair, reconstruction, and replacement of diseased or damaged parts of the body, especially bone.

Hydroxyapatite was first identified as being the mineral component of bone in 1926. It is one of a limited number of materials that forms strong chemical bonds with bone in vivo, while remaining stable under the harsh conditions encountered in the human body. These properties place hydroxyapatite into the class of biomaterials known as surface active or bioactive materials. Some researchers in the field of orthopaedic biomaterials direct their focus on the fabrication and enhancement of bioactive properties of calcium-phosphates and in particular much interest has been directed towards the use of hydroxyapatite (HAP).

Several methods of chemical synthesis have been developed to prepare HAP powder using various types of Ca and P sources [3-6].In the present thesis an attempt is made to synthesize pure and biocompatible HAP powder by Snail shell as a Ca source. The Snail shell

consists of 94-97% of $CaCO_3$ and the other 3% is $MgCO_3$ organic matter and snail pigments. The Snail shell was found to be potent source from a biological origin. Hence in this present thesis Snail shell a material taken from biological origin has been used as a calcium precursor to synthesize HAP with Ca/P ratio 1.67, through wet chemical method.

The application of HAP as useful biocompatible materials largely depends on the purity and morphology of the powder. HAP can be prepared by different routes like chemical precipitation, sol-gel route, combustion synthesis, plasma etc. The purity in the final HAP powder and stoichemetry (molar ratio of Ca/P = 1.67) can be well controlled in chemical precipitation route. The different chemical processes use precursors like $Ca(NO_3)_2$, $Ca(OH)_2$ etc. as the source of Calcium[Ca] and $(NH_4)_2 HPO_4$, H_3PO_4 etc. as the source of Phosphorus [P] during synthesis of HAP. The extremely pure HAP powder is very costly and needs high quality precursors. The most of the sources of Ca^{2+} contains different types and level of impurities mainly silica. Snail Shell consists of $CaCO_3$ with minor amount of $MgCO_3$ and other matters can be potential precursors for the production of HAP.

HAP produced by above method was convenient and easy to use. HAP was also successfully synthesized in Synthetic Body Fluid (SBF). (SBF) with ion concentration similar to those of inorganic constituents of human blood plasma were able to act as a medium for the development of hydroxyapatite.

One of major disadvantage of HAP is that it has poor mechanical strength. There it is necessary to optimize the mechanical properties of calcium phosphates bone substitutes. Nevertheless, this must not be achieved by degrading their osteoconduction properties which is linked to macropores. A compromise must be found between porosities and mechanical properties. It is therefore necessary to develop material combining an excellent biocompatibility, good resorption ability and high mechanical properties. To achieve simultaneously all these goals, these materials will have to contain a balance amount of

macropores – to allow the natural bone cells to grow inside the ceramic – and of interconnected micropores- to allow the impregnation of the material by the biological fluid – the overall porosity being kept as low as possible to maintain good mechanical properties.

However it is well known that a mechanical property of a material is depend on the porosity. With the levels of porosity encountered in macroporous bioceramic (sometimes higher than 75%) very low mechanical properties can be expected. To optimize the overall behaviour of such materials, it is therefore necessary to understand how microstructural parameters influence mechanical properties. In this aim it is useful to model the mechanical behavior as a function of the amount and morphology of porosity. Nevertheless, no attempt has been made so far to model the influence of both microporosity and macroporosity on the mechanical properties of such materials, and only polynomial fits have been assessed. In this present thesis it is thus proposed to model the variation of porosity by using Naphthalene.

The dried samples of HAP obtained by synthesis of chemical precipitation method were ground to powder by mortar and pestle and then were placed in sieve shaker to achieve particles of uniform size. The powder sample was calcined at 850^0C and ball milling at 100rpm. The calcined powder was compacted at a pressure 750MPa by uni-axial pressing into cylinder samples of 15 mm diameter. The sample was then sintered and both green as well as sintered densities of the samples were determined by Archimedes principle.

The calcined powder was then mixed with appropriate quantity of naphthalene powder in different ratio to increase their porosity. The powder mix was inserted into a plastic bottle containing zirconia balls and was left for ball milling for 24hr for thoroughly mixing the powders among each other. The powder sample was than compacted at a pressure 750MPa by uni-axial pressing into cylinder samples of 15 mm diameter. The samples were than sintered and the sintered densities of the samples were than determined by Archimedes principle.

XRD analysis were carried out for HAP powders synthesized from different routes and sintered at various temperatures at the scanning range of 2θ= 20-80. The powders were characterized using DTA/TGA, BET surface area and Malvern particle size analyzer. The pore morphology and pore size distribution of the synthesized and sintered HAP were investigated by SEM.

Hydroxyapatite prepared by precipitation route also has the feature of small size, low crystallinity and high surfacial activation which can meet different demands keeping the above points in mind, the present study was aimed to produce and to enhance the bioactivity of stoichemetric HAP prepared from garden snail shell and to evaluate its bioactivity in simulated body fluid and also study its dissolution behavior in Tris HCL.

CHAPTER 2

2.0 Review of Literature

2.1 History of Biomaterial

The following three phases can be identified when reviewing the development of biomaterials:

(1) Removal phase: In the past, diseased or damaged tissues were simply removed. This phase was before the use of biomaterials.

(2) Replacement phase: Approximately three decades ago, transplantation an implantation became possible for, and the later practice provoked the rapid progress and wide application of biomaterials.

(3) Regeneration phase: With the rapid progress in material sciences and biology, we are now entering the third phase. Scientists are now trying to form human bone by culturing bone-forming cells within a porous scaffold. Currently, tissue engineering, whether combined with gene therapy or not, has increasingly attracted attention in the area of biotechnology.

Porous ceramics can be grouped into two general categories:

(1) Reticulate ceramic: A reticulate ceramic is a porous material of interconnected voids surrounded by a web of ceramic.

(2) Foam ceramic: A foam ceramic has closed voids within a continuous matrix.

In the porous form the surface area is generally increased, which allows more cells or tissue to be carried, in comparison with dense HAP. The interconnecting channels must guarantee the supply and circulation of the necessary nutrients, through the in growth of the vascular system, and bone tissue.

Because of the above- mentioned requirement, a tissue- engineering scaffold must take the reticulate form. One of the greater advantage of using naphthalene as porogen is that it evaporates at very low temperature leaving marcopores with interconnected porosity.

The mineral component of bone is a form of calcium phosphate known as hydroxyapatite (HAP). Stoichiometric HAP has a formula $Ca_{10}(PO_4)_6(OH)_2$, and adopts a hexagonal geometry with the unit cell crystal dimensions being 9.42Å in the a and b directions, and 6.88Å along the c-axis. However, bone mineral is rarely stoichiometric, containing many substitutions such as magnesium, sodium, potassium, fluorine, chlorine and carbonate ions. The apatitic mineral in the bone is closely associated with the collagen fibers and is made up of long, flat, plate-like nanocrystals that are approximately 40nm long, 10nm wide and 1-3nm thick. This mineral component gives rise to compressive strength of bone.

In the body, bone serves a number of functions, such as providing the cells, found in marrow, that differentiate into the blood cells, and also acting as a calcium reservoir. Nevertheless, its primary purpose is to provide mechanical support for soft tissues and serves as an anchor for the muscles that generate motion.

The anisotropic structure of bone leads to mechanical properties that exhibit directionality. This directionality results from the fact that bone has evolved to be both tough and stiff, two competing properties which are optimized in bone but with an inherent loss in isotropy. [7] Nevertheless, bone exhibits extraordinary mechanical properties, displaying both viscoelastic and semi-brittle behavior. [8] Compact bone has a compressive strength in the longitudinal direction (parallel to the long axis) ranging from 131-224 MPa, and a Young's modulus between 17-20 GPa. It also exhibits good fracture toughness, which is much higher in the transverse direction than in the longitudinal one. [7, 9] The mechanical properties of trabecular bone are highly dependent upon its density. Compressive strength varies with the second power of density, where as Young's modulus scales as the second or third power,

with values ranging between 5-10 MPa and 50-100 MPa for strength and modulus, respectively.

When damaged, bone demonstrates a remarkable capacity of regeneration. Though the details process of fracture healing is complex, it can be simplified into three stages: inflammation, repair and remodeling. [10] In the first stage, the normal wound healing response occurs, resulting in a fibrin clot, when ruptured blood vessels flood the region with growth factors and signaling molecules, attracting cells such as macrophages to digest the damaged tissue. During the repair stage, a callus is formed by bone-making cells recruited to the site, osteoblasts, that produce the cartilage-like bone matrix, which eventually mineralizes through deposition of a non-stoichiometric (calcium deficient) HAP. In the final and longest stage, the bone remodels through a process of resorption and deposition, which enhances the bone to resist the applied environmental stresses. This remodeling process is ongoing throughout an individual's lifetime. A tunnel is first created by cells osteoclasts that digest the old bone by releasing acids and enzymes. This space is then invaded by osteoblasts and blood vessels to supply nutrients and remove waste. The osteoblasts line the walls with new bone matrix that eventually traps them. These entrapped cells, called osteocytes, are interconnected by microscopic processes called canaliculi, and are nourished by blood vessels that exists in a cylindrical space called Haversian canal. This leads to the osteonal structure of bone made up of concentric cylindrical layers (Fig. 2.1). As a result of this inherent regenerative capability, bone is a prime candidate for tissue engineering and reconstructive strategies in dealing with trauma to bone tissues.

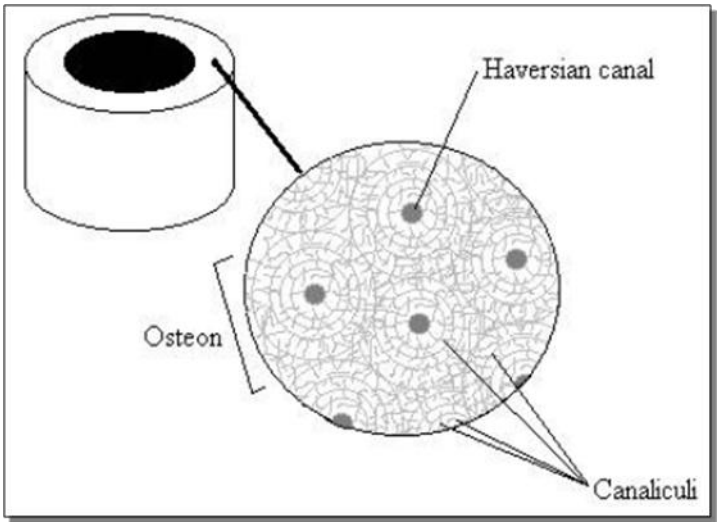

Fig. 2.1 Osteonal structure of bone made up of concentric cylindrical layers

2.1.1 The Structure and Mechanical properties of Bone

Bone is an composite material comprised of an inorganic phase, primarly hydroxyapatite ($Ca_{10}(PO_4)_6(OH)_2$) crystals, embedded in an organic matrix, primarily collagen.[11] At the micrometer level, these collagen fibril and embedded hydroxyapatite crystals bundle to form fibres.[12] The organization of these bone fibers above the micrometer level depends on the development and function of the bone area of interest.[13]

2.1.2 Bone healing

Bone healing has been studied at length in enchondral, tubular bones but much is still to be learned of the healing mechanisms of intramembranous bone, i.e. bone formed with cartilage phase. Such bone is mainly found in the cranio-facial area.

In tubular bone trauma, osteogenitor cells are recruited to the trauma site and are differentiated to bone forming cells. Multipotential cells from bone marrow and primitive fibroblasts from adjacent soft tissues may also be recruited. Biochemical, mechanical and biophysical factors are involved in this process, in which periosteal cells are activated for the repair process and the multipotential stem cells and prefibroblasts are induced to differentiate into osteoblasts.

The bone forming cells need a template to attain the proper three-dimensional structure. This is formed by the collagen network on which the hydroxyapatite crystals are deposited by the osteoblasts. This phenomenon, called osteoconduction helps to bridge large segmental defects. [14]

Fracture repair proceeds in three physiological and histologically characteristics but overlapping phases: 1) acute inflammation, 2) reparation and 3) adaptation [15-16]. Different tissue types are represented in the sequence: haetoma, granulation tissue, fibrous tissue, cartilage and bone.

In the acute inflammation phase the haematoma forms, bone necrosis occurs and cell death releases by products into the fracture site. Inflammation begins within 48 hours and lasts until cartilage and bone appear. The inflammation activates the cellular mechanisms necessary for the repair [16].

In the reparative phase the fracture gap becomes highly cellular, vascularizes and forms soft callus. Osteoblasti and chondroblasts begin to appear in the fracture gap and to replace the fibrovascular stroma[17]. The soft callus is converted by enchondral ossification to woven bone, where the collagen fibres are randomly oriented. Ossification can, however, happen without previous cartilage formation.

The last phase is adaptation (modeling and remodeling), starting early in the reparative phase [16]. The woven bone is transformed to lamellar bone with organized collagen matrix. During this process the bone shane is restored and the medullary canal is reconstructed. This process, which may take from months to years appear to be governed by Wolff's law [18].

2.1.3 Bone grafting

History

Various materials, from gold to allografts have been used to fill bony defects [19]. Despite the range of materials available today, the standard procedure for the repair of bony defects is still autogenous bone grafting.

Even if autogenous bone grafting had been used before, Leopold Ollier was the first to study bone transplantation systemically [20]. He also pointed out the difference between auto-, allo- and xenografts. In 1914 Phemister described clinically the healing of autogenous bone grafts and stressed the importance of vascularization, the various tissue components involved in bone healing and creeping substitutions [21]. After them numerous investigators contributed to the research into bone grafting, in particular after World War II, when there were a great number of victims with severe bone defects, especially in the craniofacial area.

2.1.3.1 Autografts

The autogenous bone graft has several advantages over allo- or xenografts. It has greater osteogenic capacity and it is biocompatible. As the autografts resorbs, revascularization recruits mesenchymal-type cells, which differentiate into osteogenic, chondrogenic or other cell lines [22].

The high osteogenic potential of cancellous bone derives from the bone marrow it contains, and the marrow part as such can be used to induce bone growth into different porous materials [23].

The cancellous graft is mouldable and resistant to infection; it vascularizes fast and can be obtained quite easily, usually as “chips” from the iliac crest [24]. Unfortunately the amount of cancellous bone is limited. Moreover, it cannot be used in stress bearing areas,

and the harvesting causes morbidity, such as pain, haematoma, infection and nerve injury [25] or even iliac hernia and ureteral injury [26-27]. The major complication rate amounts to 8.6% and the minor complication rate to an additional 20.6% [28]. Cortical (compact) bone is used when mechanical support is needed. Common donor sites used to be fibula, ribs and iliac crest. Unfortunately the biological properties of compact bone are poorer than those of cancellous bone, and the more compact the transplant the slower the vascular invasion. The bone grafts are replaced by local tissue through "creeping substitution", in which the graft acts as a scaffold for growing fibrovascular tissue [21]. Compact bone is probably never fully replaced or invaded by the graft site tissue; the outcome is therefore inferior integration and infections. It also has the tendency to resorb, making it an unreliable material [25, 29].

Intramembranous grafts have been considered to resist resorption better than enchondral grafts and their biological behaviour seems to be different. Cortical (and corticocancellous) grafts harvested from the calvaria (skull) are commonly used in craniofacial surgery [30].

The cortico-cancellous graft offers stability and osteogenic capacity. It can be used in weight-loaded areas, often in spinal fusions or in mandibular reconstructions. Vascularization is, however slow and large defects cannot be reconstructed due to the same complications as with cortical grafts.

Microvascular grafts have helped to overcome some of the drawbacks associated with the reconstruction of large defects. Large cortico- cancellous grafts can be harvested with their nutricient vascular pedicle, allowing the vessels to be anastomosed to suitable artery and vein in the recipient site. The healing takes place in the interface of the graft and recipient bone as in a normal bone fracture situation [31]. The donor site complications may however be more severe, because the grafts used tend to be very large.

The periosteum contains osteoprogenitor cells and can as such or as an osteo-periosteal graft be used to enhance bone formation [32]. This method has not gained much popularity though.

2.1.3.2 *Allograft*

The known limitations of autografting, e.g. secondary operation, limited availability of bone and operation morbidity, have encouraged the search for other options. The natural choice is allograft bone, human bone, usually harvested from a dead person or obtained in a hip fracture operation. The basic concept underlying allograft bone use was established in the early 1900s, when Baschirzev and Petrov showed that most of the cell components in the graft die after transplantation and that bone regeneration starts from the host bed [33].

Allografts demonstrate a lower osteogenic capacity, higher resorption rate and larger immunogenic response and, finally, less revascularization of the graft than autografts [34-35]. Despite of these drawbacks, allograft bone offers a useful adjunct to the range of bone graft materials. Bone can be minced and mixed with autogenous grafts in spinal fusions or hip prosthesis operations [24]. Allograft bone can even be used for large grafts comprising whole joints in tumour surgery. The results, however, are somewhat contradictory [36].

To maintain the availability of allograft bone, a well-organized bone bank is needed [37]. The possibility of transmitting viruses or bacteria may limit the use of allografts [38-39].

2.1.3.3 *Xenografts*

The xenogenic bone graft, that is, a graft made with bone from another species, presents similar problems to the allograft. It elicits an acute antigenic response with a high failure rate. Partial deproteination and defatting have been demonstrated to decrease the

antigenic response (Kiel bone) but at the cost of the osteoinductive capacity. Xenografts are indeed rarely used [40].

2.1.3.4 *Demineralized bone*

Demineralized (decalcified) bone was first studied in the late 19th century, when it was mainly used for filling cavities in osteomyelitis operations [41]. It is manufactured in a process whereby first the bone marrow is removed, then the bone is defatted and finally the mineral contents are decalcified with hydrogen chloride, leaving the collagen matrix intact. Demineralized bone can be used in powder form, in chips or in corticocancellous blocks. Urist and coworkers noted the osteoinductive capacity of demineralized bone, and later attributed it to the influence of morphogenetic protein [42]. Clinically demineralized bone has been used primarily for craniomaxillofacial reconstructions [43].

2.1.8 Mechanical properties of bone

Mature bone can be divided into cancellous (trabecular) or compact bone, depending upon the degree of bone porosity. Compact bone has a porosity of 5-30% and cancellous bone of approximately 30-90%, which is the proportion of the volume occupied by nonmineralized tissue [44]. The diaphyses of long (tubular) bones are composed mainly of compact bone whereas the epiphyses and methaphyses consist of cancellous bone that is continuous with the inner surface of the cortical shell and exists as a three-dimensional, sponge-like lattice composed of plates and columns of bone. The trabeculae divide the interior volume of bone into intercommunicating pores of different dimensions. The composition and true densities of compact and trabecular bone are thought to be similar [45] as are the microscopic material properties [46].

A key requirement in bone is compressive strength, and the most important factor in compressive strength is the degree of mineralization. Loss of mineralization results in increased risk of fracture [47]. A collagen and hydoxyapatite composite is advantageous from a mechanical standpoint. Mineralized tissue can be considered as a porous, two-phase composite consisting of hydroxyapatite crystals embedded in collagen matrix [48]. Increasing collagen intermolecular cross-linking is associated with increasing mineralization. The resulting composite structure is much stronger and stiffer due not only to the higher mineral content but also to the stiffening of the collagen matrix caused by the greater cross-link density [49-50]. It has been suggested that the longitudinal strength and stiffness of mineralized bone tissue are approximate proportional to the strain rate raised to the 0.06 power.

Bone can also be considered as a composite of both a solid and a fluid phase. The solid phase consists of mineralized bone tissue and fluid phase of blood vessels, blood and marrow, nerve tissue, miscellaneous cells and interstitial fluid [46].

The role of marrow, intrabecular fluids and soft tissues does not affect the compressive strength, under moderate, physiological, conditions such as walking [51]. The results at higher strain rate, 10.0 unit suggest that the presence of marrow during severe, traumatic, compressive loading *invivo* may serve to absorb considerable energy. Increasing the strain rate from 0.001 per second to10.0 per second increases the strength and stiffness of bone by a factor of approximately 2 [44].

The bone can be loaded by compression (or tension), shear, bending or torsion. The load F acting on the specimen can be measured with a testing instrument. The strength (maximal strength at breaking point) can be calculated from the load stress-strain curve by the ration of the ultimate load to the cross-sectional area of the specimen (A).

Strength = F/A

When compressive strength is measured, the displacement per unit is called strain. A stress-strain of the compressive test is shown in the Fig. 2.2

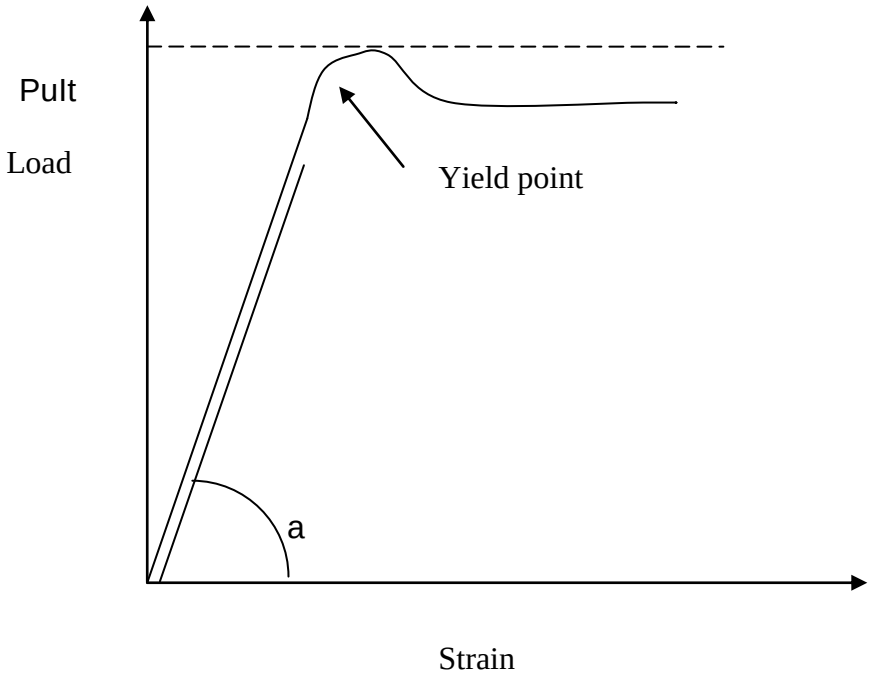

Fig. 2. 2 Stess-strain curve. PuIt is the ultimate compressive load before the final collapse of the specimen. Tan (a)-elastic modulus

At low levels of strain, stress is proportional to strain. Stress-strain curves in tension and compression consist of an initial elastic region that is nearly linear. It is followed by yielding and considerable non-elastic deformation until the breakpoint has been reached. This part of the curve reflects the irreversible, micro-damage of the bone structure.

The yielding point represents the onset of plastic deformation, which occurs at strain levels around 1% in ceramics [52]. In the zone of plastic deformation, a composite is able to absorb energy via matrix-filler debonding before ultimate failure [49].

The elastic compressive modulus is the slope of the load strain-curve in the most linear portion. Called Young´s modulus when tension or compressions are studied [50], it reflects the stiffness of bone.

The compressive strength of cortical bone varies, being in humans around 200MPa for the femur; the elastic compressive modulus is around 17GPa [53-54]. Cancellous bone is much weaker and the results obtained have varied, depending on the location of the bone [55]. Compressive strengths of 0.15-27MPa and elastic modulus from 50 to 350MPa have been reported for cancellous bone (Table 1) [44, 56-57].

2.2 Biomaterials

A biomaterial can be defined as "a material intended to interface with biological systems to evaluate, treat, augment, or replace any tissue, organ, or function of the body" [58]. There are three classes of biomaterial: metals, polymers and ceramics. The following looks briefly at some of the biomaterials used in clinical practice.

2.2.1 *Metals*

The main metals in clinical use are titanium, vitallium, aluminium and stainless steel, all of them inert and biocompatible [59]. Metal implants are used for load bearing purposes such as joint prostheses, and screws and plates. They may undergo corrosion over time due to galvanic corrosion produced by two different types of metal. Fretting corrosion may occur when the oxide film on the metal is damaged by, say, a screw in a plate hole [60].

The integration of metal prostheses to the host bone can be promoted by coating them with a bioactive ceramic such as hydroxyapatite. Coating with plasma-sprayed apatite leads to the formation of a strong bond between bone and metal implant [61]. This is particularly advantageous in hip arthroplasty, where implants have a tendency to detach with time.

Table 2.1. Studies of compressive strength on cancellous bone (adapted from Manninen 1993)

Authors(Yearof publishing)	Bone studied	Storage	Ultimate strength (MPa)	Modulus (MPa)
Sonoda 1992	Human whole lumber vertebral bodies	Fresh	6.3	-
Weavers and Chalmers (1966)	Human 3rd lumbar vertebracalcaneus	Fresh frozen	<50 yrs:4.2 >50 yrs:2.5 <50 yrs:3.9 >50 yrs:3.5	- - - -
Shoenfeld et al 1970.	Human femoral head	Fresh	0.5-13.5	340
Lindahi (1976)	Human tibia	Dried, defatted	Males 3.9 Females 2.2	35 23
Carter and Hayes (1977)	Human tibial plateaus	Fresh frozen	Marrow in situ 27.0 Without marrow 5.9	210 54
Stone et al. (1983)	Bovine humerus	Fresh frozen	8.3	-
Hvid and Jensen (1984)	Human proximal tibia	Fresh frozen	1.6 7.7	- -

Kaplan et al. (1985)	Bovine proximal humerus		12.4	
Wixon et al. (1989)	Human distal femur and proximal tibia	Dried, soft, tissue remove	5.6	150

2.2.2 *Polymers*

Polymers comprise a large group of materials of heterogenous origin. They are composed of the macromolecules that are typically formed by the bonding of one or a small number of types of subunits repeated along the length of the polymer [60]. A polymer widely used in traumatic skull defects is methyl methacrylate. It is easy to mould, cheap and nonresorbable and is even stronger than calvarial bone. The infection rate is considered to be comparable to that in bone grafting procedures but its use is not recommended for patients who previously had infections in the cranioplasty site. The use of methyl methacrylate requires good quality of the overlying soft tissues [62].

Polyhydroxyethylmethacrylate with calcium hydroxide coating (Hard Tissue Replacement, HTR®, Walter Lorenz Surgical, Inc., U.S.A), is another popular polymer composite. It is a nonabsorbable porous material allowing tissue ingrowth into pores of 150 to 350μm. It can be prefabricated in custom shapes and is mainly used in facial augmentations [63].

Porous high-density polyethylene (Medpor ®, Porex Surgical, Inc., U.S.A.) is used in facial augmentation surgery, in ear and orbital reconstruction and to fill empty eyeball sockets after enucleation or evisceration. The implants are fixed to bone or soft tissue by fibrous tissue ingrowth. The material is not resorbable, which is an advantage in

augmentation surgery. The complication rate does not seem to differ from that of bone graft procedures. Among the disadvantages of polyethylene are its rigidity and the difficulty of contouring it to the surface of complex skeletal structures [63-64]. Another polymer material is a synthetic porous composite of polyethylene polymer and aluminium (Proplast®). Although it is light, porous, resilient, malleable and easy to shape the material is currently little used due to the high complication rate associated with its application in recent years [65].

Polyglycolide and polylactide are hard synthetic crystalline polymers used as fixation material in orthopedic and craniofacial surgery. In living tissue they degrade to glycolide and lactide mainly by hydrolysis. Their unique mechanical properties are such that they can be used for manufacturing screws, pins and plates that absorb with time [66], thus eliminating the need for a secondary operation of removing the fixation material. In recent years the possibility of polyglycolide and polylactide acting as delivery material for growth factors has been investigated [67].

2.2.3 *Ceramics*

Ceramics consist of crystalline metallic oxides, carbides, nitrides and borides fused by the high temperature process known as sintering. They are brittle, have low electrical and heat conductivity and elicit very little tissue reaction [68]. Different glass ceramics are typical representatives of this group of biomaterials. In the 1970s, certain glass compositions were found to be able to bond chemically to bone, a property called bioactivity. The first bioactive glass, Bioglass®, was composed of SiO_2, Na_2O, CaO and P_2O_5. Bioactive glasses are manufactured by conventional glass manufacturing methods and even minor changes in their composition change the character of the bone-material bonding and resorption [69]. Granular and solid forms of bioactive glasses have been used clinically to reconstruct orbital walls and facial bone defects and to obliterate frontal sinuses. Bioactive glasses are osteocompatible

and the infection rate is low. The resorption rate may, however, be too high and the migration of granules can cause problems [70]. Another important group of ceramics comprises materials deriving from calcium. Such ceramics are composed of calcium sulphate, phosphate and carbonate derivates and their mixtures in dense, porous and granular forms. The following sections examine these materials in greater detail.

2.2.4 Calcium ceramics

2.2.4.1 *Calcium sulphate*

Plaster of Paris (calcium sulphate) was one of the first materials to serve as bone substitute. In 1892, Dreesman used it to fill bony defects in eight patients with nine defect sites. Six defects healed well and three remained unhealed [71]. Since then calcium sulphate has proved to be biocompatible and adsorbable but not osteoconductive. Resorption occurs in weeks and may be too fast for the bone formation process [72]. This, together with its poor mechanical properties, has limited the use of calcium sulphate as bone substitute.

Fast resorption may, however, be an advantage. In 1928, plaster of Paris was investigated by Petrova as a delivery material for antiseptics, and in the 1950s cylinders containing penicillin and sulphonamide were examined clinically [73]. Recently the properties of calcium sulphate were suggested to be suitable for a carrier of bone morphogenetic protein in a mouse model [74].

2.2.4.2 *Calcium phosphate*

Calcium phosphate biomaterials are polycrystalline ceramics deriving from individual crystals of a highly oxidized substance that have been fused together [75]. The two most important are tricalcium phosphate $Ca_3(PO_4)_2$, or ß-whitlockite, and hydroxyapatite $Ca_{10}(PO_4)_6(OH)_2$. Both materials are known to be biocompatible and osteoconductive and to

bond directly to bone. The main difference between these two materials is that tricalcium phosphate (TCP) degrades much faster than HAP [75-76]. The chemical structure of calcium ceramics resembles that of bone. Hydroxyapatite is the main inorganic salt of bone and the synthetic form has been shown to be chemically and crystallographically similar, but not identical, to naturally occurring HAP [77].

HAP is the most studied calcium phosphate material with clinical experience of its use going back to the 1970s [78]. Offering better integration to bone, porous HAP has now replaced the dense form. When HAP has been placed into bony defects, bone growth into pores has ranged from 18% to 74% (new bone area compared to total implant area) [79-80]. The entire porous space of the implant is probably never completely filled with bone [81]. Porous HAP can be manufactured in several ways. Homogenizing calcium phosphate powder with appropriately sized naphthalene particles results in macroporous material after the naphtalen has been removed. The final form is achieved after sintering at high temperatures (1100-1300°C). Another method relies on the decomposition of hydrogen peroxide to generate a pore-filled structure.

The porous structure achieved in these methods is not, however, consistent. To avoid this problem, a completely different approach was developed in the early 1970s as a joint investigation by the Materials Research Laboratory at The Pennsylvania State University and the Orthopedic Research Laboratory of the Upstate Medical Center at Syracuse, both in the U.S.A.

The idea is based on the finding that the structure of certain reef-building coral species resembles osteon evacuated bone [82]. The coral pore size is consistent and varies very little (Figure 3). A pore size of over 100µm was previously found to allow fibrovascular and bone tissue ingrowth [78]. With pore diameters of 140-160 µm, the reef-building coral genus *Porites* meets the structural requirements for bone substitute [83].

This structure can be preserved in the "replamine form process" (meaning the replication of the life forms) in which the chemical composition of coral is changed (Fig. 2.3) [84]. In 1974 Roy and Linneham refined the replamineform process and succeeded in changing the calcium carbonate ($CaCO_3$) skeleton of coral into hydroxyapatite in the "hydrothermal exchange reaction". This resulted in a hydroxyapatite implant with controlled porosity but with a chemical composition differing from that of the original coral material.

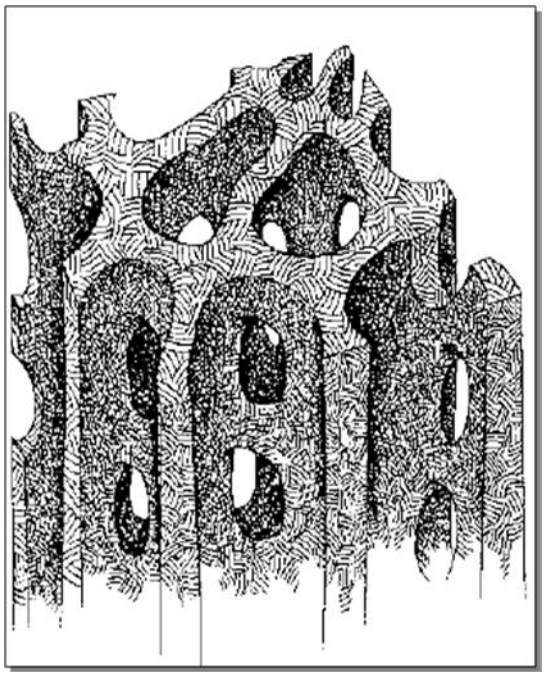

Figure 2.3 Drawing of a bone graft substitute replicated from *Porites.* Channels of osteonic diameter and channel wall fenestration mimic .

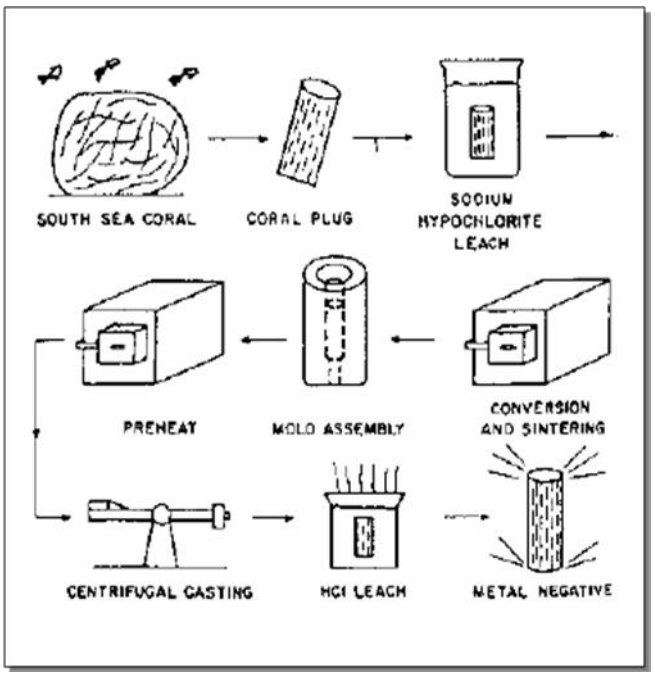

Figure 2.4 Schematic representation of the replamineform process. The coral is shaped for treatment , as shown, to yield porous implants in a variety of materials (after Chiroff 1975).

Several studies have shown that hydroxyapatite is osteoconductive, biocompatible and very inert [75, 82-83]. It resorbs with time but the degradation rate is very slow [84]. HAP has been used clinically in dental, craniofacial and orthopedic surgery, mainly in granular form [81, 85-90]. Recently a hydroxyapatite cement was developed for cranial defects. It is in paste form and can be moulded into the desired shape. The material integrates to the host bone and

is claimed to be replaced by bone, at least to some extent [91]. The high cost of the material has, however, restricted its wider use clinically.

Porous HAP is brittle and can be used only in non-loading sites. Its compressive strength is -enhanced by bone ingrowth but it is only comparable to that of cancellous bone [80]. Slow resorption is advantageous in certain clinical situations. If used as an onlay graft as in alveolar ridge augmentation, degradation is not desired. However, an ideal bone substitute should be osteoconductive, osteoinductive, biocompatible and easy to shape; it should also biodegrade after it has been occupied with new bone and is a reasonable price. Its mechanical properties should be comparable to those of cortical bone. HAP has many of these qualities but it resorbs very slowly and is brittle.

2.2.4.3 *Calcium carbonate*

Calcium carbonate ($CaCO_3$) resembles hydroxyapatite in many respects. The material is biocompatible and osteoconductive but, like HAP, has no osteoinductive properties [92]. The main difference to HAP is the resorption rate. Resorption seems to be clinically unimportant with HAP, but animal experiments have shown resorption rates of only a few weeks, when CC is used [93].

Certain coral species form a structure that resembles the matrix or bone. Each species builds a structurally and geometrically typical calcium carbonate skeleton. Choice of the appropriate species therefore enables a desired and constant implant structure to be achieved.

Coral reefs are formed by colonies of polyps ranging in size from one millimetre to several centimetres, depending on the species. Coral polyps live in symbiosis with unicellular algae, which photosynthesize compounds essential to the polyps. The outer layer of the polyp is capable of secreting a substance that calcifies in the seawater milieu and serves as matrix for the coral skeleton. The coral polyp lives only in the upper part of the skeleton, moving

slowly upwards, leaving an empty skeleton behind. Coral reefs play an important role in maintaining the equilibrium of carbon dioxide, which is absorbed from the seawater in the building process.

More than 2000 coral species have been described from the intertropical area and, of these, fourteen Scleractinian corals have been studied as possible bone substitutes.The following genera have already been used as bone grafts: Pocillopora, Acropora, Montipora, Porites, Goniopora, Fungia, Polyphyllia, Favites, Acanthastrea, Lobophyllia and Turbinaria [94]. The most promising is *Porites astreoides*, which forms massive colonies and is common throughout the Caribbean area, including the Bahamas, Bermuda and Brazil. The porosity of the skeleton is around 50% and the mean size of the pore is 150µm, the pores interconnecting with each other.

The harvested coral is purified physically and chemically and the final implant material contains no proteins and less than 0.1% amino acids. The manufacturer of the commercially available coral implant (Biocoral®) guarantees the following chemical composition of the product Table 2.2. Fig.2.5 represents picture of Snail shell.

Table 2.2 Composition of the Snail Shell

Calcium carbonate	>97%
Trace elements	0.5-1%
Magnesium	0.05-0.2%
Sodium	<1%
Potassium	<0.03%
Phosphorus	<0.05%
Water	<0.5%

Fig. 2.5 Picture of Garden Snail shell

Experimental studies on Calcium carbonate (CC) started in the early 1970s. Chiroff and coworkers placed CC in cancellous defects in dogs for 8 weeks and found that the material was biocompatible and that new bone could fill the pores. Some implants were left for 1 year and were observed to be almost completely resorbed [83]. The favourable results were confirmed when other animals, e.g. monkeys [95] and sheep and pigs [93], were used.

The first clinical reports were published in France by the Institut de Recherches Orthopédiques, Université René-Descartes Paris V in 1980[96]. Since then CC has been used clinically in maxillofacial surgery to correct periodontal defects [97-98] and to fill and reconstruct bony defects in cranial surgery [99-101]. The craniofacial bones can be augmented by the granular form of CC [102]. In orthopaedic surgery CC has been used as filler in tibial osteotomies [103], in bone tumour surgery [104] and in lower limb metaphyseal fractures to support articular surfaces [105]. The possibly most appropriate indication at the moment is

spinal fusion, where CC can be used to diminish the amount of bone grafts in conjunction with autogenous bone [106-107].

Little is known about bone ingrowth into the CC implants. Bone and fibrous tissue do grow into the pores but exact information is scarce. This may be due to the difficulty of measuring the already partially resorbed implant. The same difficulty applies to measurements of the mechanical properties, which, according to the manufacturer, are better than in cancellous bone.

Very little exact information exists also on the resorption time of CC. It seems to depend on the animal species used. When the implant was placed in the cortex of the femur in pigs, 64% of the CC blocks were resorbed after 1 month, whereas in sheep the figure was 93% [93]. The granular form has been observed to resorb completely at 24 weeks in a connective tissue site in pigs but, in humans, the same material placed in subcutis can still be found after several years [102, 108]. Roux and coworkers reported almost complete resorption after 1 year in 50% of cases when coral was used to fill craniotomy burrholes in humans [99]. Larger blocks used in humans have still been x-ray positive after 4 years [105].

Coral resorption is most active in the boneimplant contact areas and proceeds centripetally[109]. Carbonic anhydrase, an enzyme abundant in osteoclasts, plays a key role in the resorption process. Locally it lowers the pH at the osteoclast-implant interface, dissolving the CC matrix [110-112]. Resorption can be halted by the administration of the diuretic acetazolamide, a known inhibitor of carbonic anhydrase [112]. Moreover, according to Fricain and coworkers, data suggest that both fibroblasts and macrophages dissolve the coral, and that one of the mechanisms is the intracellular degradation in phagolysosomes [113]. A prerequisite for the process is direct contact between these cells and the coral matrix [114].

2.3 Induction of bone growth into calcium ceramics

2.3.1 *Enhancement of bone growth*

Porous calcium ceramics are osteocompatible [75, 115] and osteoconductive [83] but they lack the capacity to induce new bone formation from determined osteogenic precursor cells, a quality known as **osteoinduction.**

Osteoinduction can be attained by harvesting bone marrow cells as such or in conjunction with autogenous bone and placing them at a site where bone formation is needed, e.g. at bony defects caused by fracture or by pseudoarthroses. Another way is to induce bone growth by the members of the TGF-beta superfamily, a group of growth factors that make an important contribution to the bone formation process.

2.3.2 *Bone marrow*

Back in 1869 Goujon observed heterotopic (extraskeletal) bone formation after red bone marrow transplantation. Bone marrow contains osteogenic precursor cells, which are capable of differentiating into osteoblasts. When marrow is placed in a heterotopic site (subcutis, muscle), bone may derive from these cells, from endosteal osteoblasts or from the host cells at the site of grafting, induced to differentiate by bone marrow [116]. In 1971 it was found that autogenous marrow formed bone in association with various materials and that calcified matrix increased the ostegenic capacity of the marrow [117]. In 1980 Lindholm and Urist reported enhanced bone formation in composite grafts of bone matrix and bone marrow [118]. A year earlier McDavid and coworkers had placed tricalcium phosphate pellets with autogenous bone marrow under the skin of rats. At 4 weeks bone was evident only in marrow-coated implants [119]. Porous aluminate, calcium aluminate, HAP and TCP inserted together with marrow into the intermuscular space of rabbits were observed to allow bone formation [23].

Ohgushi and coworkers investigated porous calcium phosphate (60% HA and 40% TCP) blocks in a segmental rat-femur defect experiment. The group treated with bone marrow showed significantly better osseous or osteochondral union than did the control group without marrow [120]. Placing similarly treated implants into the subcutaneous pouches of rats resulted in bone in growth only into the implants treated with bone marrow; after 1 months the proportions of the pore area filled with bone for implanted HA and TCP were 16.9% and 15.1%, respectively.

After 2 months the proportions were 34.3% and 30.9 % [121]. Later, CC disks (genus *Porites)* were investigated similarly and bone formation was observed after 3 weeks. No histomorphomeric analysis was, however, performed.

2.3.3 *Transforming growth factor-beta*

The data above show that bone formation can be induced into porous calcium implants by bone marrow. The next step is to prefabricate implants with already existing potential for bone formation. Members of the transforming growth factor-beta super family play an important role in the bone formation process and may offer a solution to the manufacture of such bone substitutes.

TGF-ßs are a group of growth regulatory peptides consisting of five isoforms [122]. They form the TGF-ß superfamily together with bone morphogenetic proteins (BMPs) and the embryonical growth factors inhibin, activin and the Müllerian substance[123]. The unifying properties of these peptides are their similarity in structure and their ability to regulate development and cellular differentiation.

The five TGF-ß isoforms are encoded by closely related genes. Three of them, TGF-ß1, ß2 and ß3, are found in mammalian bone, which is the largest reservoir of TGF-ß the concentration being 100 times as high as in other tissues. TGF-ß1-3 are very similar in their way of action and are here considered together as TGF-ß.

Platelets are the most concentrated source of TGF-ß although most cells can synthesize it [123]. TGF-ß1 was first isolated from human platelets [124] and was later cloned from the human complementary DNA library (recombinant TGF-ß) [125]. The universality of its action is emphasized by the almost identical amino acid sequence in various mammalian and avian species [123].

TGF-ß is a homodimeric protein of 25kDa. It is found in the form of an inactive high molecular weight complex that is activated by an acid environment, heat and enzymatic activity. Such an environment is found close to the osteoclast. Osteoclast activity could activate TGF-ß, which then activates the osteoblasts [126] with the highest amount of TGF-ß receptors [127]. This could be an important part of bone remodeling.

TGF-ß is a major regulator of bone development, induction, repair and remodeling. It has strong mitogenic activity on osteoblasts and it enhances bone matrix collagen production [127]. It also plays an important role in soft tissue repair, chronic inflammatory fibrotic disorders, autoimmune diseases, and even in the repair of ischaemic cardial injury [128]. In 1991 Beck and coworkers showed in rabbits that a single application of TGF-ß triggers a cascade of events leading to new bone formation in the course of 49 days [129]. They used the critical size defect (CSD) model (a defect large enough not to be able to heal) [130], drilling a 12mm large hole into the parietal bone and filling it with TGF-ß mixed with 3% methylcellulose. Bone formation was minimal in the control groups.

Since then very different materials have been investigated for the delivery of TGF-ß to bone, such as calcium sulphate implants and polylactic-coglycolic acid devices [67], gelatin sponge [131] wax-like biodegradable polymer ceramics [132], tricalcium phosphate coated titanium implants [133] and demineralized bone matrix [136, 143]. The results have been encouraging, but limited bone formation has also been reported [131, 136-137]. Centrella and coworkers noted that the effect of TGF-ß on bone cell replication is biphasic and depends on both the TGF-ß concentration and the cell density in monolayer culture [138]. Dose dependence becomes more complicated when TGF-ß is released from different vehicles and when different animal species are used. Doses of between 0.4µg and 40µg have most commonly been used with conflicting results [133-134]. Ripamonti and coworkers suggested that the limited bone formation is the result of TGFß's capacity to stimulate the proliferation of only periosteal and endosteal cells rather than to initiate bone cell differentiation, as does bone morphogenetic protein [136]. They also noticed a synergism in the function of TGF-ß and BMP in a heterotopic baboon experiment and postulated that TGFß might act as a chemotactic and mitogenic factor for responding precursor cells for subsequent induction by BMP [139].

Coral has also been evaluated as a growth factor carrier, mainly in granular form. Damien and coworkers applied bone morphogenetic like protein and basic fibroblast growth factor (bFGF) to CC and noticed good ossicle formation only when BMP was present, whether with or without bFGF. The implants were placed into the subcutis of rat and they postulated that coral-collagen was a good carrier vehicle for BMP and should be tested in a bony site [140]. BMP and coral granules were later evaluated in spinal fusions in rabbit but solid fusions were obtained only in BMP groups, not in controls [141].

There are very few reports of TGF-ß in association with CC. Arnaud and coworkers tested 1µg of TGF-ß1 with coral granules and fibrin glue in a CSD model in rabbits and obtained significantly better bone formation with this combination at 2 months than with TGFß1 in methylcellulose or in fibrin glue alone [142]. Another investigation showed only marginal bone growth stimulation at 4 weeks in a canine periodontal defect model with granular coral, hydroxyethyl starch and 20µg of TGF-ß1. The authors postulated that the healing interval of 4 weeks was too short or that the experimental model itself diminished the effect of TGF-ß1 [137].

2.4 Biomaterial

A biomaterial is any material, natural or man-made, that comprises whole or part of a living structure or biomedical device which performs, auguments, or replaces a natural function. Biomaterials can have a benign function, such as being used for a heart valve, or may be bioactive and used for a more interactive purpose such as hydroxy-apatite coated hip implants (the Furlong Hip, by Joint Replacement Instrumentation Ltd, Sheffield is one such example – such implants are lasting upwards of twenty years). Biomaterials are also used every day in dental applications, surgery, and drug delivery (a construct with impregnated pharmaceutical products can be placed into the body, which permits the prolonged release of a drug over an extended period of time).

The definition of a biomaterial does not just include man-made materials which are constructed of metals or ceramics. A biomaterial may also be an autograft, allograft or xenograft used as a transplant material.

2.4.1 Biomaterial Applications

Biomaterials are used in:

- Joint replacements
- Bone plates
- Bone cement
- Artificial ligaments and tendons
- Dental implants for tooth fixation
- Blood vessel prostheses
- Heart valves
- Skin repair devices
- Cochlear replacements
- Contact lenses

Biomaterials must be compatible with the body, and there are often issues of biocompatibility which must be resolved before a product can be placed on the market and used in a clinical setting. Because of this, biomaterials are usually subjected to the same requirements of those suffered by new drug therapies. All manufacturing companies are also required to ensure traceability of all of their products so that if a defective product is discovered, others in the same batch may be traced.

2.4.2 Hydroxyapatite

Hydroxyapatite is chemically similar to the mineral component of bones and hard tissues in mammals. It is one of few materials that are classed as bioactive, meaning that it will support bone ingrowth and osseointegration when used in orthopaedic, dental and maxillofacial applications. This similarity has led to interest in the development of HAP materials for biomedical applications.

Key Properties

- The ability to integrate in bone structures and support bone ingrowth, without breaking down or dissolving (i.e it is bioactive).
- Hydroxyapatite is a thermally unstable compound, decomposing at temperature from about 800-1200°C depending on its stoichiometry .
- Generally speaking dense hydroxyapatite does not have the mechanical strength to enable it to succeed in long term load bearing applications.

The table below illustrates the chemical and structural similarities between HAP, enamel, dentin, and bone [143].

Table 2.3 Chemical and structural comparison of teeth, bone, and HAP.

Composition, wt%	**Enamel**	**Dentin**	**Bone**	**HAP**
Calcium	36.5	35.1	34.8	39.6
Phosphorous	17.1	16.9	15.2	18.5
Ca/P ratio	1.63	1.61	1.71	1.67
Total inorganic (%)	97	70	65	100
Total organic (%)	1.5	20	25	--
Water (%)	1.5	10	10	--
Crystallographic properties: Lattice parameters (±0.003 Å)				
a-axis (Å)	9.441	9.421	9.41	9.430
c-axis (Å)	6.880	6.887	6.89	6.891
Crystallinity index, (HA=100)	70-75	33-37	33-37	100

Crystallographically, hydroxyapatite belongs to the hexagonal system with the $P6_3/m$ space group. The 'P' indicates that HA is a primitive hexagonal system where a = b ≠ c, $\alpha = \beta = 90°$ and $\gamma = 60°$ [144]. A schematic representation of the crystal structure is provided in Fig. 2.4. [145].

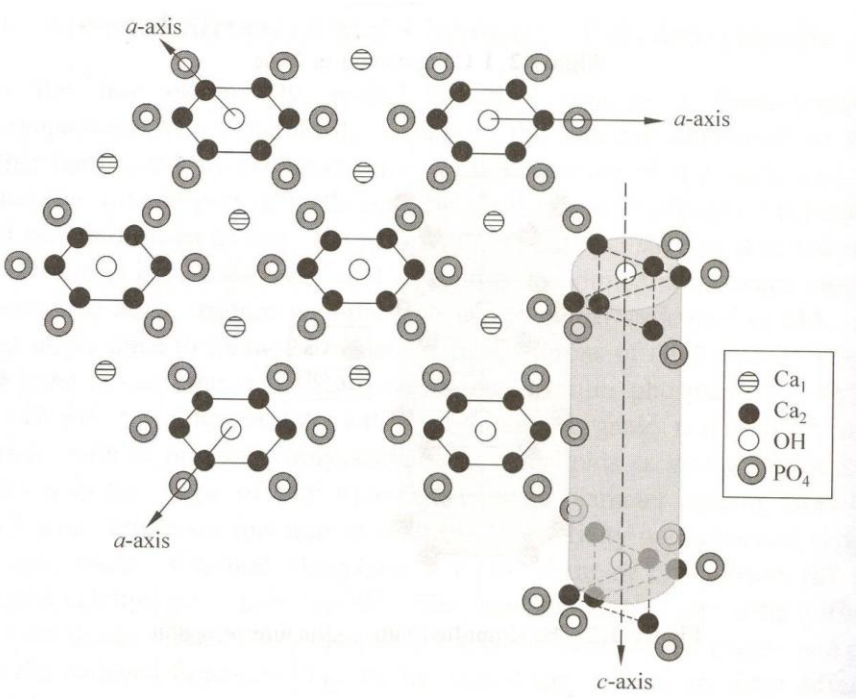

Figure 2.4 Schematic representation of hydroxyapatite crystal structure.

2.4.3 Bioactive Hydroxyapatite Ceramics

The bond formed between a metallic titanium alloy implant and the bone tissue is mediated by a so-called contact osteogenesis. Bone tissue is one-directionally growing towards to interface and „bony on-growth"occurs that is able to transmit compressive loads. However, the actual loads the interface is subjected to during movement of the patient contain also strong tensile and shear components that have to be taken care of. In the clinical practice in many cases a bioactive hydroxyapatite layer is provided that will allow bonding osteogeneses that through "bony in-growth" will be able to transmit these tensile and shear

forces. Here two ossification fronts develop, one growing from the bone towards the implant and another growing from the implant towards the bone [146]. Evidence is mounting that a 150 – 200 μm long-term stable bioactive hydroxyapatite coating will elicit a specific biological response at the interface of the implant material by control of its surface chemistry through adsorption of non-collageneous proteins such as osteocalcin, osteonectin, silylated glycoproteins and proteoglycanes. This will result of the eventual establishment of a strong and lasting osseoconductive bond between living tissue and biomaterial. The advantages of bioactive coatings include (i) the prevention of a fibrous capsule of connective tissue surrounding the implant, (ii) fast bone apposition rates through preferential adsorption of proteins, (iii) bonding osteogenesis providing a continuous and strong interface between implant and tissue that is able to transmit not only compressive but also tensile and shear loads, (iv) accelerated healing compared to implants without a bioactive coating, as well as (v) reduced release of titanium ions to the surrounding tissue thus minimizing the perceived risk of a cytotoxic response.

2.5 Defination of Biocompatibility

Biomaterials by definition are inorganic compounds that are designed to replace a part or a function of the human body in a safe, reliable, economic, and physiologically and aesthetically acceptable manner [147]. Hence they do not include renewable materials obtained from natural sources such as wood, plant fibers, hides, tendons, bone, ivory and others[1].

In increasing order of biocompatibility the interaction of biomaterials with living tissue can be defined as follows [148].

Incompatible materials are materials that release to the body substances in toxic concentrations and/or trigger the formation of antigens that cause immune reactions ranging

from simple allergies to inflammation to rejection with the associated severe health consequences.

Biocompatible materials, in contrast, are those that also release substances but in non toxic concentrations that may lead to only benign tissue reactions such as formation of a fibrous connective tissue capsule or weak immune reactions that cause formation of giant cells or phagocyts. These materials are often called ***biotolerant*** such as austenitic stainless steels or bone cement consisting of polymethylmethacrylate (PMMA).

Bioinert materials do not release any toxic material but also do not show positive interaction with living tissue. As a response of the body to these materials usually a non-adherent capsule of connective tissue is formed around the bioinert material that in the case of bone remodelling manifests itself by a shape-mediated *contact osteogenesis*. Through the bone-materials interface only compressive forces will be transmitted („bony on-growth"). Typical bioinert materials are titanium and its alloys, ceramics such as alumina, zirconia and titania, and some polymers, as well as carbon, see Table 2.4.

Bioactive materials show a positive interaction with living tissue that includes also differentiation of immature cells towards bone cells. In contrast to bioinert materials there is chemical bonding to the bone along the interface, thought to be triggered by the adsorption of bone growth-mediating proteins at the biomaterials surface. Hence there will be a biochemically-mediated strong *bonding osteogenesis*. In addition to compressive forces, to some degree tensile and shear forces can also be transmitted through the interface ("bony in-growth"). Typical bioactive materials are calcium phosphates and bioglasses, see Table 2.4.

Table 2.4. Examples of biomaterials and their applications (Willmann 1999).

Material	Application	Biological behaviour
Stainless (austenitic) steel	Osteosynthesis (bone screws)	Biotolerant
Bone cement (PMMA)	Fixation of implants	Biotolerant
cp-titanium	Acetabular cups	Bioinert
Ti6Al4V alloy	Shafts for hip implants, tibia	Bioinert
CoCrMo alloy	Femoral balls and shafts, knee implants bioinert	Bioinert
Alumina	Femoral balls, inserts of acetabular cups	Bioinert
Zirconia (Y-TZP)	Femoral balls	Bioinert
HD-polyethylene	Articulation components	Bioinert
Carbon (graphite)	Heart valve components	Bioinert
CFRP	Inserts of acetabular cups	Bioinert
Hydroxyapatite	Bone cavity fillings, coatings, ear implants, vertebrae replacement	Bioactive
Tricalcium phosphate	Bone replacement	Bioactive
Tetracalcium phosphate	Dental cement	Bioactive

2.5.1 Interaction of implant Material and Living Tissue

Fixation of an implant in the human body is a dynamic process that remodels the interface zone between the implant and living tissue at all dimensional levels from the molecular up to the cell and tissue morphology level and at all time scales from the first second up to several years after implantation [149]. This is represented in Fig. 2.6 in which the logarithmic length and time scales indicate this complex dynamic process. While immediately following the implantation a space filled with biofluid exists next to the implant surface, with time proteins will be adsorbed at the oxide surface of only several nanometers thickness covering the titanium alloy surface that will give rise to osteoinduction by proliferation of cells and their differentiation towards bone cells, revascularisation and eventual gap closing. Ideally, a strong bond will be formed between implant and tissue.

However, sometimes connective tissue is being formed at the interface resulting in a fibrous tissue capsule that prevents osteointegration (see inset) and will cause implant loosening.

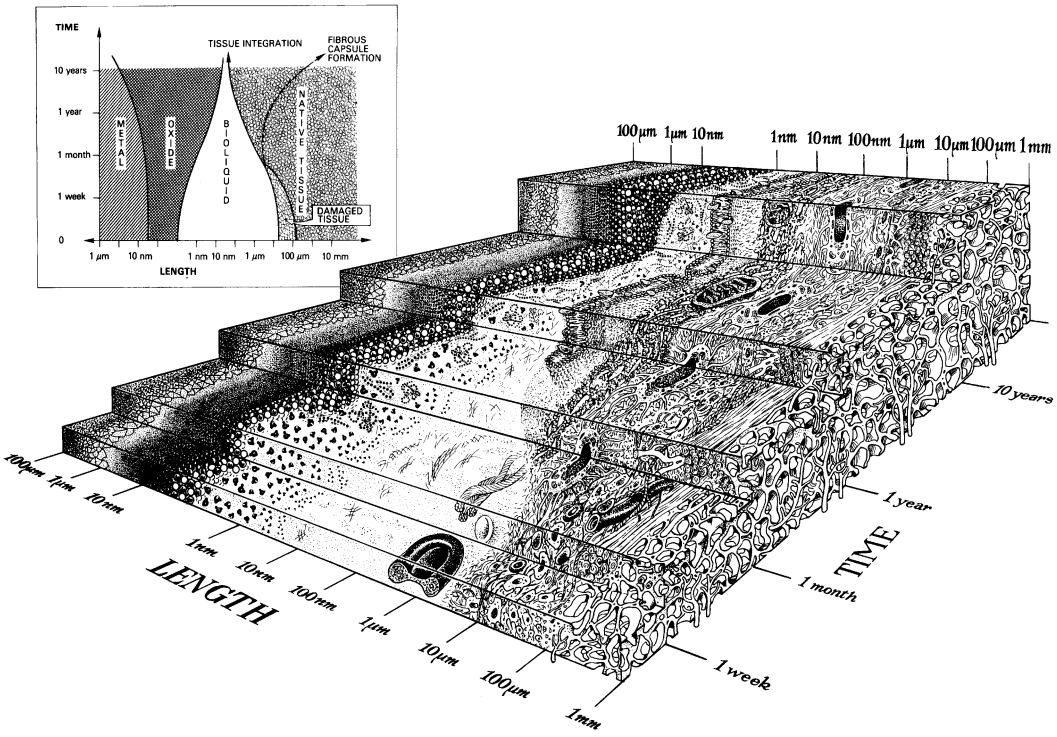

Fig. 2.5 - Dynamic behaviour of the interface between implant (left) and bony tissue (right) (Kasemo and Lausmaa 1991).

Approach of the thesis

After consideration of different synthesis processes, properties and applications, the approach was used to study the development and control of porosity in HAP by the help of porogen as naphthalene. The porogen has a negative influence on the sintering ability of ceramic probably due to the spaces generated on the way out of the organic additive on burning. Naphthalene being volatile in nature it escapes at very low temperature i.e. less than $50^{O}C$ leaving behind pores in the HAP material. The volumetric shrinkage (%) of HAP with respect to different concentration of naphthalene (wt %) is also studied. The increase in grain size and pore size behavior of the material as a function of sintering temperature, time and naphthalene concentration is studied by visualizing their microstructure with the help of Scanning electron microscope. *In vitro* studies and dissolution behavior of HAP was carried out for the test of Biocompatibility.

CHAPTER 3

3.0 OBJECTIVE

The extensive literature survey reveals the synthesis of HAP by different chemical route, has been attempted by number of researchers. However, the synthesis of HAP from Snail Shell by chemical route has not yet been reported according to best of my knowledge. Moreover, the concept of development of porous HAP by addition of different ratio of naphthalene as porogen is attempted. Hence, objectives of the present investigation can be summarized as follows:

1. To obtain, pure and thermally stable HAP powder from biological waste (Snail shell) by chemical precipitation method i.e. Route 1 and Route 2 and to synthesize HAP also in Synthetic Body fluid (SBF).
2. To analyze the thermal behavior of precursors with respect to HAP synthesized from chemical route and characterize the material like, FTIR spectral analysis, particle size analysis and BET surface area.
3. To study the morphology of the particles and crystallization behavior of the HAP synthesized from different route by XRD analysis and compares it with human bone.
4. To study the densification behavior of HAP without addition of any external additive or organic binder and to study the sintering kinetics of HAP synthesized.
5. To study the volume shrinkage behavior of porous HAP.
6. To control the porosity of HAP by adding porogen like naphthalene in different proportion and to calculate apparent porosity and bulk density.
7. To study the microstructure of porous HAP by SEM as well as to calculate average pore size with respect to increase in porosity of HAP.
8. *In vitro* study of HAP in SBF and in Tris-HCL buffer for the test of bioactivity and to study the dissolution behavior.

CHAPTER 4

4.0 EXPERIMENTAL WORK

4.1 Mineral Preparation

4.1.2 *Preparation of Calcium carbonate ($CaCO_3$) from Garden Snail Shell*

Garden snail shells (SS) were collected and their shell covering was removed carefully. Shells were washed with tap water followed by distilled water to remove the mud, sand and other impurities. The cleaned shells were dried in the direct sunlight for 2 days.

4.1.3 *Preparation of Calcium Hydroxide [$Ca(OH)_2$]*

Dry and cleaned SS were calcined at 1000^0C for 2 hours so that all organic matters and proteins escape out leaving behind Calcium Hydroxide [$Ca(OH)_2$].

$$CaCO_3 \rightarrow CaO + CO_2$$

Calcium oxide being hygroscopic in nature absorbs water from atmosphere and gets converted to Calcium Hydroxide [$Ca(OH)_2$].

4.1.3 *Preparation of Calcium Nitrate [$Ca(NO_3)_2$]*

The calcined SS were treated with requisite amount of concentrated nitric acid to convert it to $Ca(NO_3)_2$.

$$CaO + HNO_3 \rightarrow Ca(NO_3)_2 + H_2O$$

4.2 Powder Synthesis

4.2.1 Synthesis from $Ca(NO_3)_2$ and $(NH_4)_2H(PO_4)$ [Route 1]

The Calcium oxide (CaO) obtained from calcined Snail shell were converted to calcium nitrate [$Ca(NO_3)_2$] by treating with requisite amount of concentrated nitric acid followed by dilution with distilled water. The resulting solution was neutralized with liquor ammonia solution. The ammonia was added in excess to maintain a definite pH during formation of hydroxyapatite. The ammonical $Ca(NO_3)_2$ solution was added drop-wise over a period of approximately 20 – 25 minutes in a mixture containing di-ammonium hydrogen phosphate, liquor ammonia solution and distilled water. The methodology for the preparation of hydroxyapatite from Garden Snail shell is shown in Fig. 4.1.

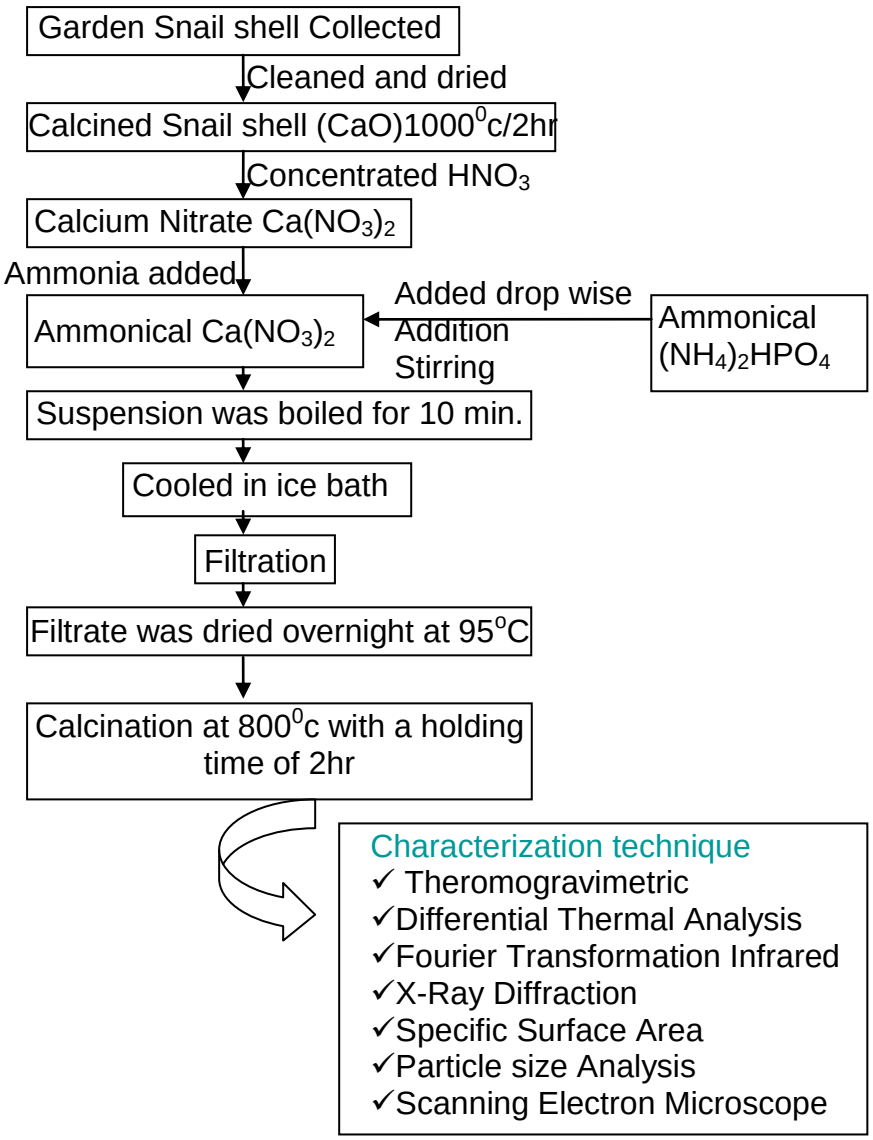

Fig. 4.1 Process Flow Chart for the Preparation of Hydroxyapatite by Route 1

The resulting suspension was boiled for 10 minutes, cooled in an ice-bath and filtered. The filter cake was then dried overnight at 95^0C. A sample of the resulting, hard, porous, brittle cake was heated in an electric kiln over a period of 115 minutes up to a final temperature of 123^0C and then cooled at room temperature to give a strong, hard translucent ceramic powder.

Chemical reaction of above method is:

$10Ca(NO_3)_2 + 6(NH_4)_2HPO_4 + 2H_2O \rightarrow Ca_{10}(PO_4)_6(OH)_2 + 12NH_4NO_3 + 8HNO_3$

4.2.2 Powder Preparation (Hydroxyapatite) from $Ca(OH)_2$ and H_3PO_4 (Route 2)

Hydroxyapatite were produced on a bench scale basic starting with requisite amount of phosphoric acid (H_3PO_4) being added to 100ml of de-ionized water to form the beginning of an acid premix. Separately calculated amount of calcium hydroxide [$Ca(OH)_2$] were added with stirring to 300 ml of de-ionized water. The phosphoric acid was then added dropwise to the stirred $Ca(OH)_2$ solution. After completing the addition, the acid premix was a clear mix with a slight yellow range and a pH of 2.1

The remainder of the stoichiometric $Ca(OH)_2$, was added with stirring to 600 ml of deionized water and the acidic premix was added drop wise to the calcium hydroxide slurry until the pH was 11. This mixture was stirred overnight and then allowed to settle for 24hours and filter. The filter cake was then dried overnight at 45^0C to obtain pure HAP. The process flow chart for the preparation of hydroxyapatite is shown in Fig. 4.2.

Chemical reaction:

$$Ca(OH)_2 + 2H_3PO_4 \rightarrow Ca(H_2PO_4)_2 + 2H_2O \text{ (acid premix) (Mixture I)}$$

$$7Ca(OH)_2 + 3Ca(H_2PO_4)_2 \rightarrow Ca_{10}(PO_4)_6(OH)_2 + 12H_2O \quad \text{(Mixture II)}$$

$$10Ca(OH)_2 + 3Ca(H_3PO_4)_2 \rightarrow Ca_{10}(PO_4)_6(OH)_2 + 18H_2O$$

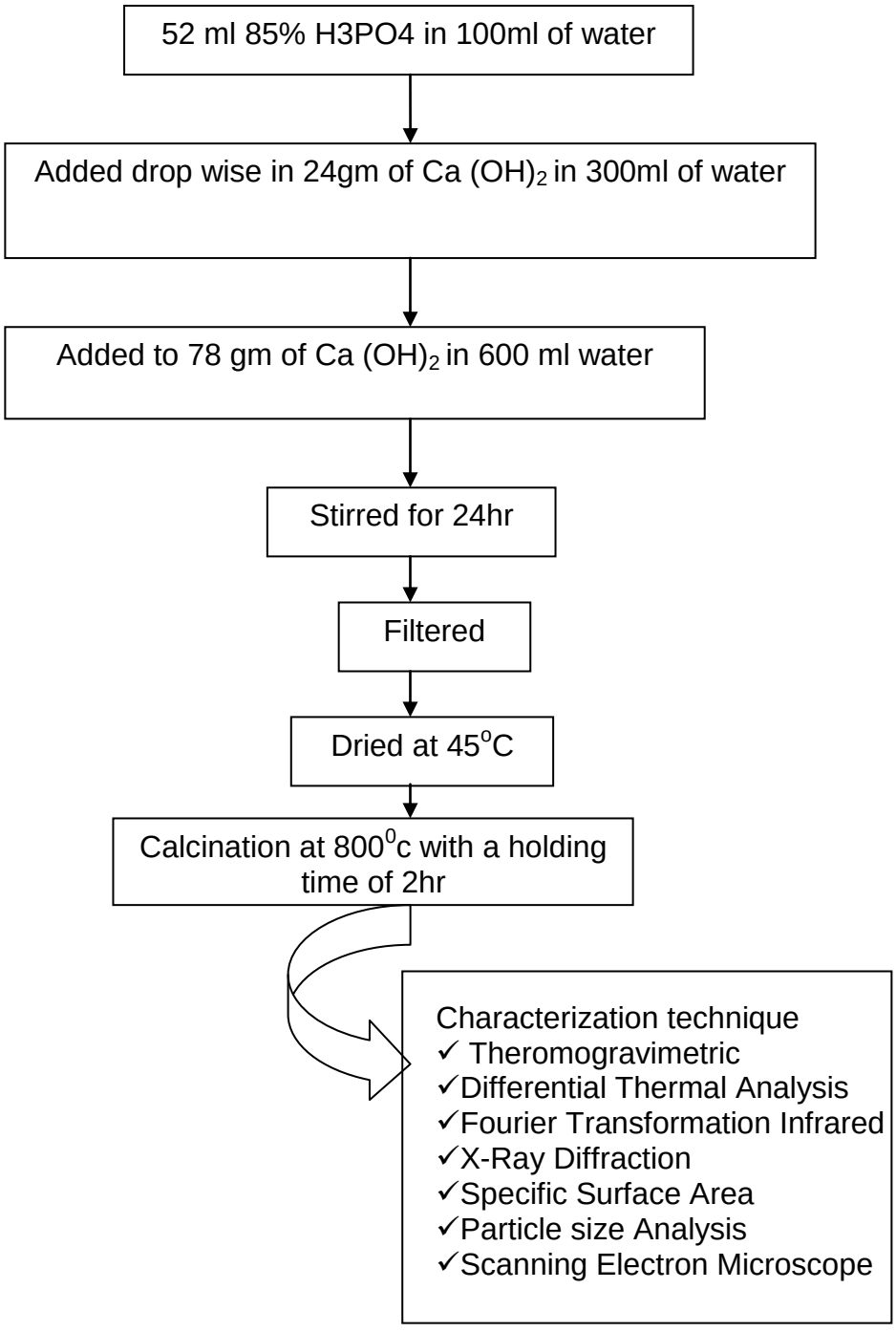

Fig. 4.2 Process Flow Chart for the Preparation of Hydroxyapatite by Route 2

4.3 Preparation of powder:

Agglomerates obtained from above two routes were grinded using mortar and pestle till we get desired fine powder. Then this powder was sieved using 50μ mesh sieve in a sieve shaker in order to get uniform size particle.

4.4 Preparation of Bone Sample

A bone sample (Femur Bone) of 60 years old lady was collected from Ispat General Hospitital, Rourkela, Orissa, India. Samples were then crushed to form a paste in mortar and pestle by the treatment with liquid nitrogen as shown in Fig. 4.3. Finally, the XRD analysis of bone sample was carried out along with the synthesized HAP powder from different routes.

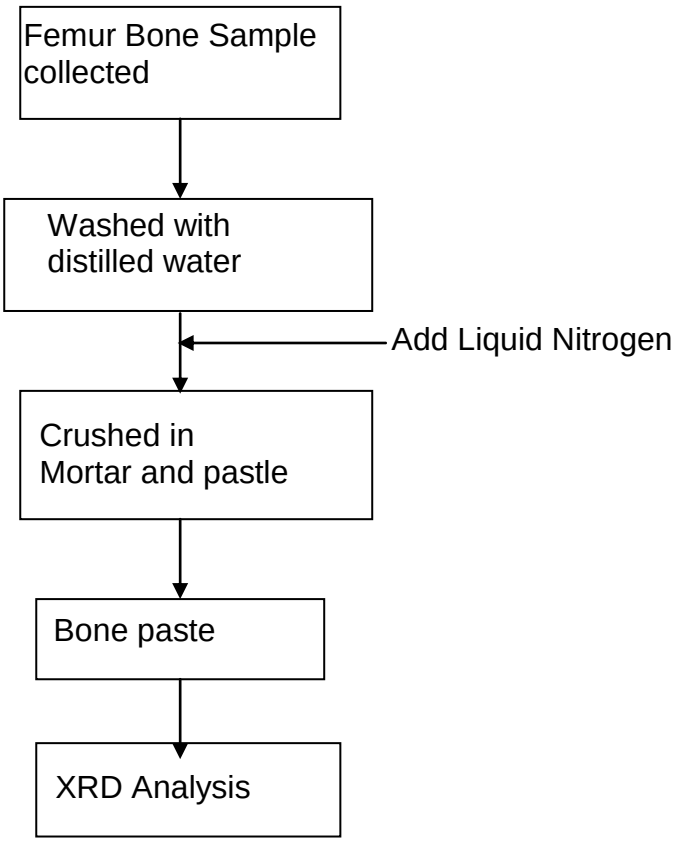

Fig. 4.3 Preparation of Bone paste

4.5 Preparation of (Synthetic Body Fluid) SBF

SBF is known to be a metastable buffer solutions [150-151]and even a small, undesired variance in both of the preparation steps and the storage temperatures, may drastically affect the phase purity and high-temperature stability of the produced HA powders, as well as the kinetics of the precipitation processes.

Merck-grade NaCl (99.5%), $NaHCO_3$ (99.5%), KCl (99.0%), $Na_2HPO_4.2H_2O$ (99.5%), $MgCl_2.6H_2O$ (99.0%), Na_2SO_4, $(CH_2OH)_3CNH_2$ (99.5%), $CaCl_2.H_2O$(99.0%) and HCl (37 vol%, Carlo-Erba, Rome, Italy) were used in the preparation of the SBF of this study.

SBF solutions [152-156] were prepared by dissolving appropriate quantities of the above chemicals in deionized water. Reagents were added, one by one after each reagent was completely dissolved in 700 ml of water, in the order given in Table 4.1. A total of 40 ml of 1 M HCl solution was consumed for pH adjustments during the preparation of 1 litre of SBF solutions. A 15 ml aliquot of this acid solution was added just before the addition of the sixth reagent, viz., $CaCl_2.2H_2O$. Otherwise, the solution would display slight turbidity. The remaining part of the HCl solution was used during subsequent titration. Following the addition of the eight reagent *tris*(hydroxymethyl) aminomethane), the solution temperature was raised from ambient to 37^0C. This solution was then titrated with 1 M HCl to a pH of 7.4 at 37^0C. During the titration process, the solution was also continuously diluted with consecutive additions of de-ionized water to make the final volume equal to 1 litre. It was observed in this study that the prepared SBF solutions can be stored at 5^0C for a month without degradation.

Table 4.1. Chemical composition of SBF solutions. ***Patent pending*****. Turkish Patent Institute, Turkey, *Appl. No.* 99-0037, 11 January 1999.**

Order	Reagent	Amount (gpl)
1	NaCl	6.547
2	$NaHCO_3$	2.268
3	KCl	0.373
4	$Na_2HPO_4.2H_2O$	0.178
5	$MgCl_2.6H_2O$	0.305
6	$CaCl_2.\ 2H_2O$	0.368
7	Na_2SO_4	0.071
8	$(CH_2OH)_3CNH_2$	6.057

4.5.1. *Synthesis of HAP powders in SBF*

$Ca(NO_3)_2.\ 4H_2O$ (99%) and $(NH_4)_2HPO_4$ (99%) solutions were used in the precipitation runs as the calcium and phosphate ion sources, respectively. NH_4OH solutions were used to adjust the pH values of the solutions when necessary. The required amounts of the starting chemicals $Ca(NO_3)_2.4H_2O$ and $(NH_4)_2HPO_4$ were first dissolved in SBF solutions contained in separate beakers at the start of precipitation experiments. As soon as both reagents were dissolved in SBF, a slight turbidity was observed in the beakers due to the immediate formation of fine precipitates, i.e., seeds. For the study of formation characteristics and phase evaluation of these fine precipitates, 23.615 g of $Ca(NO_3)_2.4H_2O$ and 5.154 g of $(NH_4)_2HPO_4$ reagents were dissolved and diluted to a total volume of 250 ml in SBF. The solutions were then left still for a day at room temperature without stirring. Thus formed and aged seeds' were removed from the mother liquors by filtration, washed two times with 100 ml of deionized water, dried in an oven at 80^0C for a day. The procedure involved the addition of pre-determined volumes of diluted NH_4OH solutions into the reaction beakers, for

pH adjustment purposes, at the beginning of the precipitation runs. These were called the *initialaddition*' experiments as described in flow diagram Fig. 4.4.

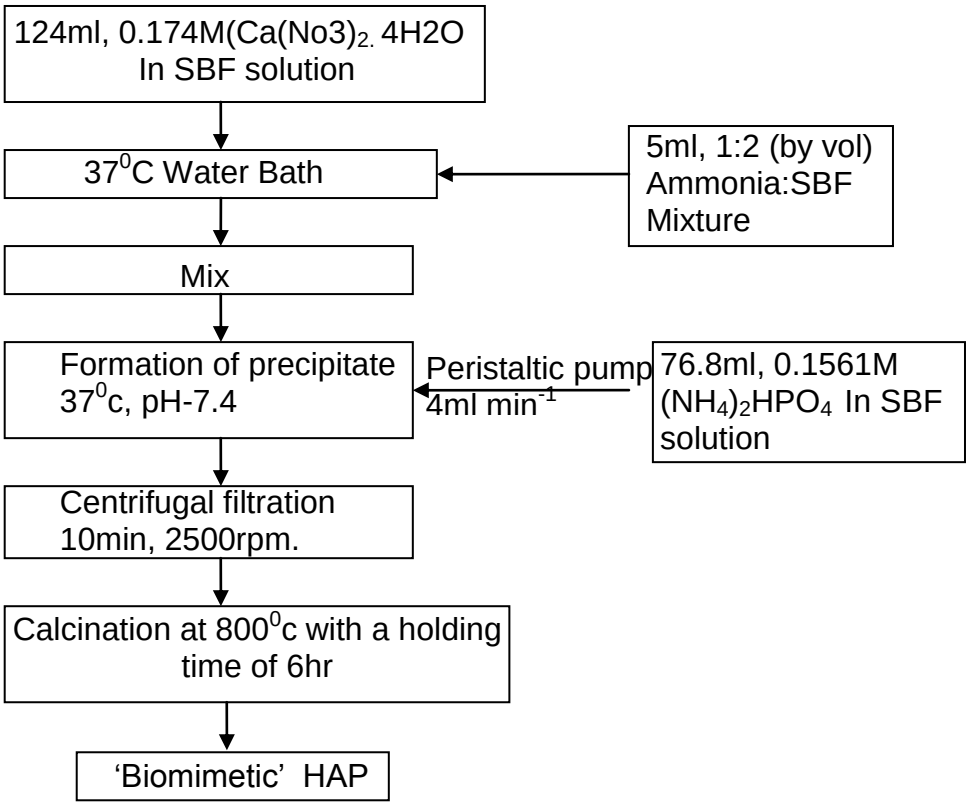

Fig. 4.4 Process flowchart for HAP synthesis in SBF by the initial addition' technique.

4.6 Sample Characterization

4.6.1. Thermal Analysis (TGA & DTA)

Differential thermal analysis (DTA) is a thermo analytic technique, similar to differential scanning calorimetry. In DTA, the material under study and an inert reference are made to undergo identical thermal cycles, while recording any temperature difference between sample and reference. This differential temperature is then plotted against time, or

against temperature (DTA curve or thermogram). Changes in the sample, either exothermic or endothermic, can be detected relative to the inert reference. Thus, a DTA curve provides data on the transformations that have occurred, such as glass transitions, crystallization, melting and sublimation. The area under a DTA peak is the enthalpy change and is not affected by the heat capacity of the sample.

Thermo Gravimetric (TG) and Differential Thermal Analysis (DTA) analyses were carried out in (NETZSCH-Geratebau GmbH Thermal Analyser) system in air with the heating rate of 10^{o}C per minute. Samples were ground to make fine powders. For TGA, sample was loaded onto an accurate balance and heated at a controlled rate, to record the weight loss at different temperatures. When a material undergoes physical or chemical change it absorbs or releases thermal energy which is a characteristic of the range. The temperature difference of a sample with respect to a reference inert material (α-Al_2O_3) during heating or cooling is shown in DTA as the deviation from zero base line. Exothermic or endothermic changes are shown in opposite directions of the baseline.

4.6.2. Fourier Transformed Infrared (FTIR) Analysis

The term Fourier transform infrared spectroscopy (FTIR) originates from the fact that a Fourier transform (a mathematical algorithm) is required to convert the raw data into the actual spectrum. FTIR is a technique which is used to obtain an infrared spectrum of absorption, emission, photoconductivity or Raman scattering of a solid, liquid or gas. Fig. 4.5 represents a typical apparatus of Fourier Transform Infra Red (FTIR) spectroscopy.

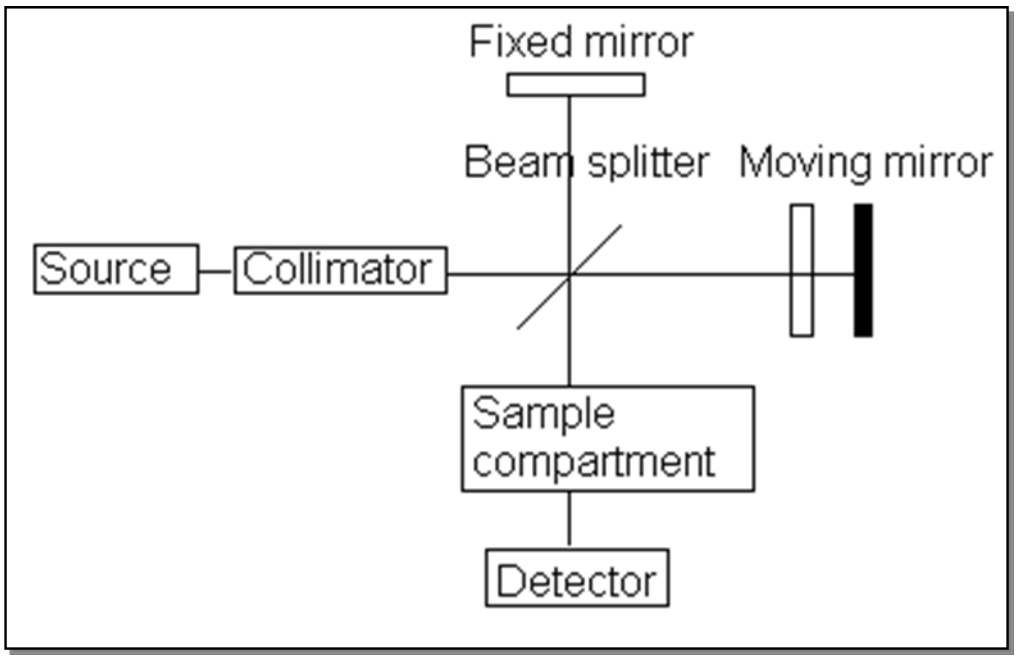

Fig. 4.5 Typical apparatus Fourier transform infrared (FTIR) spectroscopy

FTIR analysis of calcined HAP was done by using KBr pallet method. Calcined HAP powder was taken and a homogenous mixture of sample and KBr was made in the ratio of 1:50 by grinding in a mortar and pestle. This was done to remove scattering effect from large crystals. The pallet was made from this homogeneous mixture using hydraulic press by applying a pressure of 1.5 ton for 2 minutes to make a translucent pellet through which spectrometer can pass easily. Then the pellet was placed in pallet holder and the analysis was carried out and the spectrogram of the sample was observed on a video monitor. Finally, the graphic representation of the spectra was taken.

4.6.3. Phase Analysis by X-Ray Diffractometer

X- ray diffraction techniques are based on observing the scattered intensity of an X-ray beam hitting a sample as a function of incident and scattered angle, polarization, and wavelength or energy. Fig. 4.6 represents schematic of X-ray powder diffraction.

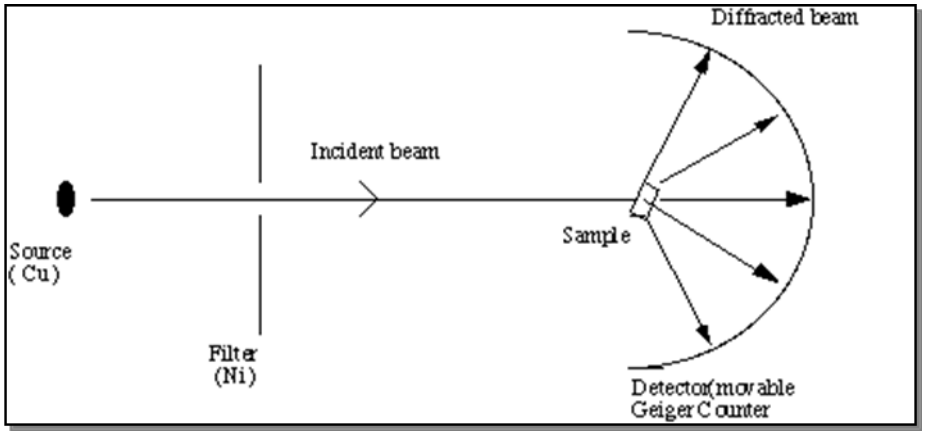

Fig. 4.6 Schematic of an X-ray powder diffractometer

A powdered mineral sample is packed on a sample stage so that it can be irradiated by the X-ray tube. To detect the diffracted X-rays, an electronic detector is placed on the other side of the sample from the X-ray tube, and allowed rotate the sample to produce angles from 0 to 90^{o}. The instrument used to rotate both the X-ray tube and the detector is called a goniometer. The goniometer keeps track of the angle θ, and the detector records the rate of X-rays coming out of the other side of the sample (in units of counts/sec) and sends this information to the computer. The identification of different phases is carried out by powder X-ray diffraction study. For the phase analysis of dried gel and calcined powder, X-ray data were collected using a fully automated Philips X-pert system (PHILIPS PW1830) with Cu-Kα radiation. The voltage and current were set at 35 kV and 30mA respectively with the copper target, with a step size of 0.020 (2θ) and a count time of 1s per step. After scan of the sample, the X-ray intensity (counts/sec) was plotted against the angle theta (θ).

4.6.4. Particle Size Distribution

The particle size distribution (PSD) of a powder, or granular material, or particles dispersed in fluid, is a list of values or a mathematical function that defines the relative amounts of particles present, sorted according to size. The stability, chemical reactivity,

opacity, flow ability and material strength of many materials are affected by the size and characteristics of the particles within them. There are many particle size and size distribution analysis technologies. The most common ones are laser diffraction for sizing particles from submicron to millimeter in size, Counter Principle for sizing and counting particles from micron to millimeter in size, and dynamic light scattering for sizing submicron and nanometer particles.

A laser diffraction method with a multiple scattering technique was used to determine the particle size distribution of calcined powder. The particles size distribution (volume percent) of the suspension was carried out in computer-controlled particle size analyzer (Malvern, Mastersizer 2000, UK) via a software program. The powders must not be agglomerated and completely dispersed in the liquid so that they are separated into discrete unattached particles. A well-dispersed and agglomerate-free suspension was obtained using Ultrasonic treatment (Sidilu Ultrasonics, India). Powdered samples were used to be well dispersed in a liquid medium of known density and viscosity.

4.6.5. Surface Area

Specific surface area of ultrafine submicron ceramic powder is an important objective to predict the green compaction and sintering characteristics. This can be measured by a common BET method. The BET method (Brunauer, Emmet and Teller after the developers of the basic calculations) involves adsorbing a monolayer of liquid nitrogen onto the surface of particles, then measuring the amount of nitrogen that is released when that monolayer is vaporized. Based on this nitrogen quantity, the surface area of the sample can be calculated from the BET equation:

$$\frac{1}{V}\left(\frac{x}{1-x}\right) = \frac{c-1}{cVm}x + \frac{1}{cVm}$$

V = volume of gas adsorbed, Vm = volume of gas adsorbed at monolayer coverage, X = P/Po, P = Ambient Pressure, Po = total pressure, C, a constant that is related to the heat of adsorption. A plot of (1/V)(x/(1-x)) versus x gives a straight line with slope = m= (c-1)/(cVm), Intercept = b= 1/cVm, The value of Vm and c are worked out, Vm = 1/(slope + intercept). This is normalized by the mass of particles tested to give a specific surface area (m2/gm) Specific surface area of HAP powders was determined by the surface area Coulter SA 3100 BET. Surface area was determined as per BET method. About 2-3 gm of sample was taken in the sample cell and degassed at 110^{o}C in vacuum up to a maximum of 3mbar. The sample holder mouth was closed by a stopper. Sample was cooled and the cell was placed in liquid nitrogen bath. The equipment measured the amount of gas adsorbed on the surface of the sample and calculated the specific surface area.

4.7 Fabrication of Green Discs

The synthesized HAP dried powder was calcined at 800^{0}C for 2 hrs [157]. After being calcined HAP powder were consolidated by uniaxial pressing in high carbon steel mould in a hydraulic press with a capacity of 2.5 tons for 1 minutes using 15 mm cylidndrical dye. Every time before loading sample into it, they were cleaned with acetone and stearic acid. Subsequently, uniaxially pressed samples were placed in rubber moulds, followed by vacuum suction to remove air. Sealed rubber moulds were placed inside the cylindrical chamber of isostatic press (laboratory model) in a fluid bath consisting of oil-water mixture. All samples were isoststically pressed at 750 MPa for 2 minutes. Green densities were measured through weight/volume data. The green samples and the sintered samples were used to measure the volume shrinkage (%) taking place. Weight was measured from electronic balance, whereas

volume was calculated from the dimension of the specimens. The final volume shrinkage was calculated by using formulae:

$$\text{Volume shrinkage (\%)} = \frac{V_1}{V_2} \times 100$$

Where V_1= Difference between initial volume and final volume shrinkage of the sample

And V_2= Initial volume

4.8 Processing of porous HAP by Dry mixing method:

Porous hydroxyapatite was prepared by the following methods using Naphthalene as porogen. The process outline for each of the two pore former has been outlined:

4.8.1 Porous HAP using Naphthalene as pore former:

Naphthalene (Aldrich chemical co.) was used as a porogen for the development and control of porosity in HAP. The naphthalene balls were grinded by mortar and pastel to give the shape of powder. The powder material was sieved in sieve shaker (Mesh size 50µ) and particle in the size of 50µ were selected. Weighed amount of calcined HAP powder was dry mixed well with naphthalene powder (Naphthalene 0, 5, 10, 20, 30, 40, 50 weight %) in high-density polythene bottle for 24 hours containing high purity zirconia balls as shown in Table 4.2

Table 4.2. Batch Composition of Green specimen

Batch	Identification	Calcined HAP Powder (800^0C/2Hours)	Napthalene(N) as Pore Former
1	H	100 wt % of HAP	0 wt % Napthalene
2	HAN	95 wt % of HAP	5 wt % Napthalene
3	HBN	90 wt % of HAP	10 wt % Napthalene
4	HCN	80 wt % of HAP	20 wt % Napthalene
5	HDN	70 wt % of HAP	30 wt % Napthalene
6	HEN	60 wt % of HAP	40 wt % Napthalene
7	HFN	50 wt % of HAP	50 wt % Napthalene

The synthesized powder of each batch was thoroughly mixed with its corresponding naphthalene and was processed as per the flow sheet Fig. 4.7. The mixed powders were consolidated by uniaxial pressing in high carbon steel mould in a hydraulic press with a capacity of 750MPa. The dry powder was pressed in a cylindrical die (diameter 12.0 mm). The green pellets were sintered at 1250^0C for 4 hours at a heating rate of 3^0C per minute. The sintered pellet was characterized as mentioned above. The flow chart for the processing of porous HA scaffold using naphthalene is shown below:

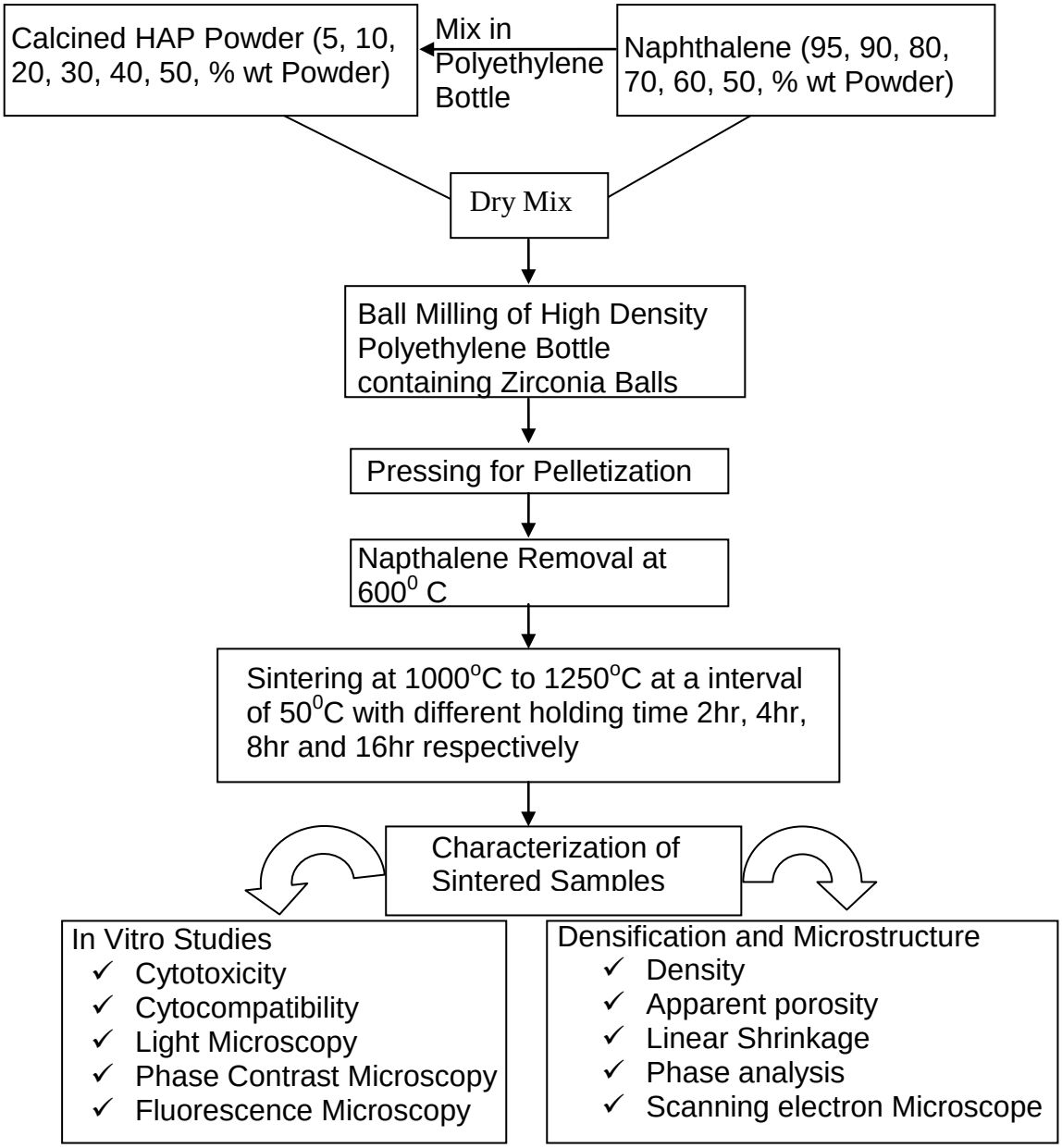

Fig.4.8 Flow Chart for Processing of Porous HAP by Dry mixing method and its Characterization techniques

4.9 Sintering

Understanding the sintering behavior of hydroxyapatite powders is important, because this allows designing ceramics with controlled grain growth, microstructure and mechanical properties. In the present thesis, the effect of powder characteristics on densification, micro structural development and mechanical properties of HAP compacts were studied.

The pellets were sintered in an electrical furnace (Nabertherm Super Kanthal, Germany) Molybdenum disilicide ($MoSi_2$) heating elements and alumina insulation boards as chamber walls (size of the chamber 250x150x150mm). The thermal regime of the furnace was controlled through a programmer cum- controller of 'Eurotherm' within 2^0C. The sintering temperature was varied from 1000^0C to 1250^oC with an interval of 50^0C at a heating rate 3- 4^0C/minute and different soaking times for 2hour, 4hour, 8 hour and 16 hour respectively. The main problem of sintering is cracking. Previous literature shows that HAP calcined at 800^0C [157] will give good results, but again the problem will appear during powder compaction. Some binder is needed to improve the green strength but the use of binder hampers the quality of sintered product.

4.9.1 Apparent Porosity and Bulk Density

The apparent porosity and bulk density of the sintered samples were measured using Archimedes's principle. Firstly dry weight of the sintered sample was taken in an electronic balance. The samples were then dipped inside kerosene and kept under a vacuum for two hours to ensure that kerosene filled up the open pores completely and had removed all the air present inside the pores of the sintered pellets. Then, soaked (in kerosene) and suspended weights were measured. Then applying formula Bulk density and apparent porosity was measured.

$$\text{Bulk Density} = \frac{\text{Dry weight}}{\text{Soaked weight} - \text{Suspended weight}} \quad \text{(without the effect of open pores)}$$

$$\text{\% Apparent Porosity} = \frac{\text{Soaked weight} - \text{Dry weight}}{\text{Soaked weight} - \text{Suspended weight}}$$

$$\text{\% Relative Density} = \frac{\text{Bulk density x 100}}{\text{Theoretical density}}$$

4.10 Microstructure and Phase Analysis

4.10.1. Scanning Electron Microscope (SEM)

The scanning electron microscope (SEM) is a type of electron microscope that images the sample surface by scanning it with a high-energy beam of electrons in a raster scan pattern. The electrons interact with the atoms that make up the sample producing signals that contain information about the sample's surface topography, composition and other properties such as electrical conductivity.

Phase assemblage of the materials was analyzed through a Scanning Electron Microscope (SEM). An SEM was used to study the micro structural feature of samples as it had a much higher resolution power compared to an optical microscope. In SEM, a hot tungsten filament electron gun under vacuum emits electrons which pass through a series of electromagnetic lenses. The sample is then bombarded with a fine beam of electrons having acceleration potentials range from 1-30 KV. A part of the beam is reflected as back scattered electrons (BSE) along with low energy secondary electron emission (SE), cathode luminescence, x-ray excitation beam and electron transmission also take place. Images formed from the (SE) beam were studied in the extrinsic mode of SEM. While the images appeared very real as if they are photographed by ordinary means, the apparent illumination was a function of particle emission rather than radiation. The emitted secondary electrons are detected and displayed on a scanning TV display. A bright image will be the result of high secondary electron emission, while the primary influence on high emission is the surface structure of the specimen. The end result is therefore brightness associated with surface characteristics and an image which looks very much like a normally illuminated subject.

SEM micrograph of sample was obtained by JEOL JSM-6480LV. The samples were coated with platinum for 1 minute and a current of 10mA was applied before the SEM micrograph was obtained.

4.11 In vitro Studies (Test for Biocompatibility)

The *in vitro* bioactive evaluation of synthesized Hydroxyapatite powder was performed in SBF media of pH 7.40 at a ratio of 1mg/ml in a water bath at 37^{O}C. HAP pellet sintered at 1200^{O}C was taken as the starting material for our study. The important factor during the preparation is to observe that the pH of SBF should be around 7.40 and the ionic concentration of SBF should be equal to that of blood plasma. The change in pH of SBF was measured at predetermined intervals with the help of pH meter.

4.11.1 Surface characterization of HAP

The surface morphology and structure of HAP before and after soaking period in SBF was observed by Scanning electron microscopy study JEOL JSM-6480LV at 15mA. The chances of contamination are more while transfer of HAP soaked in synthetic body fluid to Scanning electron microscopy analysis. So care must be taken and it should be handled very carefully because a minute contamination in the sample may lead to drastic result.

4.11.2 *In-vitro* Biodegradation:

The *in vitro* degradability of the porous HAP was determined by their weight loss percentage in a Tris-HCL buffer solution. The Tris-HCL buffer solution was prepared by dissolving 0.1MTris- HCl solution in distilled water. The pH of solution was maintained 7.4 at 37^{0}c by adding 1MHCl. Porous HAP with naphthalene (5-50 wt %) in the form of pellets were soaked in 24 days in polystyrene bottles containing Tris-HCl buffer solution in a water bath

shaker. At each time the samples were taken out rinsed with distilled water and dried in oven at 150^0c. Finally, weight loss of sample was determined by the formulae as given below:

$$\% \text{ Weight Loss} = \boxed{\frac{W_1 - W_2}{W_2} \times 100}$$

Where, W_1 = initial weight of sample before soaking in Tris-HCL solution.

W_2 = final weight of sample after soaking in Tris-HCl solution.

CHAPTER 5

5.0 RESULTS AND DISCUSSION

5.1 Synthesis, Characterization and Development of Porous Hydroxyapatite and study of its Biocompatibility.

In the present work a novel attempt is made to convert the calcium carbonate skeleton of widely available garden snail shell to Hydroxyapatite based bioceramics. The porosity was well controlled by the help of porogen as Napthalene with varying concentration as shown in Table 4.2. The synthesized powder in the form of pallets was soaked in stimulated body fluid (SBF) medium for various periods of time in order to evaluate its bioactivity. The changes of the pH of SBF medium were measured. High bioactivity of prepared HAP powder due to the formation of apatite on its surface was observed.

5.1.1 Powder Synthesis:

Hydroxyapatite was prepared by Chemical Precipitation Method[158] as shown in Fig. 4.1. The prepared HAP powder was calcined to a temperature 800^0C for 2 Hours. The different characterization techniques were adopted both for calcined snail shell and HAP synthesized like X-ray Diffraction (XRD) and Thermal Analysis (DTA/TGA). Finally, particle characteristics of synthesized HAP powder were carried out by BET surface area analyzer, Particle size analyzer and Transmission Electron Microscopy.

The weight loss and thermal stability of the samples were evaluated from the thermo gravimetric analysis data.

5.1.2 DTA/TGA of snail shell (SS)

Fig. 5.1.2 differential and thermo-gravimetric analysis (DTA/TGA) analysis of Snail Shell showed the weight loss at temperature between 90^0C – 120^0C that is due to the physically adsorbed water. Over a wide range of temperature from 250^0C – 400^0C the weight loss is due to the decomposition of $MgCO_3$ combined with the combustion of hydrocarbons. The weight loss along with endothermic peak at 750^0C - 850^0C indicates the decomposition of $CaCO_3$ following the reaction.

$$CaCO_3 \longrightarrow CaO + CO_2\uparrow$$

The change of phase from $CaCO_3$ to $Ca(OH)_2$ at a temp 750 – 850^0C is confirmed from the XRD analysis Fig. 5.1.8.1 and Fig. 5.1.8.2. So it is confirmed from the thermal analysis that Snail Shell mainly contains $CaCO_3$ along with small amount of $MgCO_3$ and other organic matters.

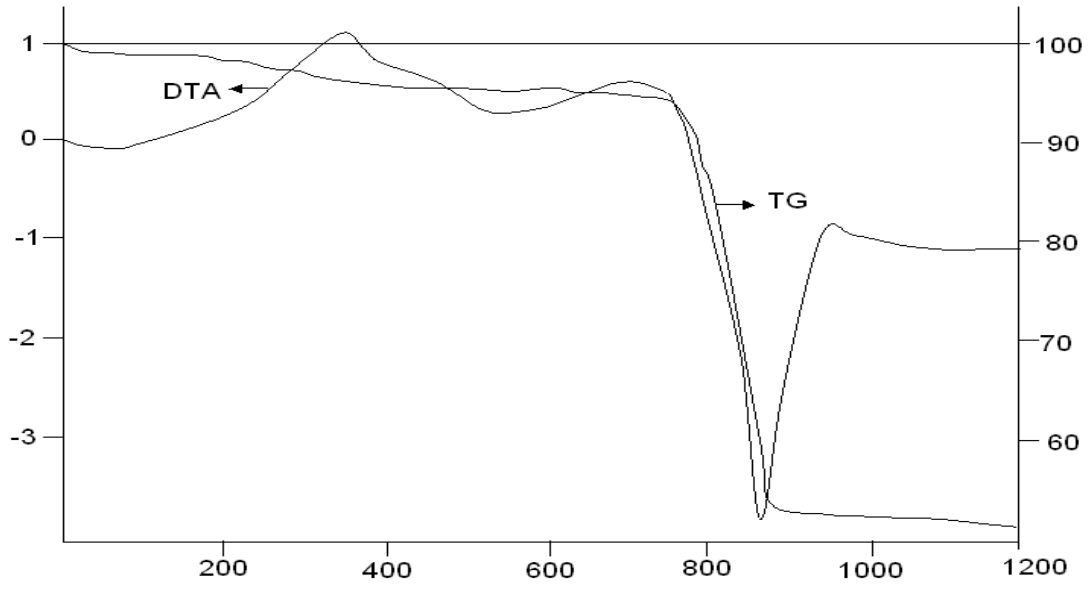

Fig. 5.1.2 shows the TGA/DTA analysis of as dried Snail shell

5.1.3 DTA/TGA of Synthesized HAP powder

The DTA/TG analysis of the HAP powder was carried out from room temperature to 1200^{o}C in order to understand the phase transformation being taking place. Fig. 5.1.3 showed the weight loss at the beginning of TG plot from 40^{0}C to 200^{0}C that is due to the physically adsorbed water. There is around 11% loss of weight associated with it. It indicates that a lot of moisture has been adsorbed. Adsorbed water is removed from the surface at temperature below 200^{o}C. The weight loss is also between 300^{0}C to 800^{0}C is due decomposition of HPO_4^{2-} in HAP as shown in the reaction:

$$2HPO_4^{2-} \longrightarrow P_2O_7^{4-} + H_2O$$

$$P_2O_7^{4-} + 2OH^- \longrightarrow 2PO_4^{3-} + H_2O$$

The weight loss is also confirmed with sharp peaks in the DTA plot at temperature 200^{0}C and 500^{0}C to 550^{0}C. The peak around 200^{0}C is due the thermal dissociation of hydroxyl group and temperature between 500^{o}C -550^{0}C was most probably associated with the crystalline of HAP from the amorphous phase. This fact is also confirmed by XRD studied Fig 5.1.3 where crystalline peaks started appearing at 500^{0}C. So the exothermic peak at 500^{0}C and 550^{0}C has been associated with crystallization of hydroxyapatite.

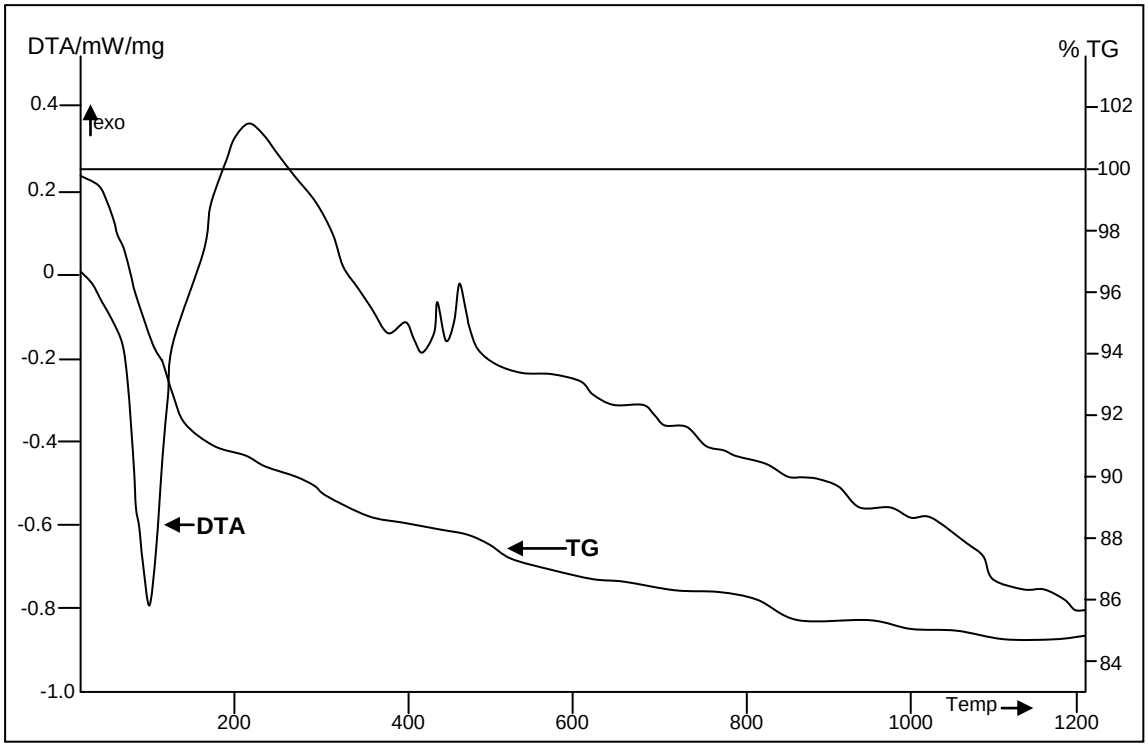

Fig. 5.1.3. DTA/TGA of Synthesized HAP powder

5.1.4 FTIR Analysis

Infrared characterization was carried out for the sample to study the spectral characteristics indicative of the chemical bonding in the synthesized HAP powder. The spectrum Fig. 5.1.3 can be divided into four regions with peaks having wave numbers around 3500, 1420, 1100 and 600cm^{-1}. The peak observed around 3431.8cm^{-1} is due to the presence of –OH bond [159]. This peak is mainly due to O-H stretching vibration in HAP[160]. The peak at 1036.2 cm^{-1} is associated with the stretching modes of the P-O bonds of HAP[160, 163]. The double peak at 603.1 cm^{-1} and 567.4cm^{-1} are due to bending modes of P-O bonds in phosphate groups [161]. Thus, the presence of PO_4^{3-} - group in HAP is almost confirm from IR studies. The pH of the medium during synthesis of HAP was maintained using ammonium solution and it was removed from the suspension with repeated washing with distilled water. In spite of all efforts to remove ammonia from the solution, there is a possibility of small amount of it in the

HAP powder. The IR analysis shows a small broad peak at 1422.6cm^{-1}; which is characteristics peak of NH_4^+- group[162-164].

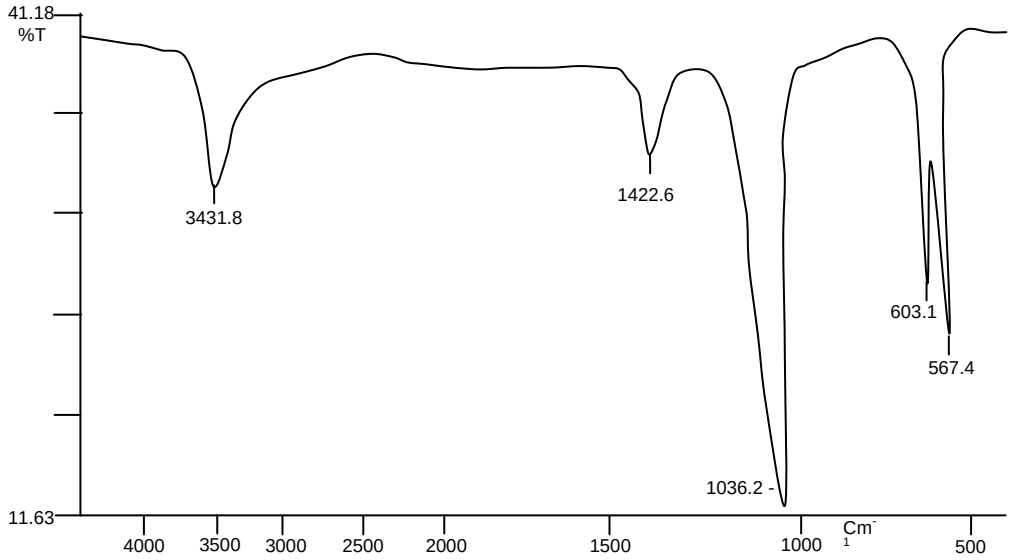

Fig. 5.1.4 FTIR spectrum of HAP powder

5.1.5 Particle size analysis:

Particle size analysis of HAP powder was carried out following Laser technique and pattern of particle size distribution is plotted in Fig. 5.1.5 Average particle size was found to be 2.63 μm. Small amount of fine particles (0.2-0.3 μm) are also present in the synthesized powder.

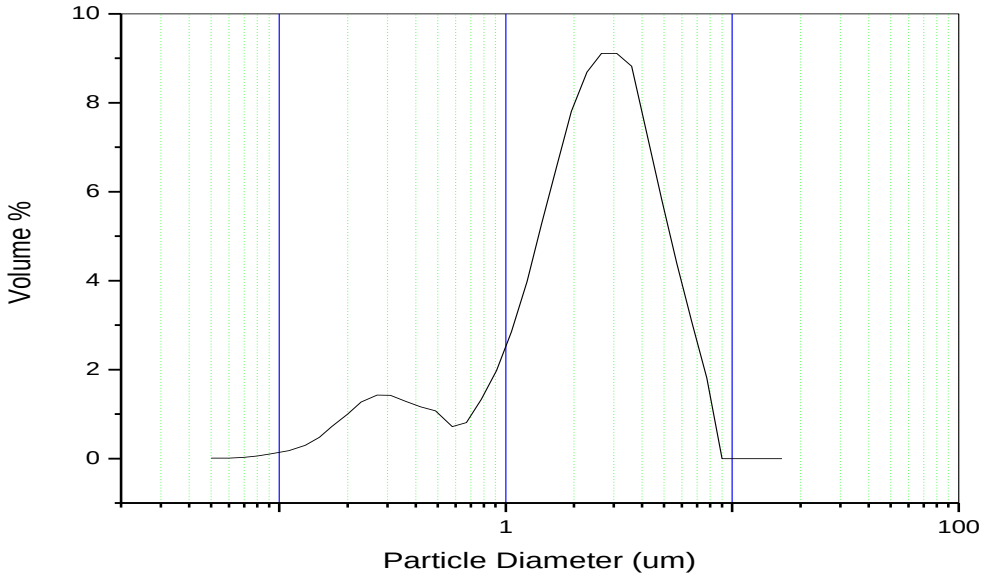

Figure 5.1.5 Particle Size Analysis of HAP powder

5.1. 6 Surface Area Measurement:

The surface area of the synthesized hydroxyapatite powder and calcined HAP is determined to be ~76m^2/gm and ~20m^2/gm respectively. Powders are agglomerated during calcinations; but HAP powders have to be calcined to remove volatile impurities like ammonia.

5.1.7 Scanning Electron Microscope (SEM):

The morphologies of as synthesized and calcined HAP powders are shown in Fig. 5.1.7 Uncalcined HAP powders are almost regular and round in shape Fig. 5.1.7 (a); whereas calcined HAP powders are agglomerated Fig. 5.7.1 (b). Thus, SEM micrograph of the calcined powder confirmed the presence of soft agglomerates that break up easily during compaction. The microstructure as reveals from SEM is in well- agreement with the particle size analysis and BET surface area analyzer results.

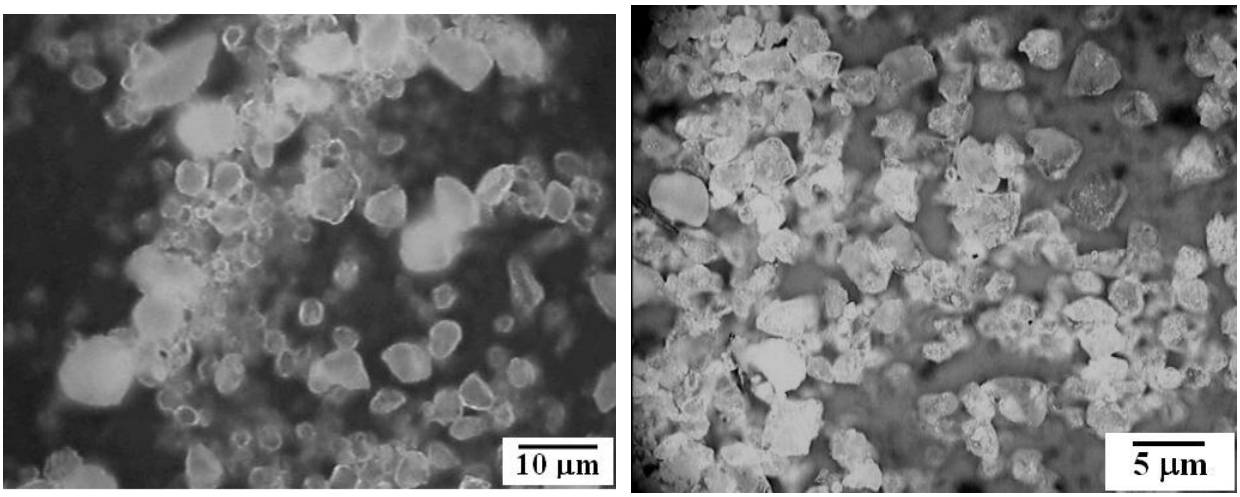

Fig.5.1.7 SEM Micrograph of (a) Synthesized HAP powder (b) Calcined (850^{o}C/2h) HAP powder

5.1.8 XRD Analysis

A typical XRD profile of Snail Shell and calcined Snail Shell has been shown in Fig.5.1.8. The raw SS showed the presence of $CaCO_3$ phase, where as CaO was detected in the calcined Snail shell. The appearance of calcined SS was soft, porous and white in colour. However, due to delay in recording some amount of CaO was converted to $Ca(OH)_2$ by adsorbing moisture from the atmosphere which is depicted in Fig. 5.1.8.

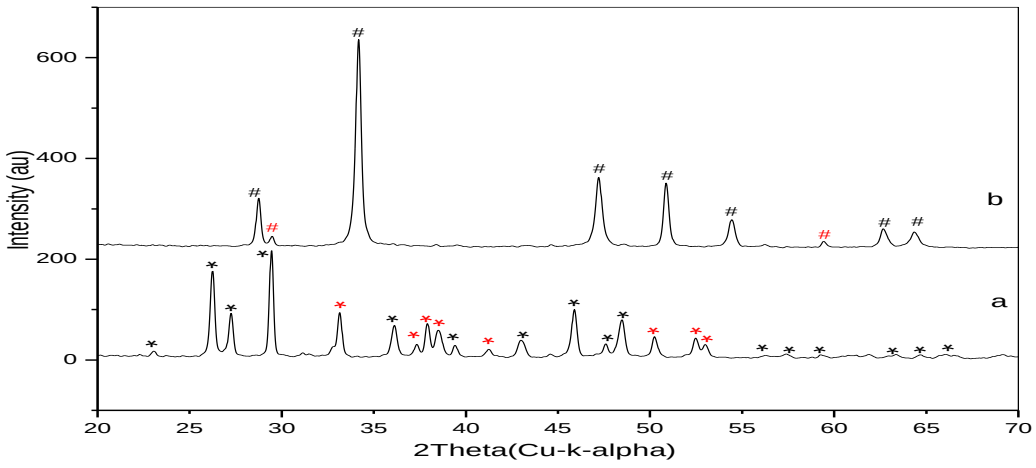

Fig. 5.1.8 XRD patterns of (a), Snail shell; (b), Calcined snail shell at 1000^{0}C/2Hr. The abbreviation for the phase * represents $CaCO_3$ peaks and # represents CaO.

Fig. 5.1.8.1 shows the composite XRD graphs of calcined powder from 400^0C to 625^0C where as Fig. 5.1.8.2 shows the next set of XRD pattern of calcined powder from 650^0C to 1000^0C. The patterns shows the presence of both $CaCO_3$ and $Ca(OH)_2$. But at higher temperature, peaks corresponding to $CaCO_3$ gradually diminish and $Ca(OH)_2$ peaks appear. At around 850^oC $CaCO_3$ decomposes to CaO. The thermal analysis DTA/TGA analysis of Snail Shell is also supporting the decomposition of $CaCO_3$ to CaO at this temperature as shown in Fig. 5.1. But due to the presence of moisture in the atmosphere this CaO reacts with water and gets transformed into $Ca(OH)_2$.[165].

$$\mathbf{CaCO_3 \longrightarrow CaO + CO_2 \uparrow}$$

$$\mathbf{CaO + H_2O \rightarrow Ca(OH)_2}$$

So instead of CaO peak, we get $Ca(OH)_2$ peak.

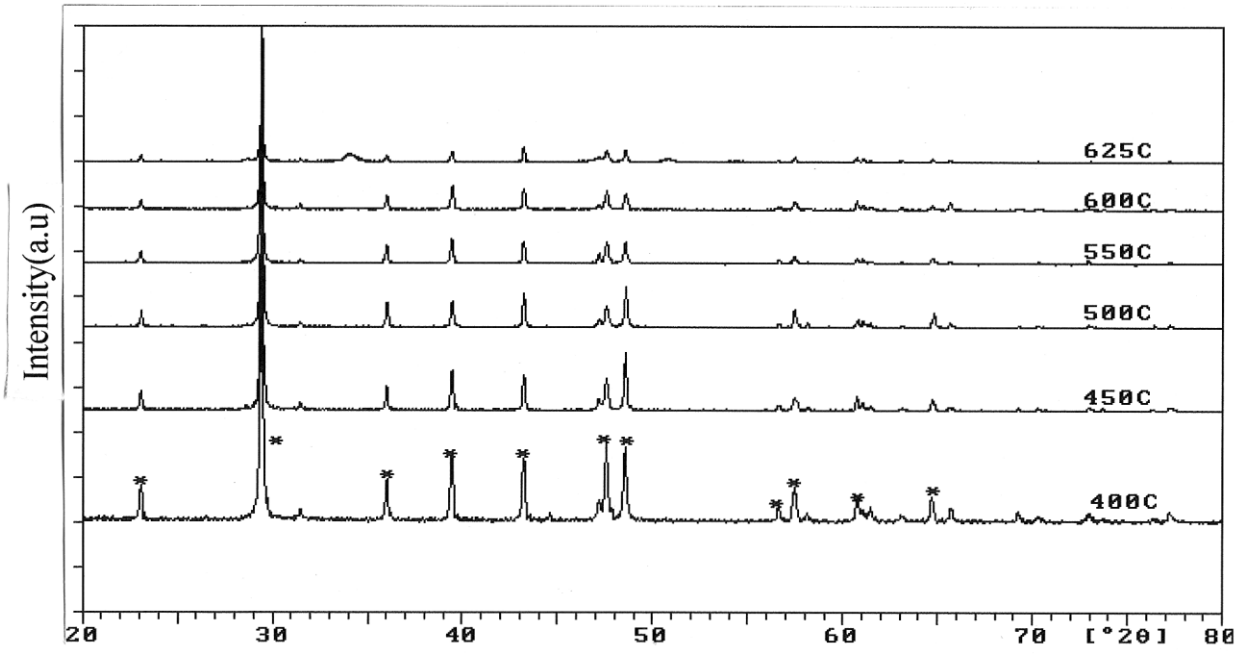

Fig. 5.1.8.1. Composite X-ray treatment of calcined eggshells at temperature between 400^OC to 625^OC. The abbreviation for the phase * represents $CaCO_3$ peaks.

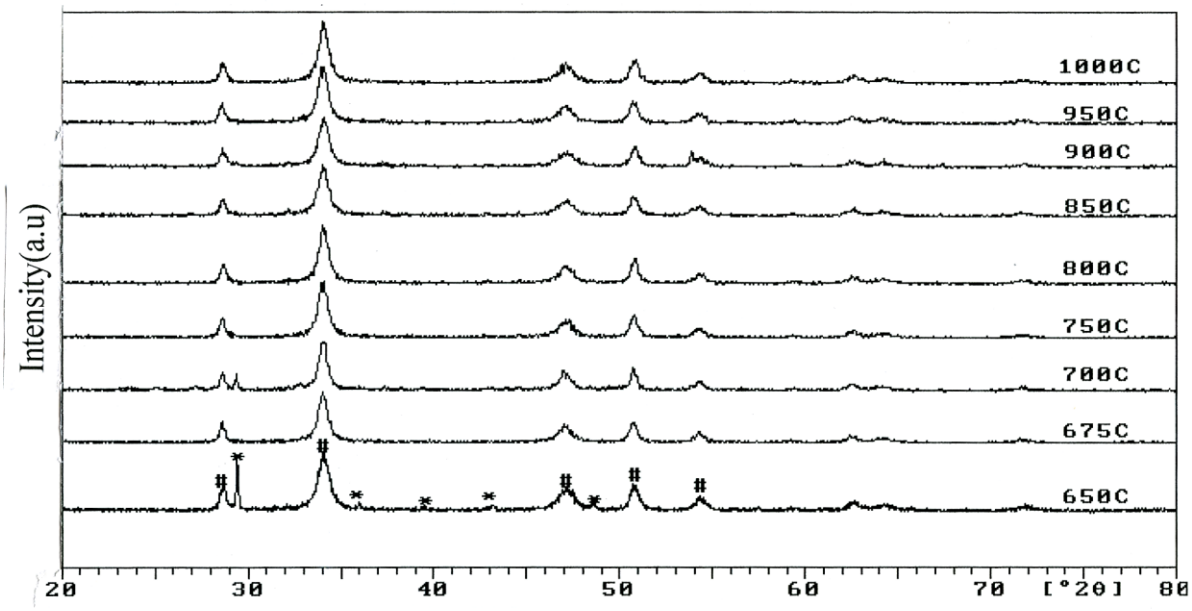

Fig. 5.1.8.2 Composite X-ray treatment of calcined eggshells at temperature between 650^0C to 1000^0C. The abbreviation for the phases: * represents $CaCO_3$ peaks, # represents $Ca(OH)_2$ peaks.

X-ray analysis of synthesized HAP showed that there was an absence of other calcium phosphate or other undesirable phases, such as tri-calcium phosphate (TCP) or calcium oxide (CaO). The XRD phase analysis of HAP powder has been shown in Fig.5.1.8.3. Three-high-intensity peaks located at $2\theta = 31.7^0$, 32.2°and 32.9°with Cu-Kα radiation are difficult to be exactly recognized from their diffraction patterns. An XRD pattern reveals the formation of HAP and is well resembled with the standard JCPDS card number 09-0432. The unindexed peak at 30.75^0 in Fig. 5.1.8.3 may be due to β-tricalcium phosphate; which indicates the initiation of conversion of HAP to β-tricalcium phosphate on heating HAP above 800^0C. The calcined HAP exhibits well crystallized sharp peaks of characteristics HAP. The HAP powders, thus synthesized from Snail Shell precursor, are very pure and chemical analysis of powders confirms the same observation.

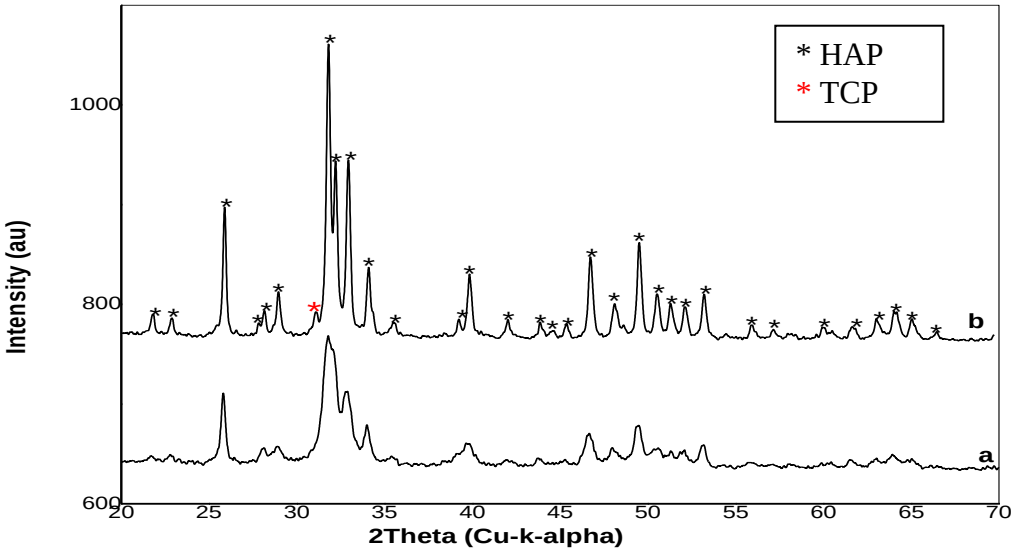

Fig. 5.1.8.3 XRD Pattern of: (a), HAP (synthesized); (b) Calcined HAP (synthesized) 800^0C/2Hr

The XRD analyses of HAP synthesized from different routes namely Route 1 and Route 2 is shown in Fig.5.1.8.4. HAP synthesized from two different routes namely Route 1 and route 2 by chemical precipitation method is shown in Fig. 4.1 and Fig. 4.2 respectively. The phase purity of synthesized HAP powder was analyzed. It was found that there was no change in purity in HAP powder synthesized from two different routes and all the peaks corresponds to JCPDS card number 09-432. X -ray analysis showed that there was an absence of other calcium phosphate or undesirable phases, such as tricalcium phosphate (TCP) or calcium oxide (CaO). The XRD result is in agreement with the FTIR result which revealed no other phases such as calcium carbonate or calcium oxide present in synthesized HAP powder. The source powder exhibit a low degree of crystallinity, which is known to be a typical characteristic of calcium phosphate being synthesized by chemical precipitation method. [166, 167]

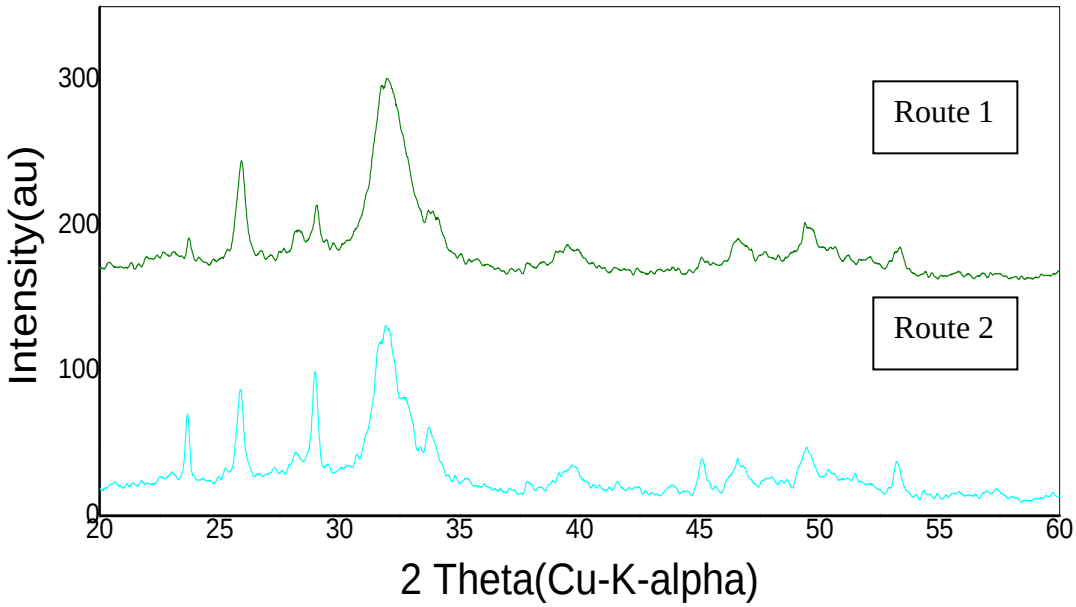

Fig. 5.1.8.4 XRD pattern of HAP synthesized from Route 1 and Route 2.

Bone sample was isolated as shown in Fig. 4.3. XRD analysis of bone samples along with the HAP synthesized by chemical precipitation method (Route 1) was carried out Fig. 5.1.8.5. It is well known that the composition of human bone is an inorganic/organic hybrid consisting of ~ 70% apatitic calcium phospthate and 30% organic (largely collagen) constituents by weight [168]. The submicroscopic crystal of calcium phosphate in bone resembles the crystal structure of synthetic Hydroxyapatite [HAP, $Ca_{10}(PO_4)_6(OH)_2$][169] . The important characteristics of HAP peaks is the formation of three-high-intensity peaks located at $2\theta = 31.7^0$, 32.2°and 32.9° which is depicted in Fig. 5.1.8.5.

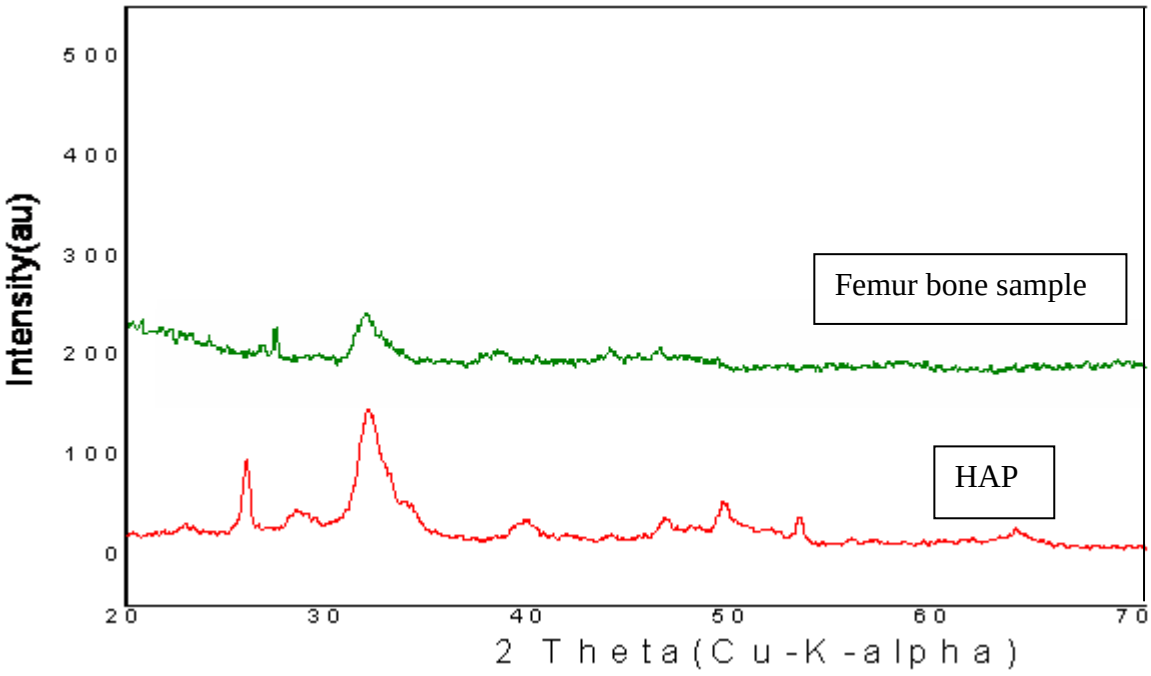

Fig. 5.1.8.5. XRD analysis of HAP and Femur bone sample.

Figure 5.1.8.6 depicts the XRD pattern of synthesized HAP by chemical precipitation method and HAP synthesized in Synthetic Body fluid (SBF). HAP was synthesized in SBF as shown in Fig. 4.4 by 'initial addition technique'. The strongest peaks in the XRD pattern were characteristics of pure HAP and closely matched with the JCPDS card No. 09-432 of calcium Hydroxyapatite. The XRD pattern clearly indicates the absence of β - TCP phase.

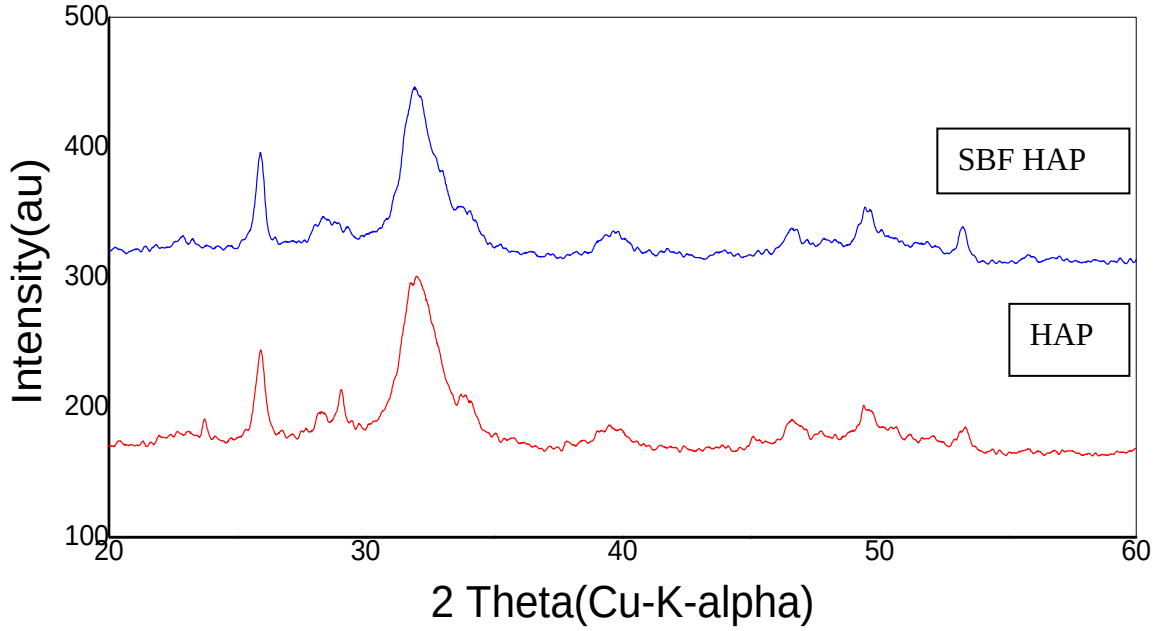

Fig. 5.1.8.6. XRD Analysis of synthesized HAP and HAP synthesized in SBF

Fig.5.1.8.7 shows that after calcination at higher temperature from 1000^{O}C to 1200^{0}C the powder showed a substantial increase in peak height and an associated drop in peak width, which corresponds to an increase in crystallinity. It was also noted that the presence of TCP begins once the calcinations temperature reaches 1000^{0}C and above. This may not be desirable, as pure, clean powder is an essential criteria for any implantology in biomedical application. Hence, a calcination temperature of 1000^{0}C or below may be ideal.

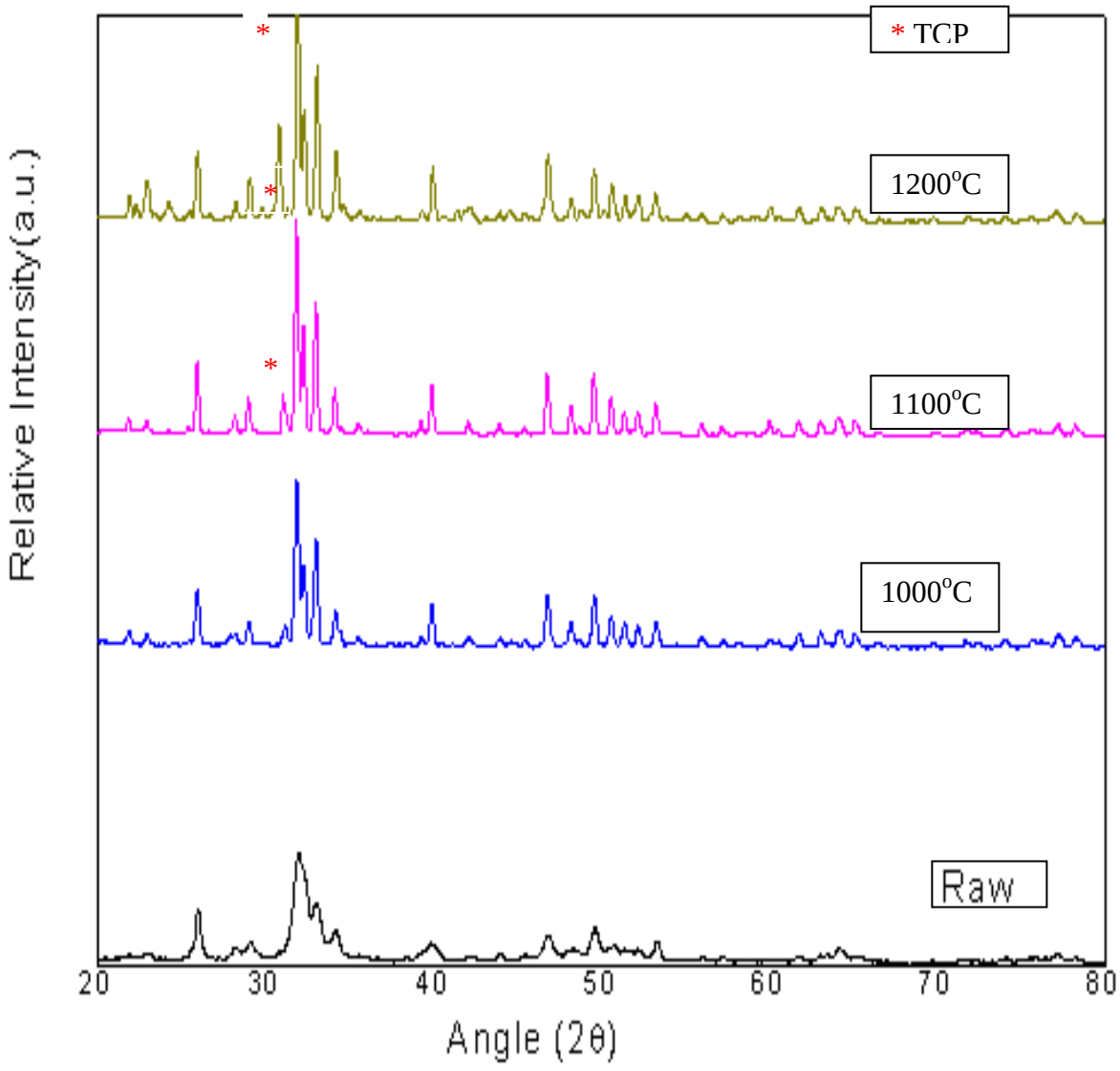

Fig. 5.1.8.7:XRD pattern of HAP calcined at various temperatures from 1000 to 1200^{0}C.

5.1.9 Density

HAP powder synthesized by calcium precipitation method and after being calcined at 800^{O}C for 2 Hr was ball milled at 200 rpm for 2 Hr. It was than compacted at different pressure from 450 to 950 MPa.

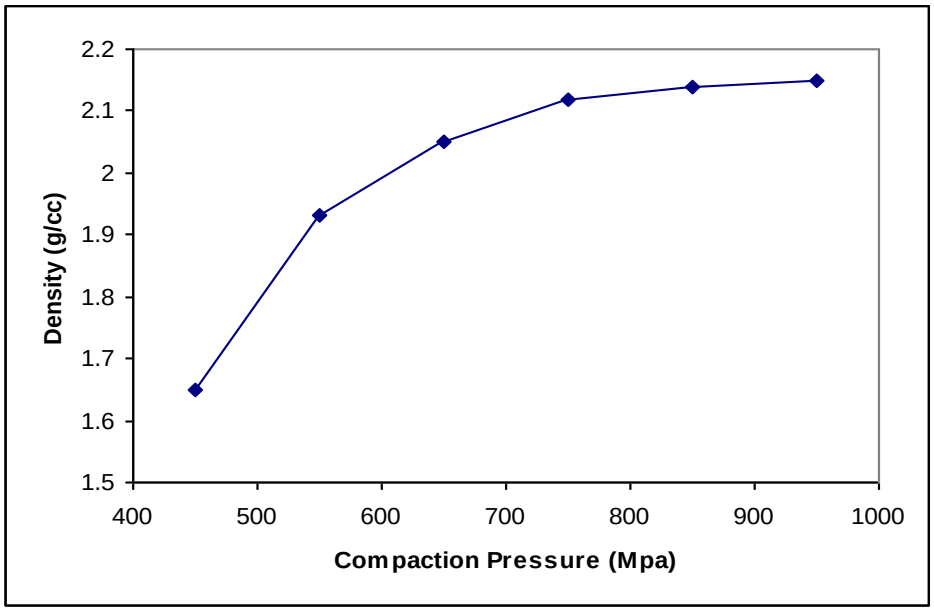

Fig. 5.1.9.1 Green density of HAP samples at various compaction pressure

From the above graph shown in Fig. 5.1.9.1 it is clear that beyond 750 MPa compaction pressure there is no significant enhance in green density. Sintered pellets compacted at pressure greater than 750MPa were found to develop cracrks. Hence the maximum pressure that can be applied was choosen as 750MPa. The calcined HAP powders were thus compacted at 750MPa to give a shape in the form of pallets and sintered at different temperatures 900 to 1250^{O}C.

5.1.9.2 Relative Density

Sintering is a method for making objects from powder, by heating the material in a sintering furnace below its melting point until its particles adhere to each other [170]. The word "sinter" comes from the Middle High German *Sinter*, a cognate of English "cinder**.**

The variation of sintered density with sintering temperature for HAP calcined at 800^{0}C is shown in Table 5.1.9.2.The relative density plot showed a increase in measured density from 50.68% (sintered at 1000^{O}C) to 95.02% (sintered at 1300^{0}C). The powder calcined at 800^{0}C and sintered at temperature 1250^{O}C attains a maximum sintered density of 95.66 % of Thereotical Density (T.D). The maximum density of less than 96% was measured for samples

sintered at 1200 to 1300^{O}C. These measured densities are in agreement with some of the values reported in the literature of HAP ceramic sintered up to 1300^{O}C. [171,172,173]

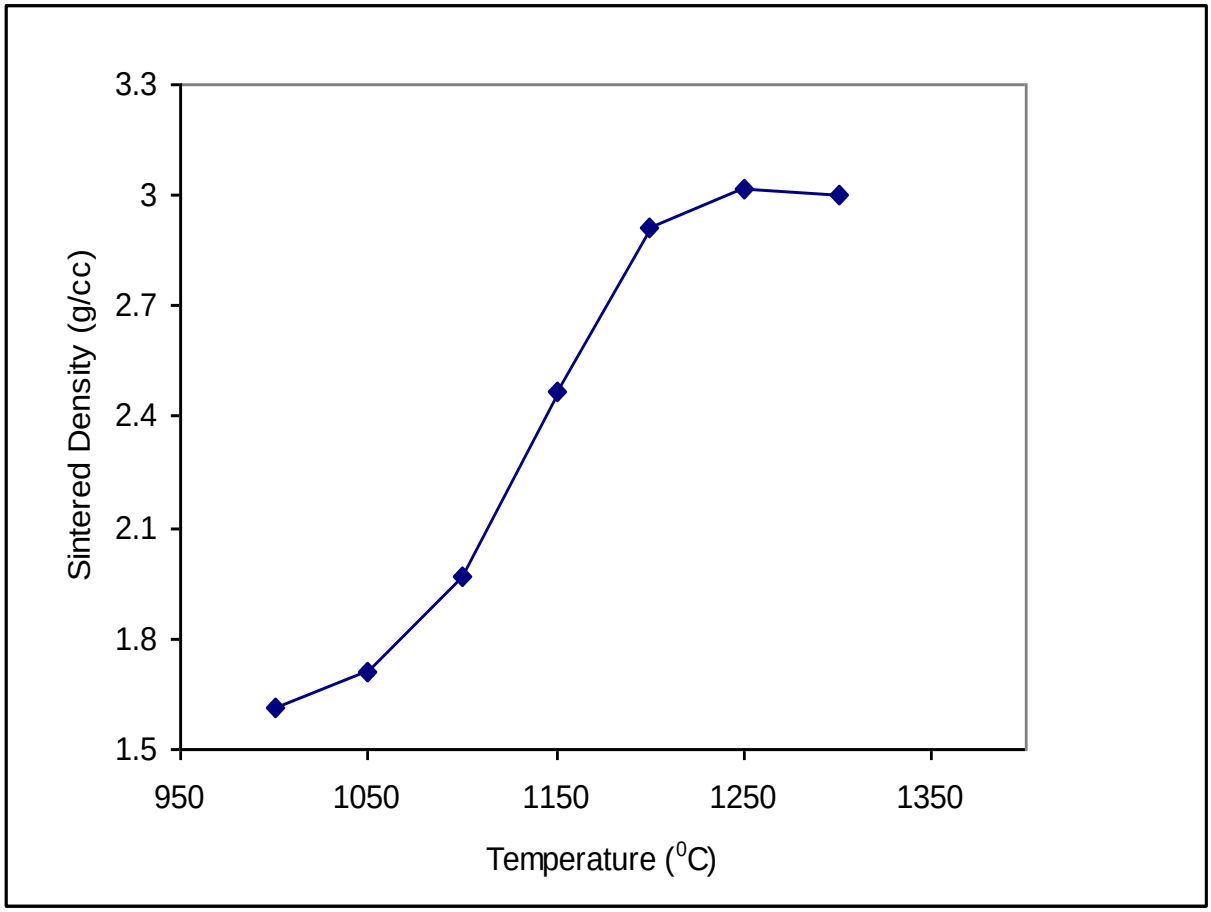

Fig. 5.1.9.2 Variation in sintered densities of the sample with the varying sintering temperature.

Fig. 5.1.9.2 resembles very closely exhibiting a sigmoidal shape with an inflexiuos point around 1250^{O}C. This point marks the temperature where maximum densification start to take place. From the graph it is clear that as the sintering temperature increases the density is also increased, but after a temperature of 1250^{0}C there is no substantial increase in density took place. The possible reason for reduced density at higher sintering temperature would be decomposition of HAP into other calcium phosphate as shown in Fig. 5.1.8.7.

The formation of HAP to tricalcium phosphate [$Ca_3(PO_4)_2$] (TCP) begins at temperature greater than 1000^{0}C. Pure HAP has got poor mechanical properties, but can be improved by the presence of TCP phase. The application of TCP in biological system can be summarized as below:

a) Porous TCP scaffolds are employed as drug carrier system for local drug delivery in bone.
b) TCP can be used as a tissue replacement for bony defects where autogenous bone graft is not feasible or possible. It may be used alone or in combination with a biodegradable, resorable polymer such as polyglycolic acid.
c) Another practical application is its use in gene transfection.

5.1.9.3 Volume Shrinkage

The effect of sintering temperature on the volume shrinkage (%) of calcined HAP is shown in Fig. 5.1.9.3.1.

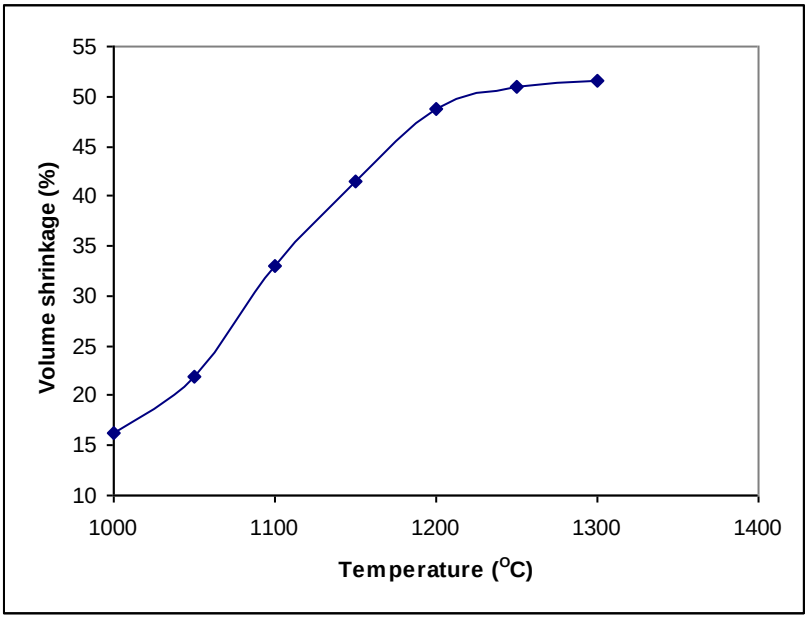

Fig. 5.1.9.3.1 Variation in volume shrinkage (%) of HAP samples with increase in sintering temperature.

From the above graph it is clear that the volume shrinkage increases from 16.249% at 1000^{O}C to 51.0243% at 1300^{O}C. There was substantial increase in volume shrinkage (%) of HAP samples with increase in sintering temperature from 1000 to 1300^{O}C. The maximum volume shrinkage 51.553% of HAP samples took place at temperature 1250^{O}C. Further increase in sintering temperature above 1250^{O}C results not much change in the volume shrinkage of the samples. This point marks the temperature where maximum densification starts to take place.[174]

HAP samples were mixed with different proportion of naphthalene and were sintered at temperature from 1000 to 1250^{O}C to study the volume shrinkage (%) of the HAP samples. The batch composition of green specimen is given in Table. 5.1.9.3.1.

Table. 5.1.9.3.1 Batch composition of green specimen.

Identification	HAP calcined at 800^{O}C/2Hr	Naphthalene (N) as porogen
HAP5N	**95% of HAP**	**5% N**
HAP10N	**90% of HAP**	**10% N**
HAP10N	**80% of HAP**	**20% N**

Fig. 5.1.9.3.2 shows the volume shrinkage of calcined HAP mixed with 5% Naphthalene with increase in sintering temperature from 1000 to 1250^{O}C. The graph showed increase in volume shrinkage with increase in sintering temperature. The maximum volume shrinkage (%) occurred at temperature 1250^{O}C was 50.693.

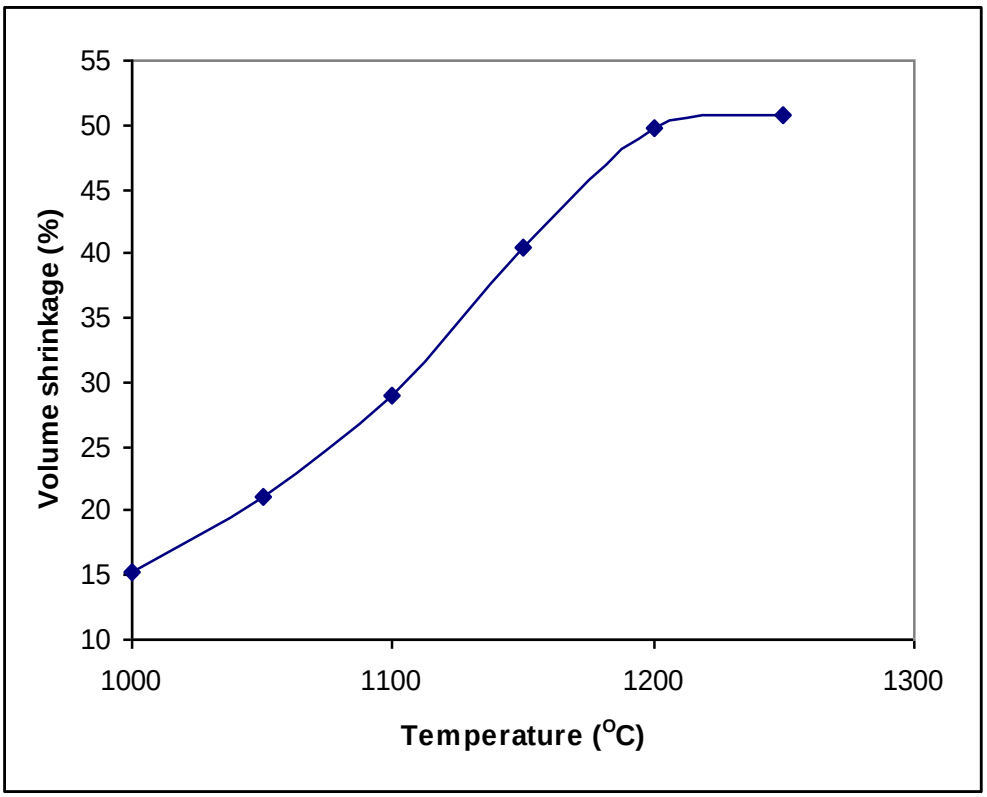

Fig. 5.1.9.3.2 Variation in volume shrinkage (%) of HAP mixed with 5% naphthalene with increase in sintering temperature

Fig. 5.1.9.3.3 shows the volume shrinkage of calcined HAP mixed with 10% Naphthalene with increase in sintering temperature from 1000 to 1250^{O}C. The graph showed increase in volume shrinkage with increase in sintering temperature. The maximum volume shrinkage (%) occurred at temperature 1250^{O}C was 50.817.

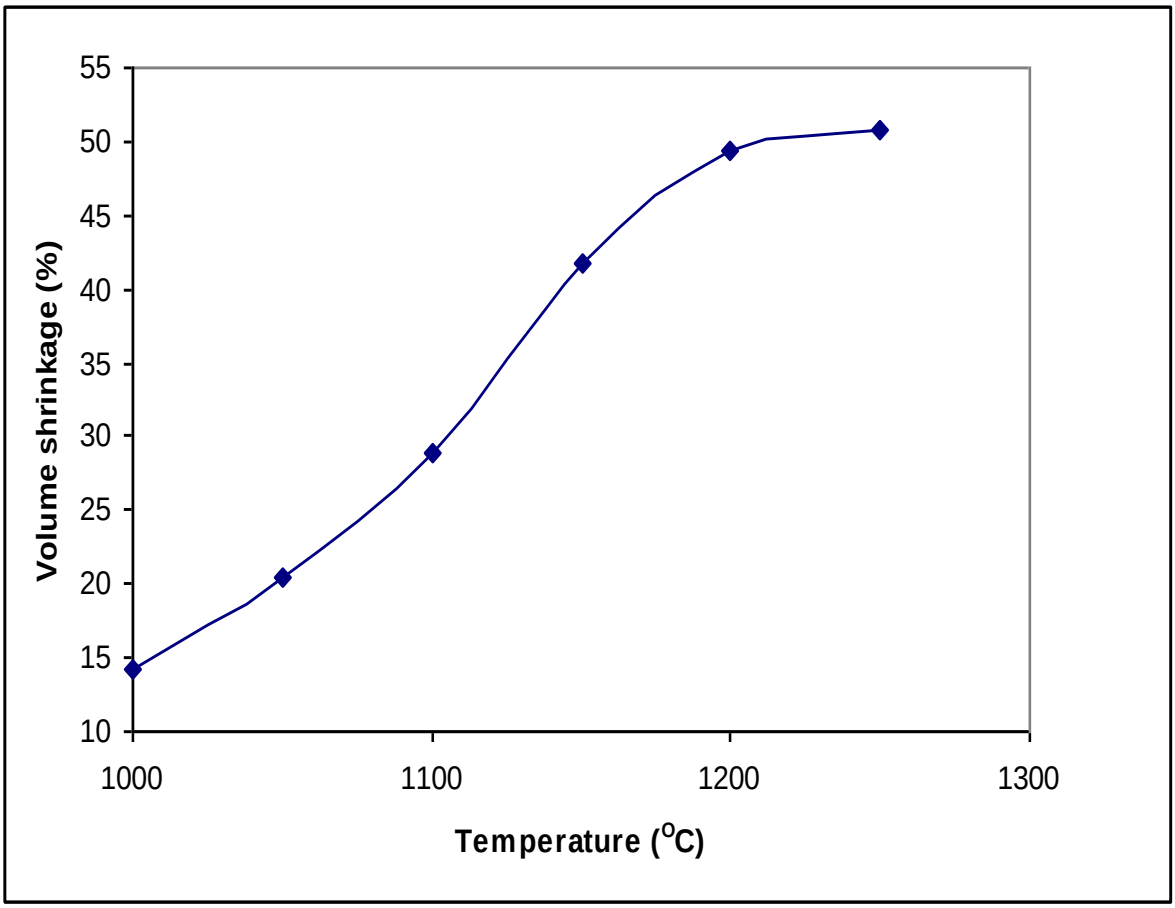

Fig. 5.1.9.3.3 Variation in volume shrinkage (%) of HAP mixed with 10% naphthalene with increase in sintering temperature

Fig. 5.1.9.3.4 shows the volume shrinkage of calcined HAP mixed with 20% Naphthalene with increase in sintering temperature from 1000 to 1250^{O}C. The graph showed increase in volume shrinkage with increase in sintering temperature. The maximum volume shrinkage (%) occurred at temperature 1250^{O}C was 51.686.

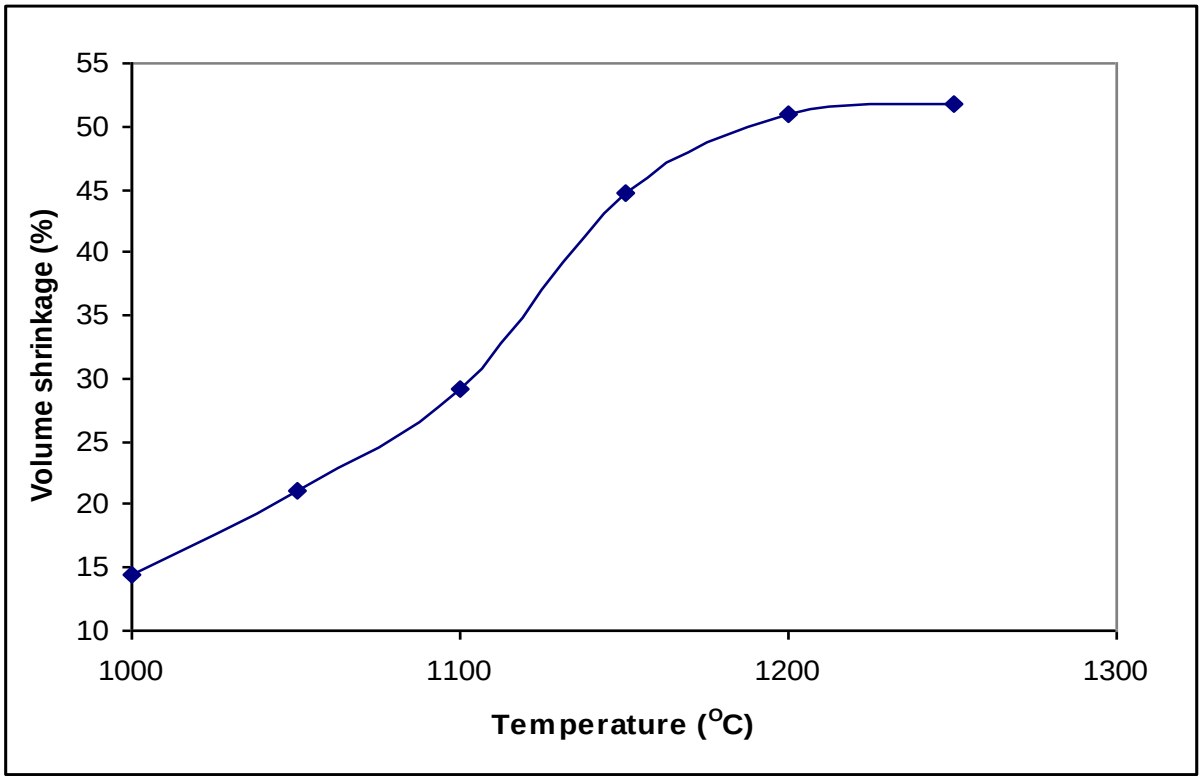

Fig. 5.1.9.3.4 Variation in volume shrinkage (%) of HAP mixed with 20% naphthalene with increase in sintering temperature.

Thus from the above study it was finally concluded that maximum volume shrinkage (%) took place for the calcined HAP mixed with 20% Naphthalene sintered at temperature 1250^{O}C. The volume shrinkage of sample is a function of sintering temperature which increases with increase in sintering temperature of the sample. The volume shrinkage (%) decreases at higher sintering temperature more than 1300^{O}C probably due to decomposition of

HAP to other calcium phosphates. A remarkable feature to notice is that nearly half the volume shrinkage % from initial volume took place when HAP was sintered from temp 1000 to $1300^{O}C$.

5.1.10 Development of Porous Hydroxyapatite.

The chemical synthesis and characterization of HAP powder have been explained in section 5.1 The calcined HAP powder of each batch were thoroughly mixed with its corresponding (wt%) of naphthalene as a porogen by dry mixing method Fig. 4.6. The development of porosity is an important parameter in the implant in order to make it light as well as to facilitate rapid vascularization. Further, porous HAP has the advantage of becoming infiltrated by fibro vascular tissue, thereby providing resistance to infection, migration and extrusion. [175, 176, 177]

5.1.10.1 Bulk density and Porosity of Porous HAP prepared by Dry mixing method

The change in bulk density (g/cc) and apparent porosity (%) of sintered HAP as a function of increase in naphthalene (wt %) is shown in Fig. 5.1.10.1. The maximum apparent porosity for the sample fired at $1000^{O}C$/2hr was measured to be 77.56 % at naphthalene (50 wt %) and minimum 49% at naphthalene (0 wt %) and the maximum bulk density was 1.61 (g/cc) at naphthalene (0 wt %) and minimum 0.71g/cc at naphthalene (50wt%). The result clearly showed that with the increase in concentration of naphthalene (wt %) from 0 to 50 (wt %) there was increase in apparent porosity (%) with substantial decrease in bulk density (g/cc) of porous HAP. The porosity increases because after sublimation naphthalene particles escape out leaving behind as pores.

Thus, the apparent porosity is increased due to increase in pore volume and the increase in total volume of sintered compacts powder because of increase in porosity. The greater advantage of using naphthalene is that HAP with 50% porosity has pores that are open, but they are not always connected. After adding naphthalene, porosity increases and the pores obtained are interconnected.[178]

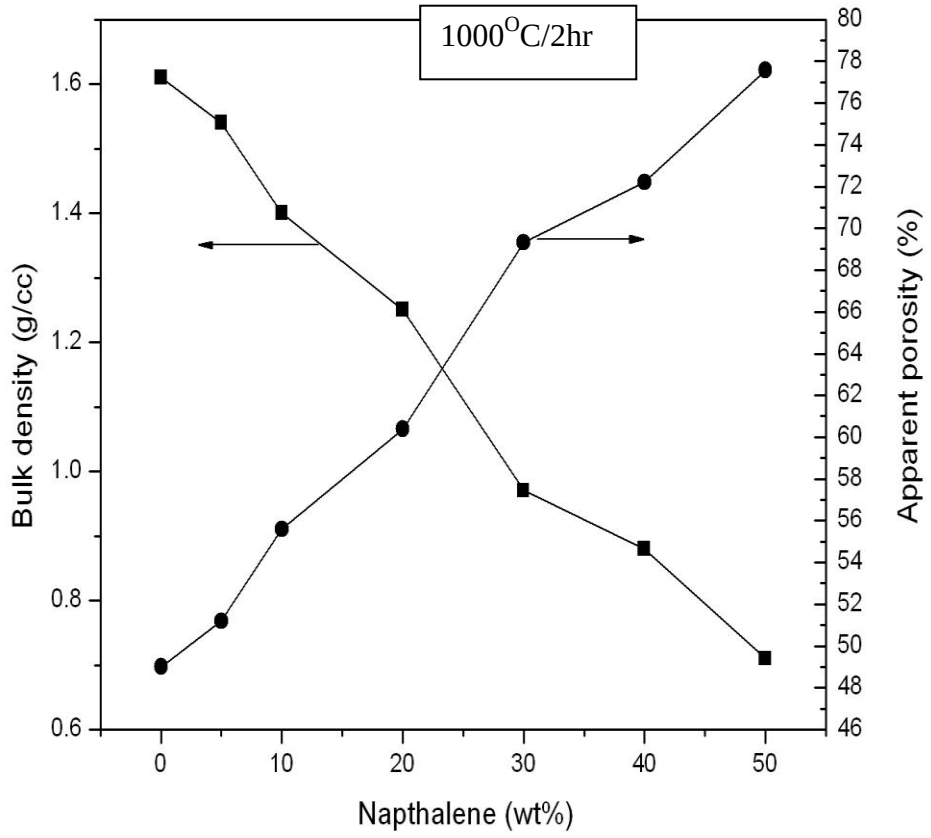

Fig. 5.1.10.1 Variation in Bulk density (g/cc) and Apparent porosity (%) of porous HAP with increasing Naphthalene (wt %) at 1000^{O}C/2Hr

Fig. 5.1.10.2 showed variation in Bulk density (g/cc) and apparent porosity (%) of porous HAP with increasing Naphthalene (wt %) at 1050^{O}C/2Hr. The maximum apparent porosity for the porous HAP fired at 1050^{O}C/2hr was measured to be 73.23 % at naphthalene (50 wt %) and minimum 45.83% at naphthalene (0 wt %) where as maximum bulk density of 1.71 (g/cc) was obtained for naphthalene (0 wt %) and minimum 0.85g/cc at naphthalene (50 wt %) respectively.

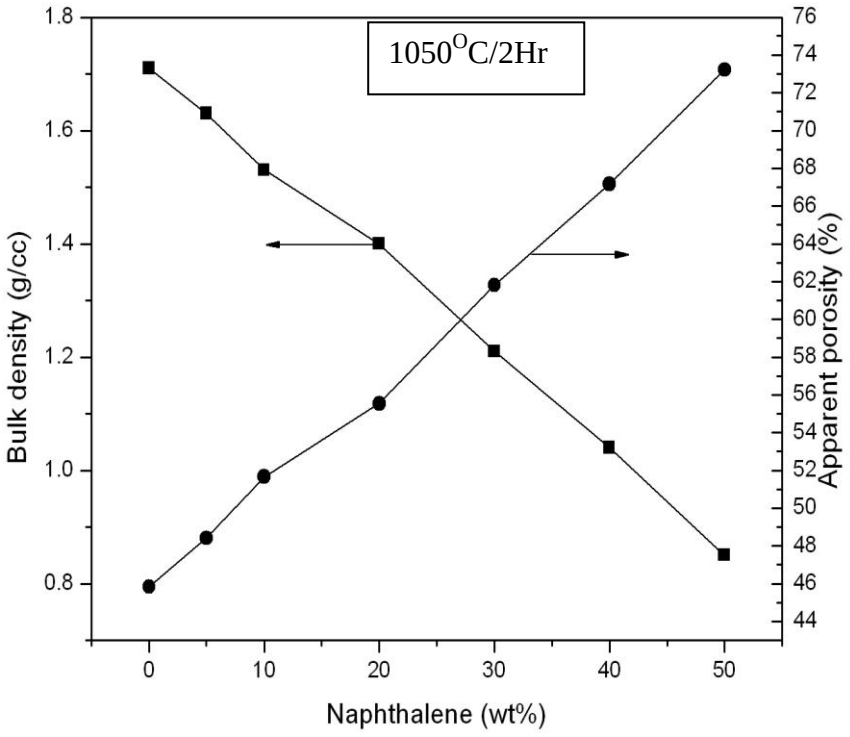

Fig. 5.1.10.2 Variation in Bulk density (g/cc) and Apparent porosity (%) of porous HAP with increasing Naphthalene (wt %) at 1050^{O}C/2Hr

Fig. 5.1.10.3 showed variation in Bulk density (g/cc) and Apparent porosity (%) of porous HAP with increasing naphthalene (wt %) at 1100^{O}C/2Hr. The maximum apparent porosity for the porous HAP fired at 1100^{O}C/2hr was measured to be 66.3 % at naphthalene (50 wt %) and minimum 39.49% at naphthalene (0 wt %) where as maximum bulk density of 1.91 (g/cc) was obtained for naphthalene (0 wt %) and minimum 1.06g/cc at naphthalene (50 wt %) respectively.

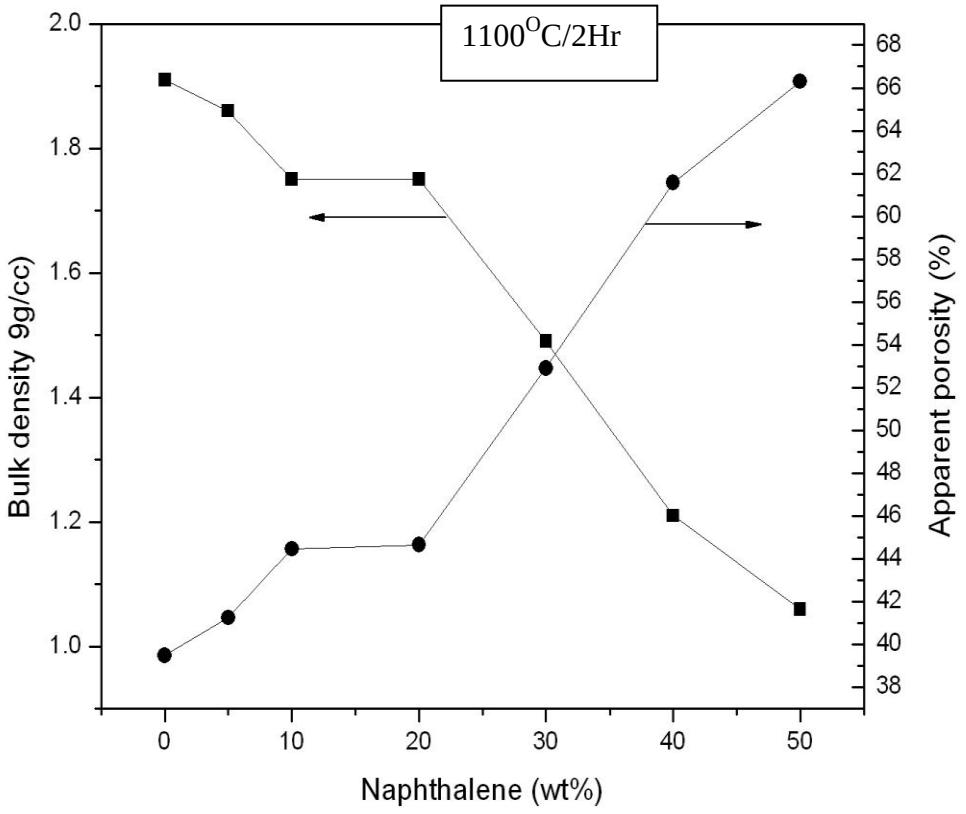

Fig. 5.1.10.3 Variation in Bulk density (g/cc) and Apparent porosity (%) of porous HAP with increasing Naphthalene (wt%) at 1100^{O}C/2Hr.

Fig. 5.1.10.4 showed variation in Bulk density (g/cc) and Apparent porosity (%) of porous HAP with increasing naphthalene (wt%) at 1150^{O}C/2Hr. The maximum apparent porosity for the porous HAP fired at 1150^{O}C/2hr was measured to be 61.3 % at naphthalene (50wt%) and minimum 21.76% at naphthalene (0wt%) where as maximum bulk density of 2.47(g/cc) was obtained for naphthalene (0wt%) and minimum 1.22g/cc at naphthalene (50wt%) respectively.

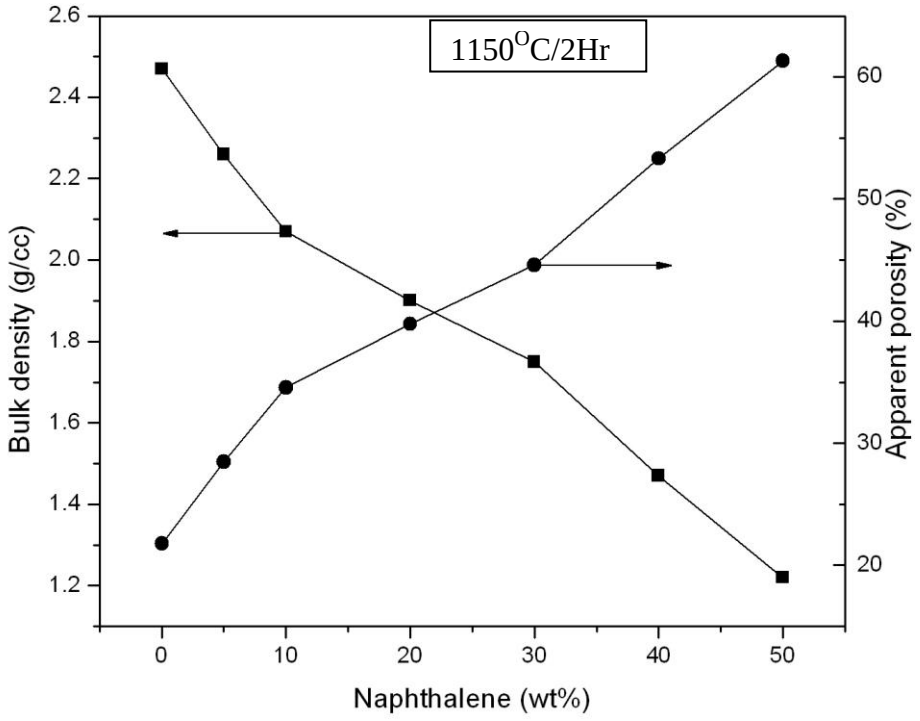

Fig. 5.1.10.4 Variation in Bulk density (g/cc) and Apparent porosity (%) of porous HAP with increasing Naphthalene (wt %) at 1150^{O}C/2Hr

Fig. 5.1.10.5 showed variation in Bulk density (g/cc) and Apparent porosity (%) of porous HAP with increasing naphthalene (wt %) at 1200^{O}C/2Hr. The maximum apparent porosity for the porous HAP fired at 1200^{O}C/2hr was measured to be 57.30% at naphthalene (50 wt %) and minimum 9.09% at naphthalene (0 wt %) where as maximum bulk density of 2.87(g/cc) was obtained for naphthalene (0 wt %) and minimum 1.35g/cc at naphthalene (50wt%) respectively.

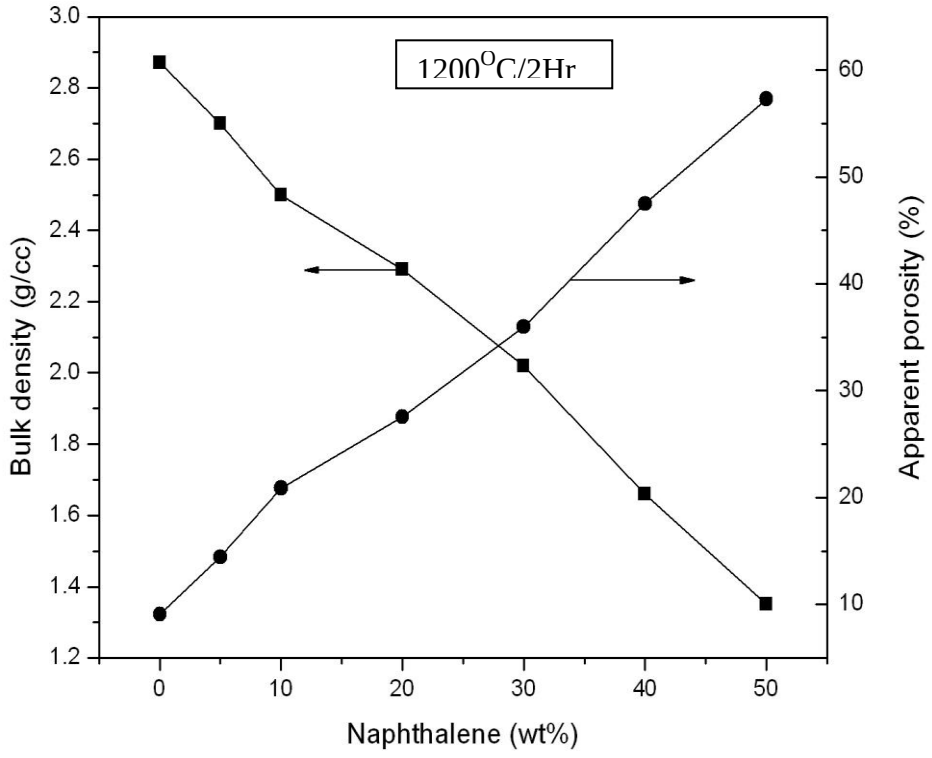

Fig. 5.1.10.5 Variation in Bulk density (g/cc) and Apparent porosity (%) of porous HAP with increasing Naphthalene (wt%) at 12000^{O}C/2Hr.

Fig. 5.1.10.6 showed variation in Bulk density (g/cc) and apparent porosity (%) of porous HAP with increasing naphthalene (wt %) at 1250^{O}C/2Hr. The maximum apparent porosity for the porous HAP fired at 1200^{O}C/2hr was measured to be 50.99% at naphthalene (50 wt %) and minimum 5.28% at naphthalene (0 wt %) where as maximum bulk density of 2.99(g/cc) was obtained for naphthalene (0wt%) and minimum 1.55g/cc at naphthalene (50wt%) respectively.

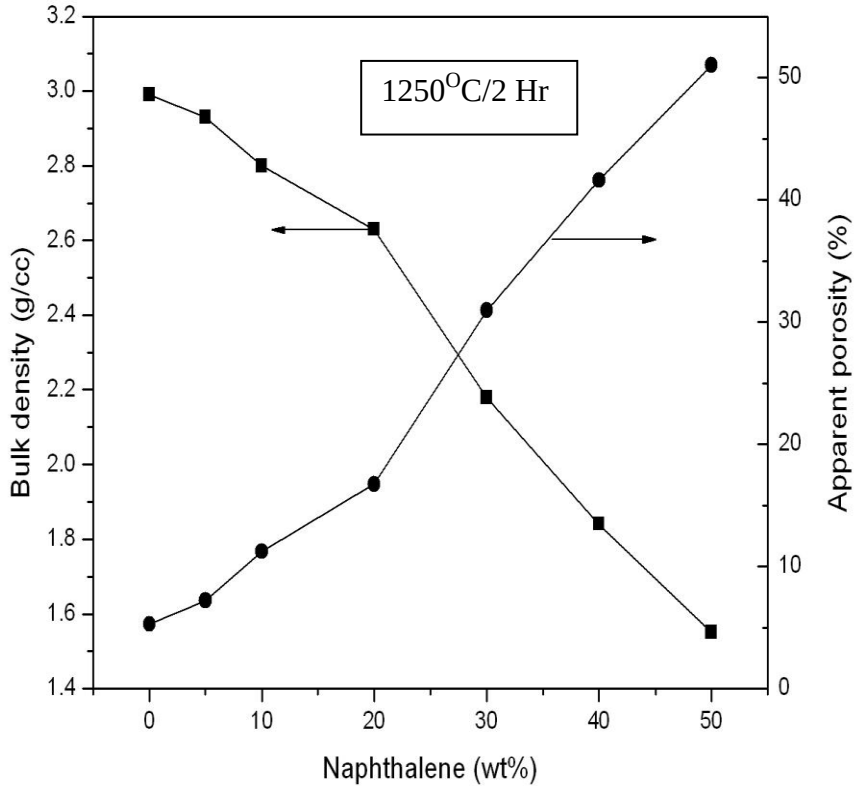

Fig. 5.1.10.6 Variation in Bulk density (g/cc) and apparent porosity (%) of porous HAP with increasing Naphthalene (wt %) at 1250^{O}C/2Hr.

Fig. 5.1.10.7 showed variation in Bulk density (g/cc) and apparent porosity (%) of porous HAP with increasing naphthalene (wt %) at 1000^{O}C/4Hr. The maximum apparent porosity for the porous HAP fired at 1000^{O}C/4hr was measured to be 76.05% at naphthalene (50 wt %) and minimum 50.44% at naphthalene (0 wt %) where as maximum bulk density of 1.56(g/cc) was obtained for naphthalene (0 wt %) and minimum 0.76g/cc at naphthalene (50 w t%) respectively.

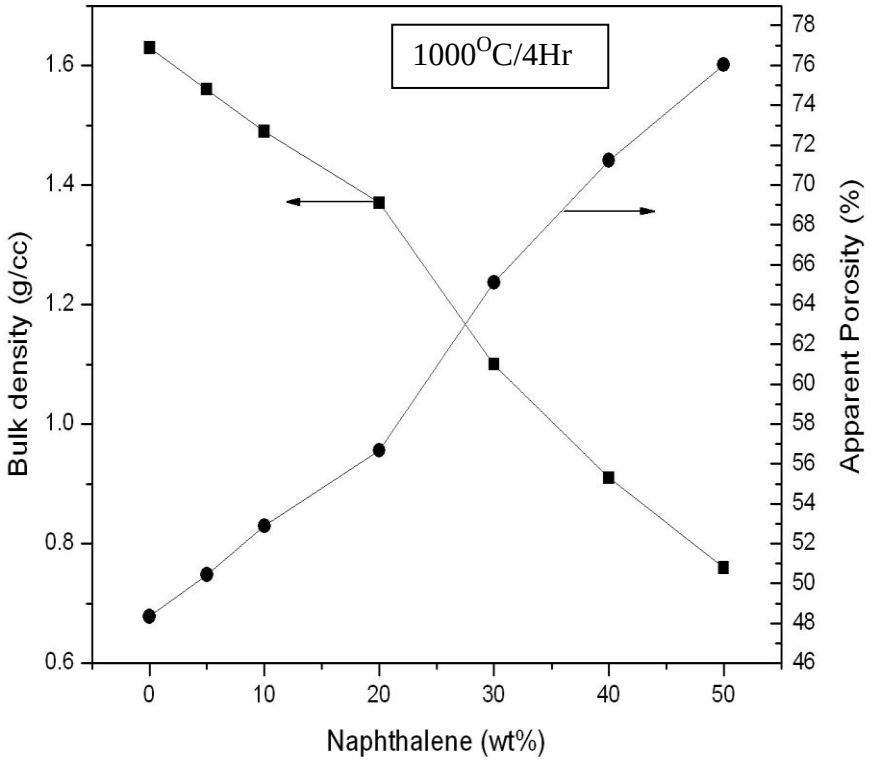

Fig. 5.1.10.7 Variation in Bulk density (g/cc) and apparent porosity (%) of porous HAP with increasing Naphthalene (wt %) at 1000^{O}C/4Hr.

Fig. 5.1.10.8 showed variation in Bulk density (g/cc) and apparent porosity (%) of porous HAP with increasing naphthalene (wt %) at 1050^{O}C/4Hr. The maximum apparent porosity for the porous HAP fired at 1050^{O}C/4hr was measured to be 72% at naphthalene (50 wt %) and minimum 45.14% at naphthalene (0 wt %) where as maximum bulk density of 1.73(g/cc) was obtained for naphthalene (0 wt %) and minimum 0.88g/cc at naphthalene (50wt%) respectively.

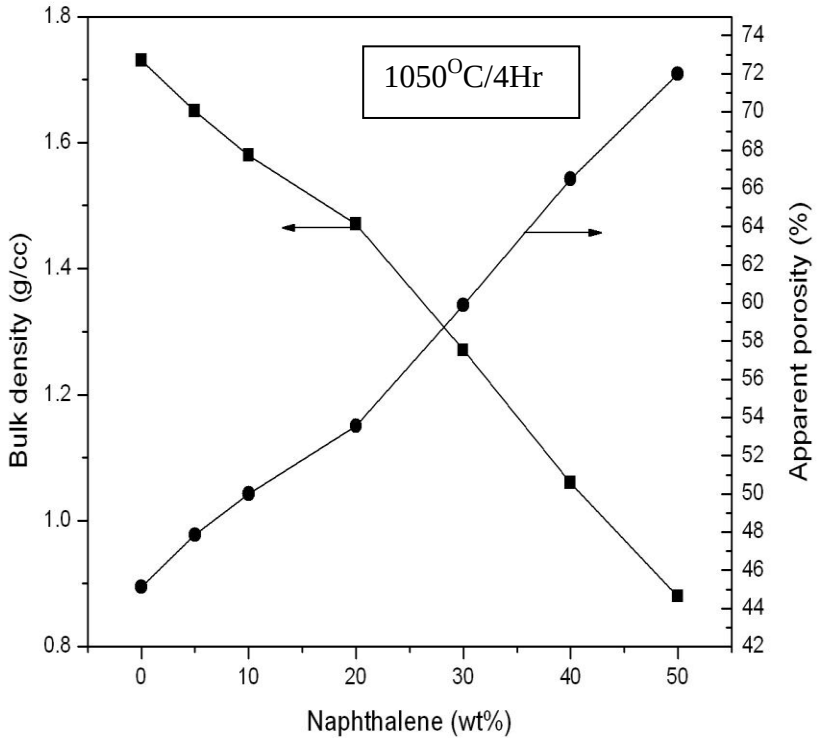

Fig. 5.1.10.8 Variation in Bulk density (g/cc) and Apparent porosity (%) of porous HAP with increasing Naphthalene (wt %) at 1050^{O}C/4Hr.

Fig. 5.1.10.9 showed variation in Bulk density (g/cc) and apparent porosity (%) of porous HAP with increasing naphthalene (wt %) at 1100^{O}C/4Hr. The maximum apparent porosity for the porous HAP fired at 1100^{O}C/4hr was measured to be 63.67% at naphthalene (50 wt %) and minimum 37.33% at naphthalene (0 wt %) where as maximum bulk density of 1.98(g/cc) was obtained for naphthalene (0 wt %) and minimum 1.15g/cc at naphthalene (50 wt %) respectively.

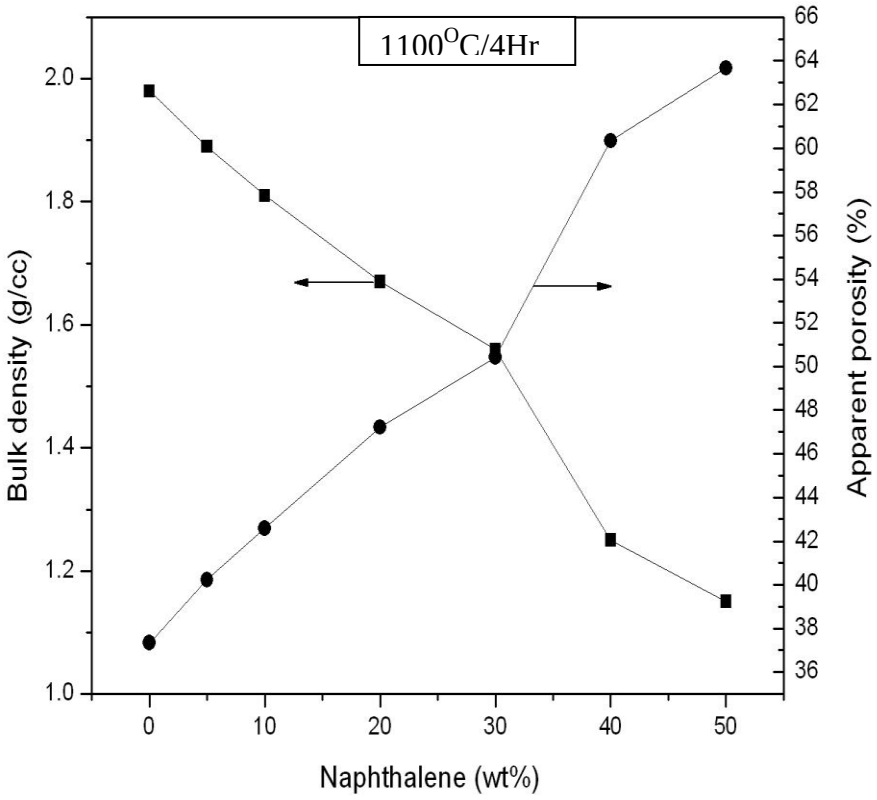

Fig. 5.1.10.9 Variation in Bulk density (g/cc) and Apparent porosity (%) of porous HAP with increasing Naphthalene (wt %) at 1100^{O}C/4Hr.

Fig. 5.1.10.10 showed variation in Bulk density (g/cc) and Apparent porosity (%) of porous HAP with increasing naphthalene (wt %) at 1150^{O}C/4Hr. The maximum apparent porosity for the porous HAP fired at 1150^{O}C/4hr was measured to be 57.34% at naphthalene (50 wt %) and minimum 18.94% at naphthalene (0wt%) where as maximum bulk density of 2.56(g/cc) was obtained for naphthalene (0 wt %) and minimum 1.35g/cc at naphthalene (50wt%) respectively

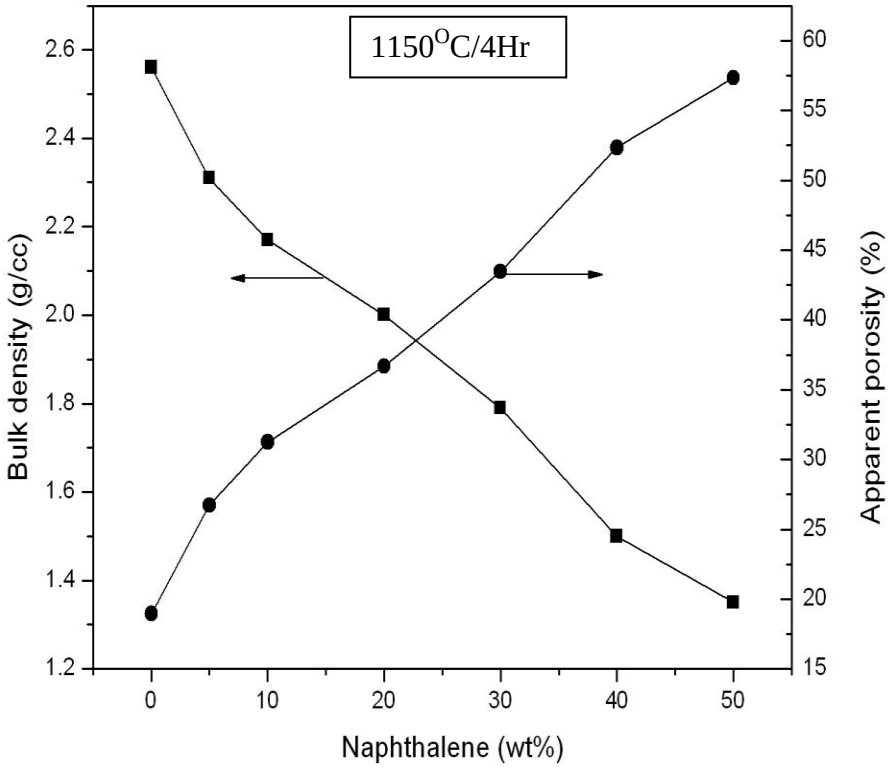

Fig. 5.1.10.10 Variation in Bulk density (g/cc) and Apparent porosity (%) of porous HAP with increasing Naphthalene (wt %) at 1150^{O}C/4Hr.

Fig. 5.1.10.11 showed variation in Bulk density (g/cc) and apparent porosity (%) of porous HAP with increasing naphthalene (wt %) at 1200^{O}C/4Hr. The maximum apparent porosity for the porous HAP fired at 1200^{O}C/4hr was measured to be 53.70% at naphthalene (50 wt %) and minimum 7.17% at naphthalene (0 wt %) where as maximum bulk density of 2.93 (g/cc) was obtained for naphthalene (0 wt %) and minimum 1.46g/cc at naphthalene (50 wt %) respectively

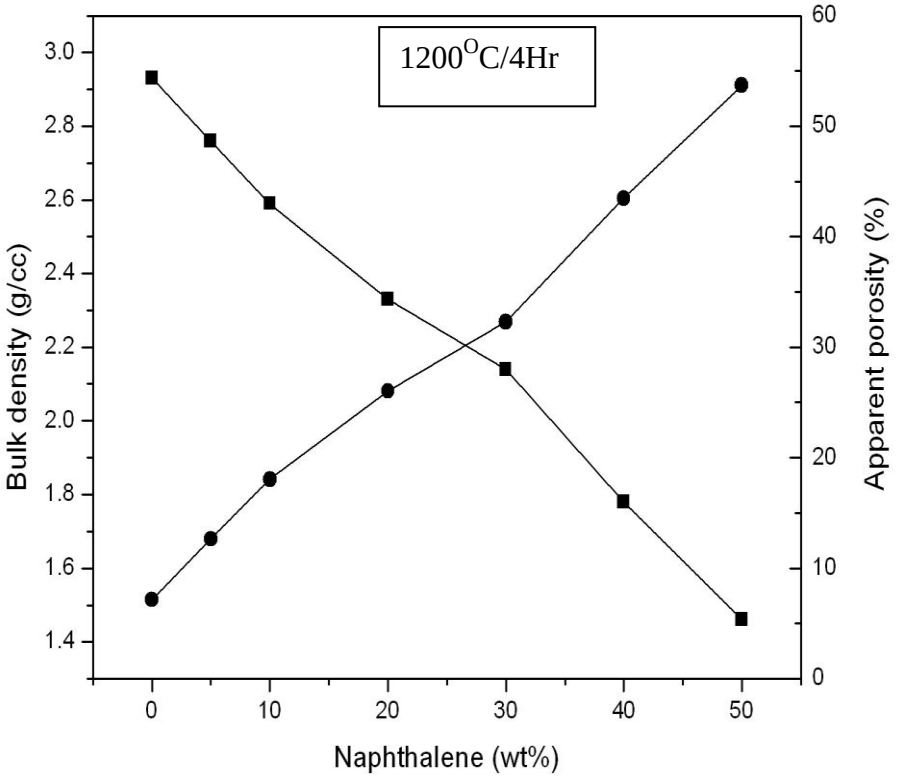

Fig. 5.1.10.11 Variation in Bulk density (g/cc) and apparent porosity (%) of porous HAP with increasing Naphthalene (wt %) at 1200^{O}C/4Hr.

Fig. 5.1.10.12 showed variation in Bulk density (g/cc) and apparent porosity (%) of porous HAP with increasing naphthalene (wt %) at 1250^{O}C/4Hr. The maximum apparent porosity for the porous HAP fired at 1250^{O}C/4hr was measured to be 49.89% at naphthalene (50 wt %) and minimum 4.40% at naphthalene (0 wt %) where as maximum bulk density of 2.94 (g/cc) was obtained for naphthalene (0 wt %) and minimum 1.58g/cc at naphthalene (50 wt %) respectively

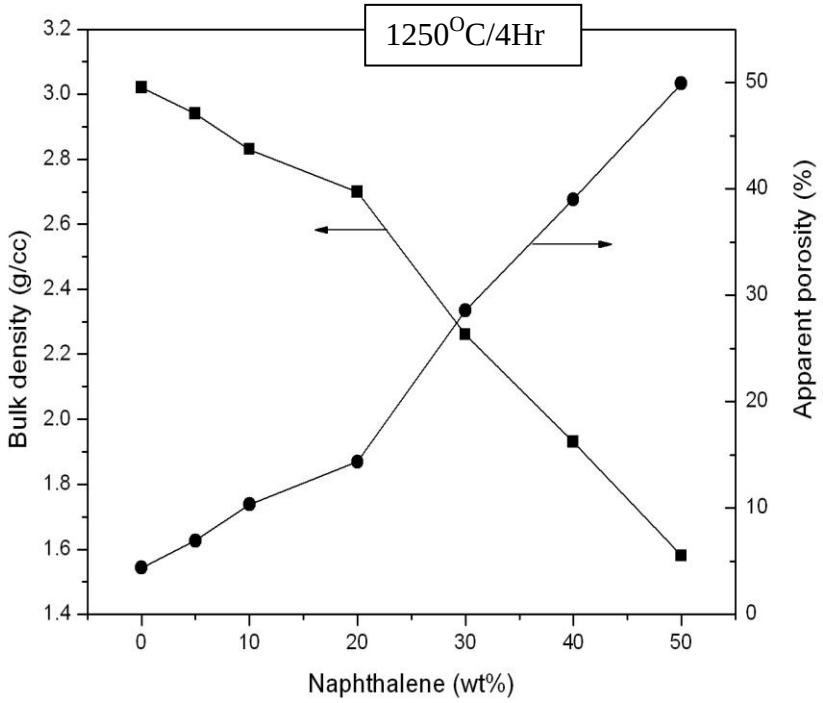

Fig. 5.1.10.12 Variation in Bulk density (g/cc) and apparent porosity (%) of porous HAP with increasing Naphthalene (wt %) at 1250^{O}C/4Hr.

Fig. 5.1.10.13 showed variation in Bulk density (g/cc) and apparent porosity (%) of porous HAP with increasing naphthalene (wt %) at 1000^{O}C/8Hr. The maximum apparent porosity for the porous HAP fired at 1000^{O}C/8hr was measured to be 75.31% at naphthalene (50 wt %) and minimum 50.10% at naphthalene (0 wt %) where as maximum bulk density of 1.58(g/cc) was obtained for naphthalene (0 wt %) and minimum 0.78g/cc at naphthalene (50 wt %) respectively

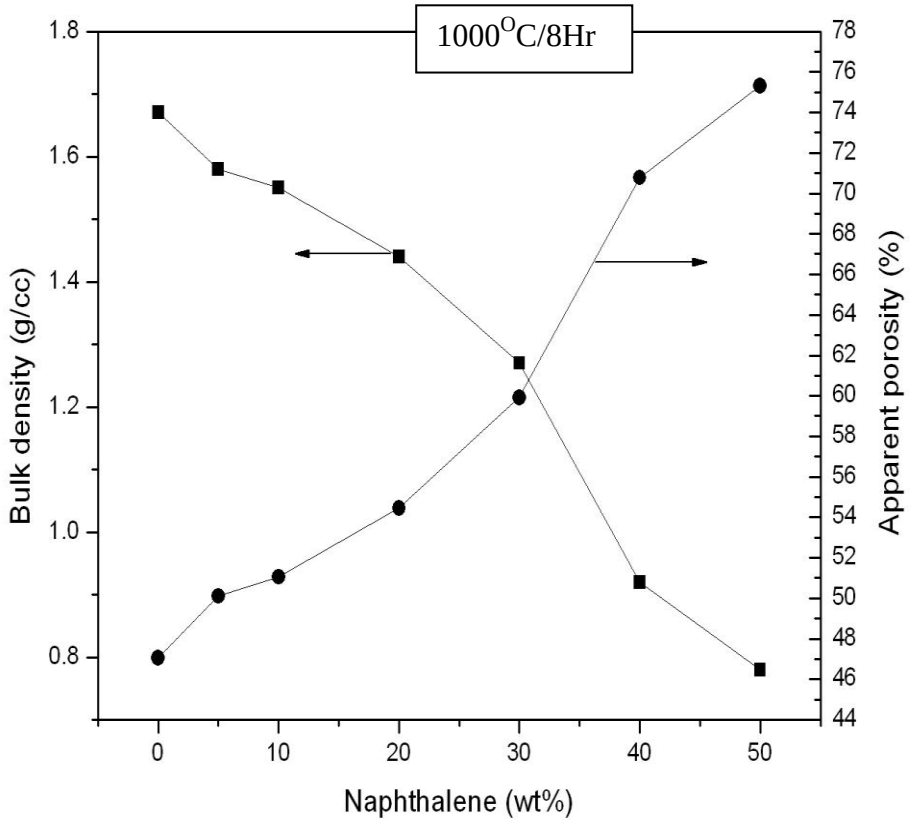

Fig. 5.1.10.13 Variation in Bulk density (g/cc) and apparent porosity (%) of porous HAP with increasing Naphthalene (wt %) at 1000^{O}C/8Hr.

Fig. 5.1.10.14 showed variation in Bulk density (g/cc) and apparent porosity (%) of porous HAP with increasing naphthalene (wt %) at 1050^{O}C/8Hr. The maximum apparent porosity for the porous HAP fired at 1050^{O}C/8hr was measured to be 71.20% at naphthalene (50 wt %) and minimum 44.97% at naphthalene (0 wt %) where as maximum bulk density of 1.74(g/cc) was obtained for naphthalene (0 wt %) and minimum 0.91g/cc at naphthalene (50 wt %) respectively

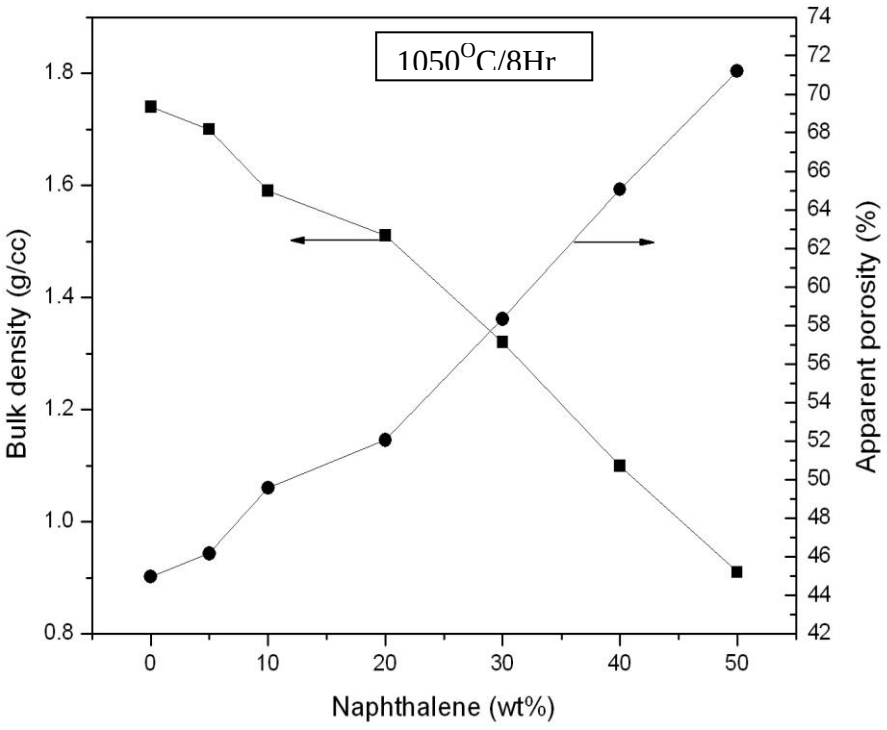

Fig. 5.1.10.14 Variation in Bulk density (g/cc) and apparent porosity (%) of porous HAP with increasing Naphthalene (wt %) at 1050^{O}C/8Hr.

Fig. 5.1.10.15 showed variation in Bulk density (g/cc) and apparent porosity (%) of porous HAP with increasing naphthalene (wt %) at 1100^{O}C/8Hr. The maximum apparent porosity for the porous HAP fired at 1100^{O}C/8hr was measured to be 62.34% at naphthalene (50 wt %) and minimum 35.48% at naphthalene (0 wt %) where as maximum bulk density of 2.04(g/cc) was obtained for naphthalene (0 wt %) and minimum 1.19g/cc at naphthalene (50 wt %) respectively

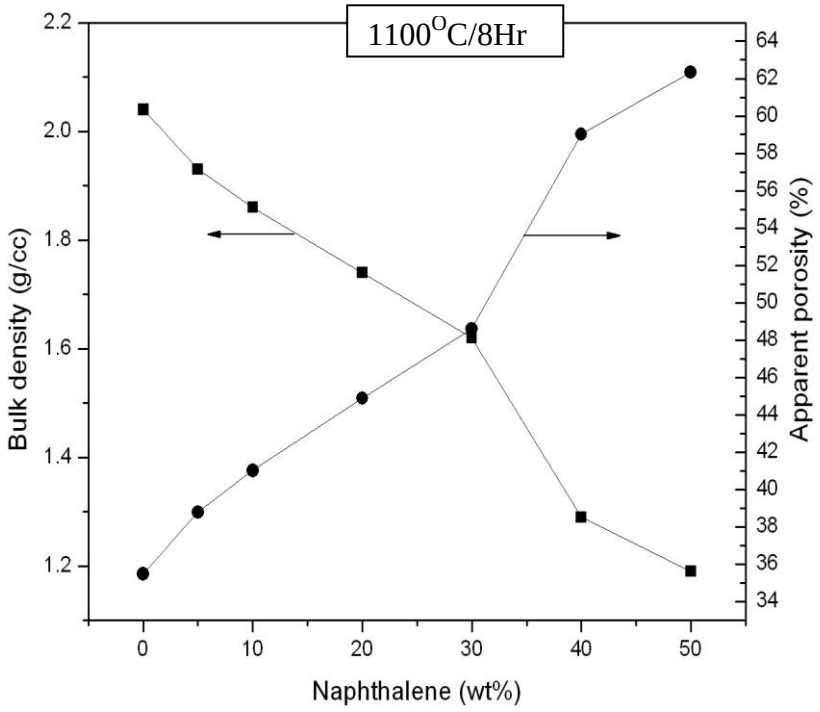

Fig. 5.1.10.15 Variation in Bulk density (g/cc) and Apparent porosity (%) of porous HAP with increasing Naphthalene (wt %) at 1100^{O}C/8Hr.

Fig. 5.1.10.16 showed variation in Bulk density (g/cc) and Apparent porosity (%) of porous HAP with increasing naphthalene (wt %) at 1150^{O}C/8Hr. The maximum apparent porosity for the porous HAP fired at 1150^{O}C/8hr was measured to be 56.05% at naphthalene (50 wt%) and minimum 15.38% at naphthalene (0wt%) where as maximum bulk density of 2.67(g/cc) was obtained for naphthalene (0wt%) and minimum 1.39g/cc at naphthalene (50 wt %) respectively.

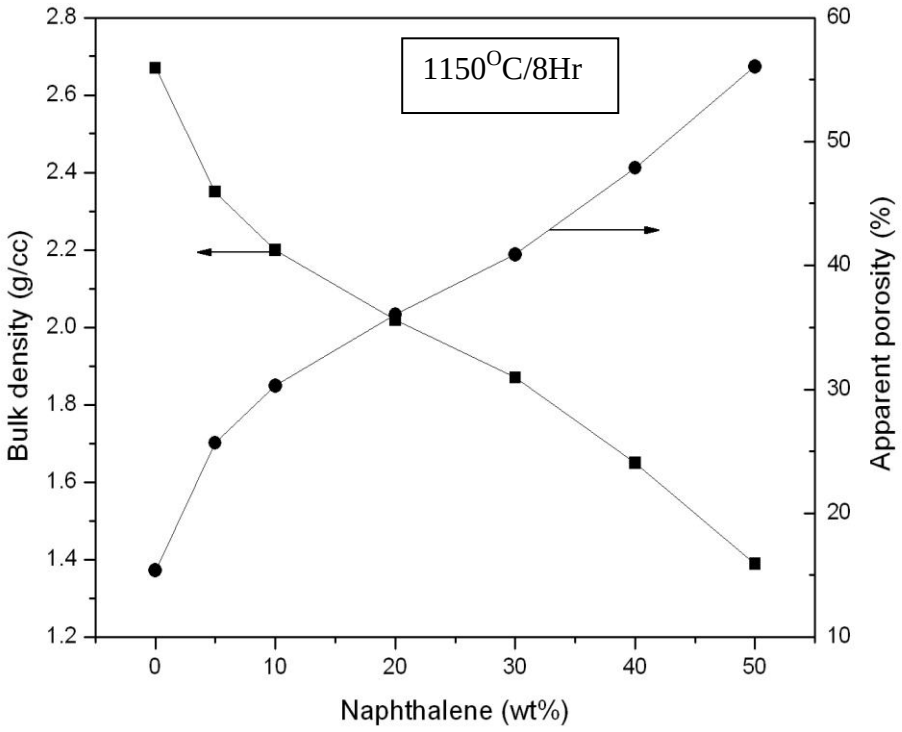

Fig. 5.1.10.16 Variation in Bulk density (g/cc) and Apparent porosity (%) of porous HAP with increasing Naphthalene (wt %) at 1150^{O}C/8Hr.

Fig. 5.1.10.17 showed variation in Bulk density (g/cc) and Apparent porosity (%) of porous HAP with increasing naphthalene (wt %) at 1200^{O}C/8Hr. The maximum apparent porosity for the porous HAP fired at 1200^{O}C/8hr was measured to be 52.05% at naphthalene (50 wt %) and minimum 6.20% at naphthalene (0 wt %) where as maximum bulk density of 2.96 (g/cc) was obtained for naphthalene (0 wt %) and minimum 1.51g/cc at naphthalene (50 wt %) respectively.

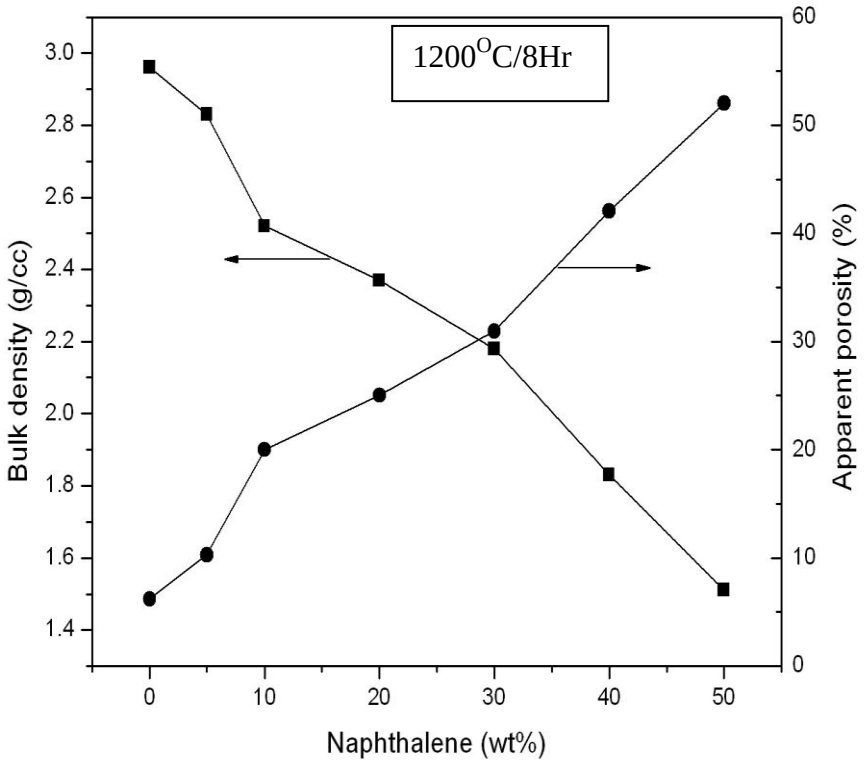

Fig. 5.1.10.17 Variation in Bulk density (g/cc) and Apparent porosity (%) of porous HAP with increasing Naphthalene (wt %) at 1200^{O}C/8Hr.

Fig. 5.1.10.18 showed variation in Bulk density (g/cc) and apparent porosity (%) of porous HAP with increasing naphthalene (wt %) at 1250^{O}C/8Hr. The maximum apparent porosity for the porous HAP fired at 1250^{O}C/8hr was measured to be 49.0% at naphthalene (50wt%) and minimum 3.5% at naphthalene (0 wt %) where as maximum bulk density of 3.05(g/cc) was obtained for naphthalene (0 wt %) and minimum 1.61g/cc at naphthalene (50wt%) respectively

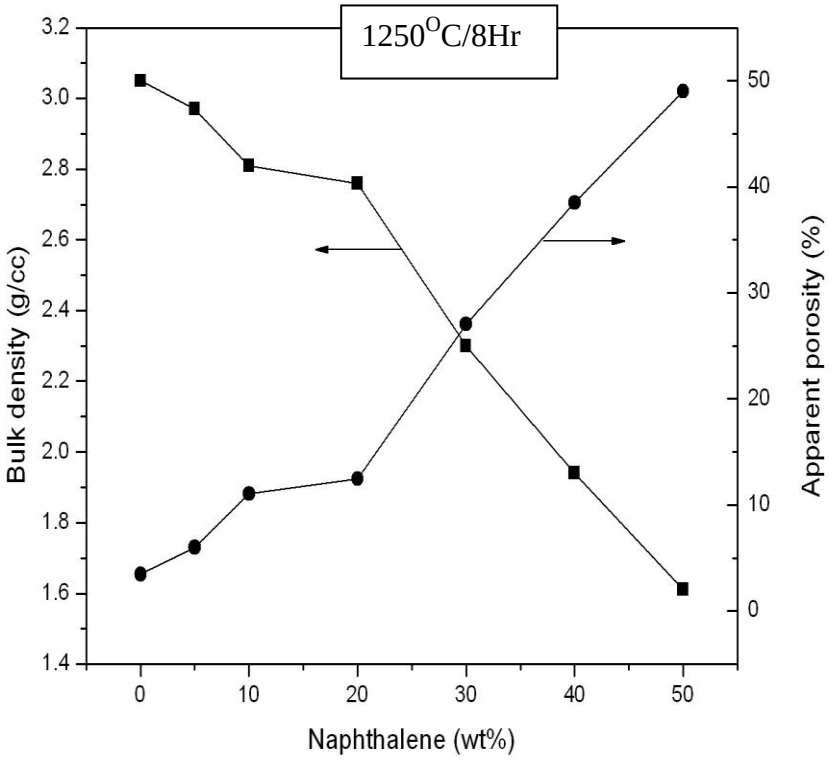

Fig. 5.1.10.18 Variation in Bulk density (g/cc) and Apparent porosity (%) of porous HAP with increasing Naphthalene (wt %) at 1250^{O}C/8Hr.

Fig. 5.1.10.19 showed variation in Bulk density (g/cc) and apparent porosity (%) of porous HAP with increasing naphthalene (wt %) at 1000^{O}C/16Hr. The maximum apparent porosity for the porous HAP fired at 1000^{O}C/16hr was measured to be 75.31% at naphthalene (50 wt %) and minimum 50.10% at naphthalene (0 wt %) where as maximum bulk density of 1.58 (g/cc) was obtained for naphthalene (0 wt %) and minimum 0.78g/cc at naphthalene (50 wt %) respectively

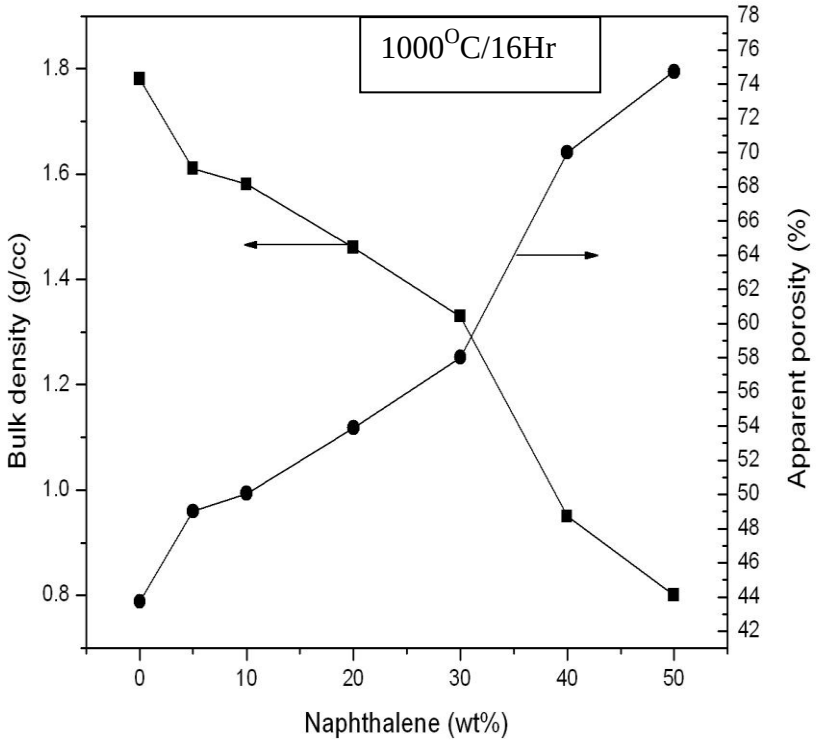

Fig. 5.1.10.19 Variation in Bulk density (g/cc) and apparent porosity (%) of porous HAP with increasing Naphthalene (wt %) at 1000^{O}C/16Hr.

Fig. 5.1.10.20 showed variation in Bulk density (g/cc) and apparent porosity (%) of porous HAP with increasing naphthalene (wt %) at 1050^{O}C/16Hr. The maximum apparent porosity for the porous HAP fired at 1050^{O}C/16hr was measured to be 71.20% at naphthalene (50 wt %) and minimum 44.97% at naphthalene (0 wt %) where as maximum bulk density of 1.74(g/cc) was obtained for naphthalene (0 wt %) and minimum 0.91g/cc at naphthalene (50 wt %) respectively.

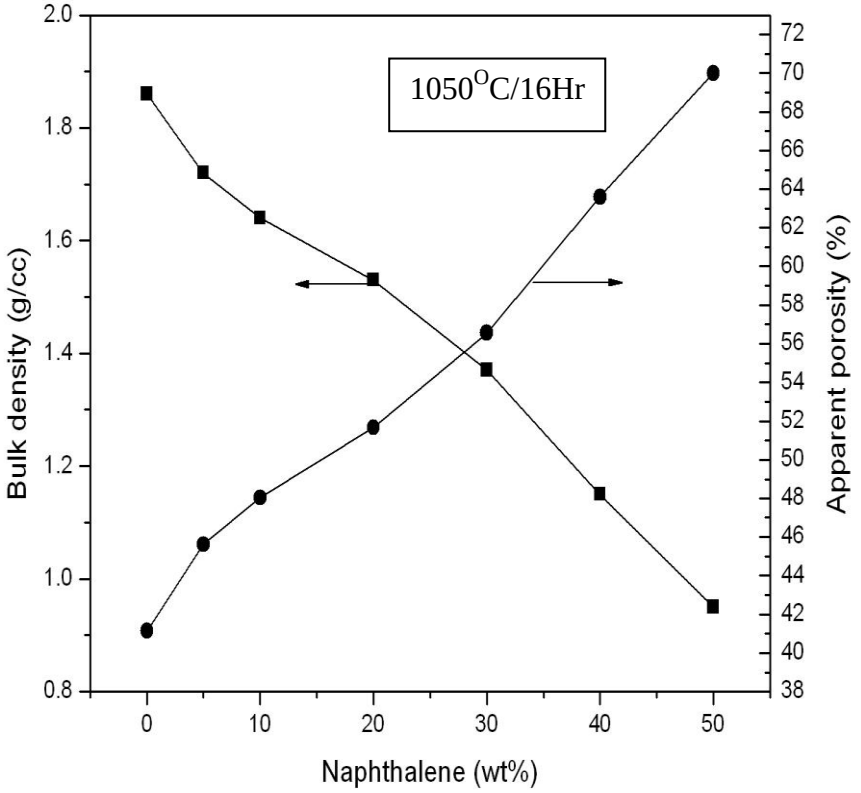

Fig. 5.1.10.20 Variation in Bulk density (g/cc) and Apparent porosity (%) of porous HAP with increasing Naphthalene (wt%) at 1050^{O}C/16Hr.

Fig. 5.1.10.21 showed variation in Bulk density (g/cc) and Apparent porosity (%) of porous HAP with increasing naphthalene (wt %) at 1100^{O}C/16Hr. The maximum apparent porosity for the porous HAP fired at 1100^{O}C/16hr was measured to be 62.34% at naphthalene (50 wt %) and minimum 35.48% at naphthalene (0wt%) where as maximum bulk density of 2.04(g/cc) was obtained for naphthalene (0 wt %) and minimum 1.19g/cc at naphthalene (50 wt %) respectively.

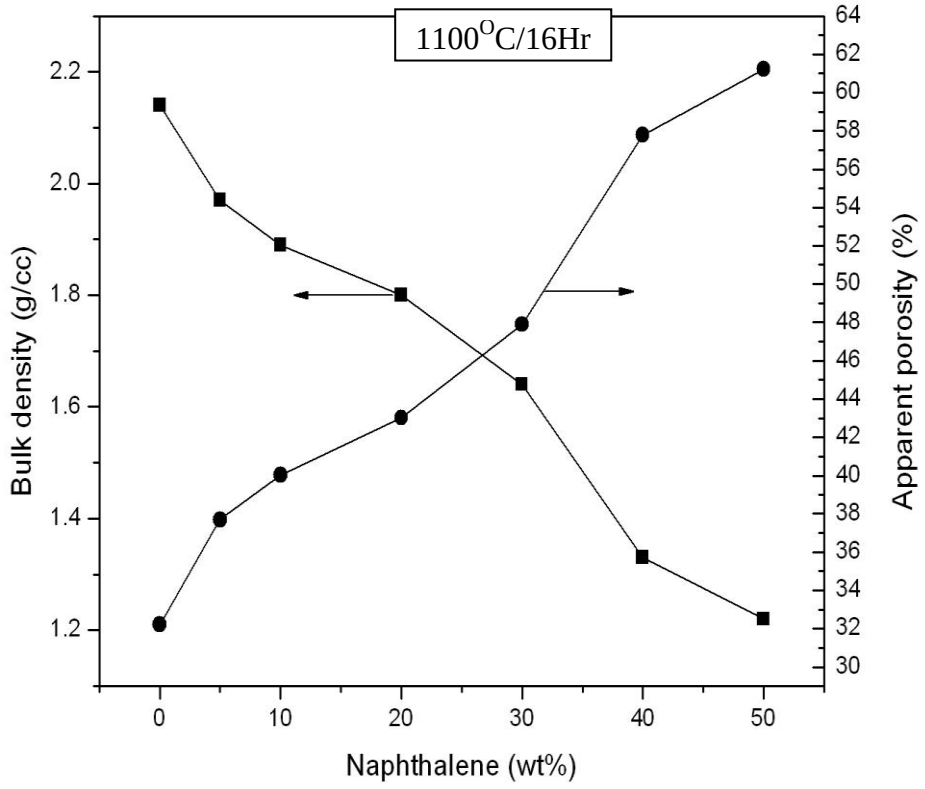

Fig. 5.1.10.21 Variation in Bulk density (g/cc) and apparent porosity (%) of porous HAP with increasing Naphthalene (wt %) at 1100^{O}C/16Hr.

Fig. 5.1.10.22 showed variation in Bulk density (g/cc) and apparent porosity (%) of porous HAP with increasing naphthalene (wt %) at 1150^{O}C/16Hr. The maximum apparent porosity for the porous HAP fired at 1150^{O}C/16hr was measured to be 56.05% at naphthalene (50 wt%) and minimum 15.38% at naphthalene (0 wt %) where as maximum bulk density of 2.67(g/cc) was obtained for naphthalene (0 wt %) and minimum 1.39g/cc at naphthalene (50wt%) respectively**.**

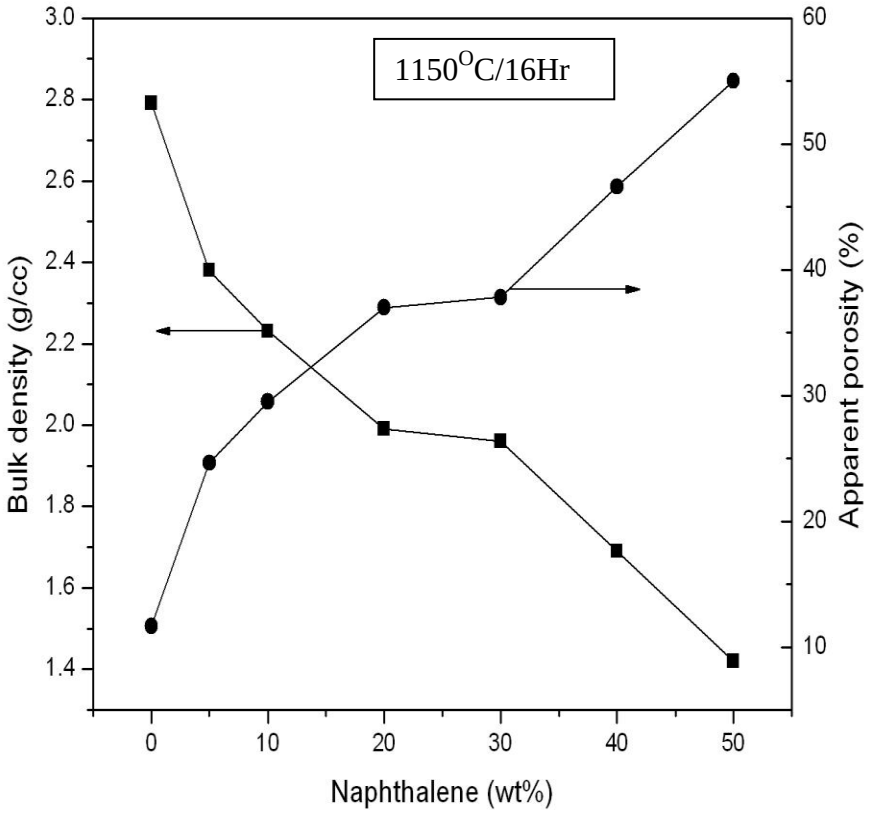

Fig. 5.1.10.22 Variation in Bulk density (g/cc) and Apparent porosity (%) of porous HAP with increasing Naphthalene (wt%) at 1150^{O}C/16Hr

Fig. 5.1.10.23 showed variation in Bulk density (g/cc) and Apparent porosity (%) of porous HAP with increasing naphthalene (wt %) at 1200^{O}C/16Hr. The maximum apparent porosity for the porous HAP fired at 1200^{O}C/16hr was measured to be 52.05% at naphthalene (50 wt %) and minimum 6.20% at naphthalene (0 wt %) where as maximum bulk density of 2.96 (g/cc) was obtained for naphthalene (0 wt %) and minimum 1.51g/cc at naphthalene (50 wt %) respectively**.**

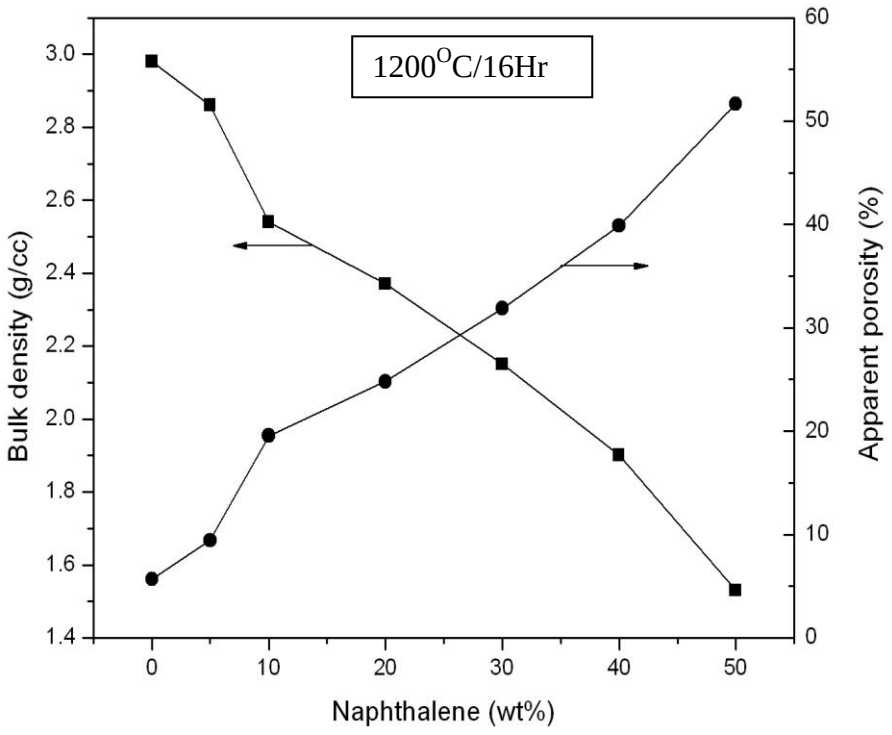

Fig. 5.1.10.23 Variation in Bulk density (g/cc) and Apparent porosity (%) of porous HAP with increasing Naphthalene (wt %) at 1200^{O}C/16Hr.

Fig. 5.1.10.24 showed variation in Bulk density (g/cc) and Apparent porosity (%) of porous HAP with increasing naphthalene (wt %) at 1250^{O}C/16Hr. The maximum apparent porosity for the porous HAP fired at 1250^{O}C/16hr was measured to be 49.00% at naphthalene (50 wt%) and minimum 3.50% at naphthalene (0wt%) where as maximum bulk density of 3.05(g/cc) was obtained for naphthalene (0 wt%) and minimum 1.61g/cc at naphthalene (50 wt%) respectively**.**

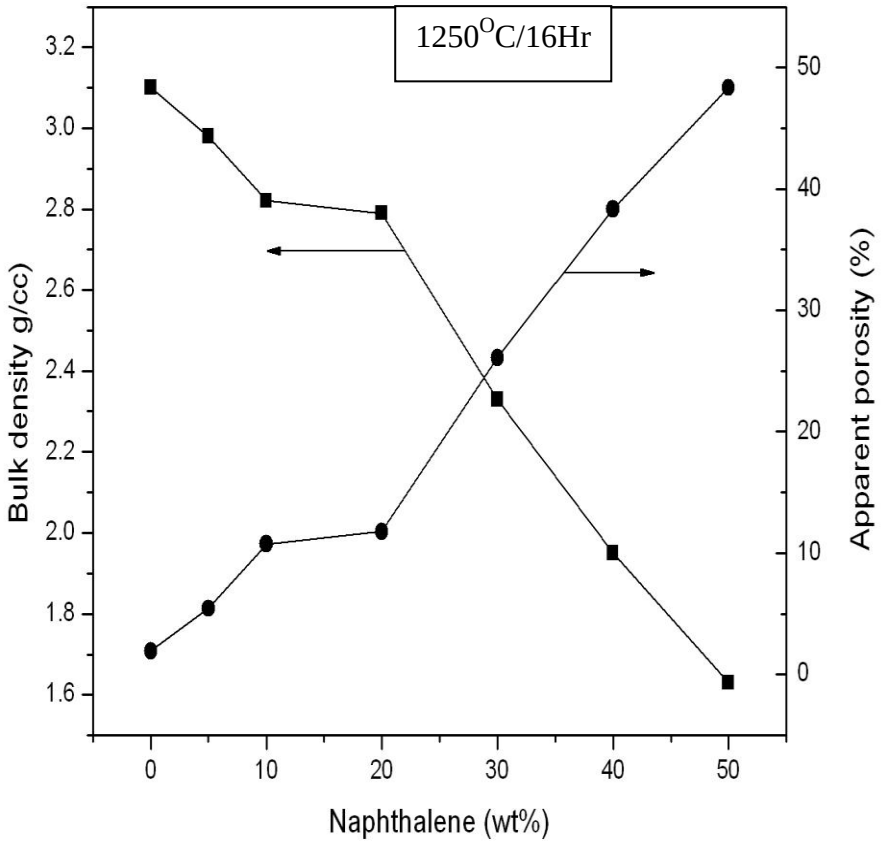

Fig. 5.1.10.24 Variation in Bulk density (g/cc) and Apparent porosity (%) of porous HAP with increasing Naphthalene (wt %) at 1250^{O}C/16Hr.

Fig. 5.1.10.25 shows evolution of total porosity (%) as a function of sintering temperature (^{O}C) and naphthalene (wt %) for soaking period 2Hr. From the graph it is well understood that with the increase in sintering temperature there is reduction in apparent porosity (%) and as the naphthalene (wt %) is increased there is also increase in apparent porosity (%) as discussed in Section 5.1.10.1. The maximum apparent porosity that was achieved for a soaking period of 2Hr with increasing in sintering temperature from 1000 to 1250^{O}C and increase in naphthalene (wt %) concentration from 0-50 (wt %) was 77.56% at 1000^{O}C of sintering temperature and naphthalene (50 wt %) and minimum porosity of 5.28% at 1250^{O}C and 0% naphthalene (wt %). The apparent porosity of samples can be well controlled by adding with different proportion of naphthalene (wt %) in calcined HAP (wt %).

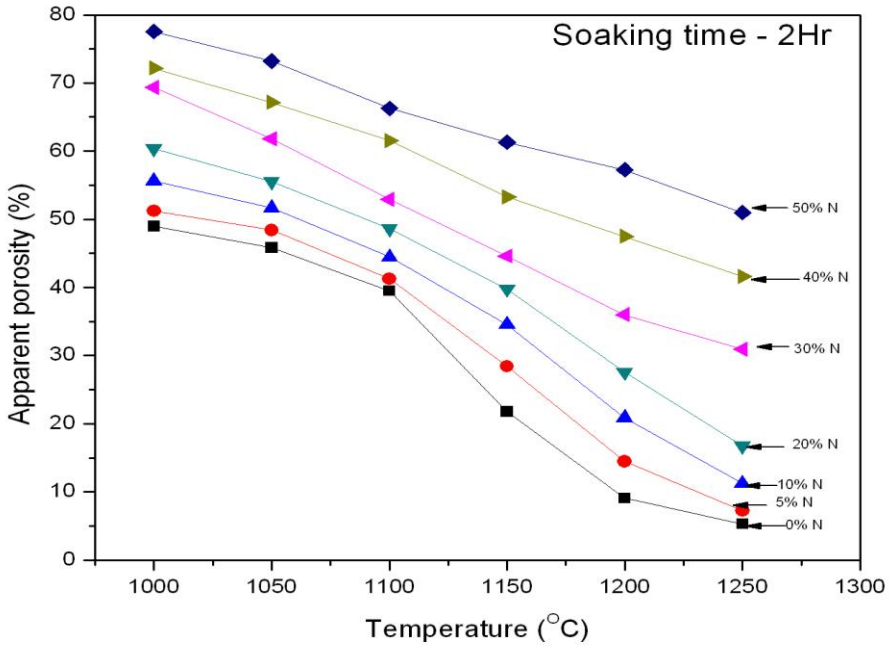

Fig.5.1.10.25 Evolution of total porosity (%) as a function of sintering temperature (^{O}C) and naphthalene (wt%) for soaking period 2Hr.

Fig. 5.1.10.26 shows evolution of total porosity (%) as a function of sintering temperature (^{O}C) and naphthalene (wt %) for soaking period 4Hr. The maximum apparent porosity that was achieved for a soaking period of 4Hr with increasing in sintering temperature from 1000 to 1250^{O}C and increase in naphthalene (wt %) concentration from 0-50 (wt %) was 76.05% at 1000^{O}C sintering temperature and naphthalene (50 wt %) and minimum porosity of 4.4% at 1250^{O}C and 0% naphthalene (wt %).

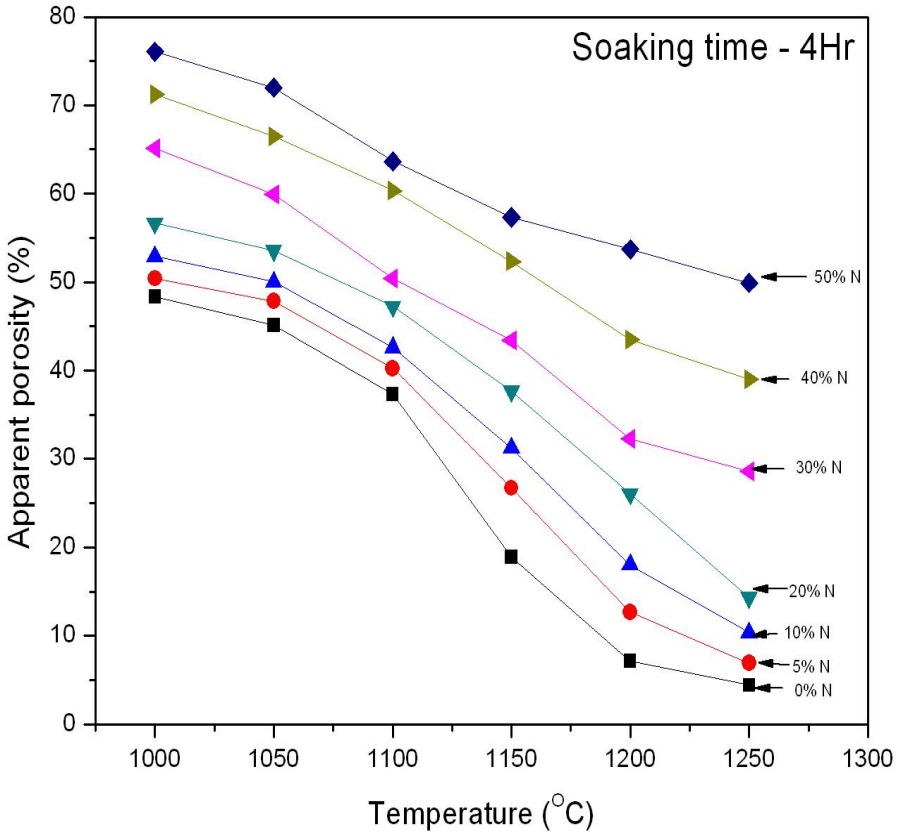

Fig.5.1.10.26 Evolution of total porosity (%) as a function of sintering temperature (^{O}C) and naphthalene (wt %) for soaking period 4Hr.

Fig. 5.1.10.27 shows evolution of total porosity (%) as a function of sintering temperature (^{O}C) and naphthalene (wt %) for soaking period 8Hr. The maximum apparent porosity that was achieved for a soaking period of 8Hr with increasing in sintering temperature from 1000 to 1250^{O}C and increase in naphthalene (wt %) concentration from 0-50 (wt %) was 75.31% at 1000^{O}C sintering temperature and naphthalene (50 wt %) and minimum porosity of 3.5% at 1250^{O}C and 0% naphthalene (wt %).

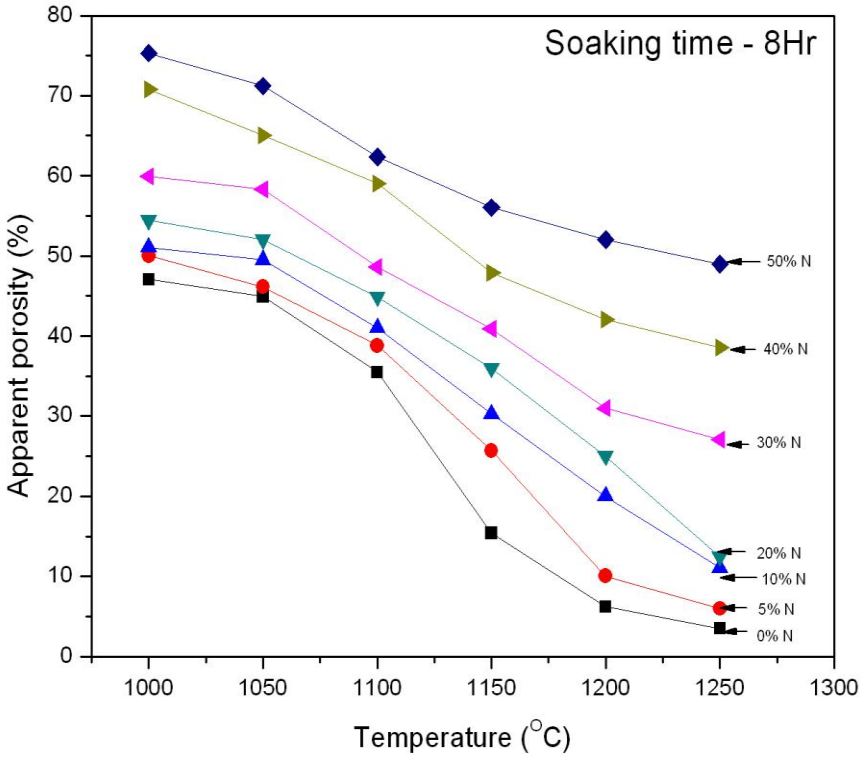

Fig.5.1.10.27 Evolution of total porosity (%) as a function of sintering temperature (^{O}C) and naphthalene (wt %) for soaking period 8Hr.

Fig. 5.1.10.28 shows evolution of total porosity (%) as a function of sintering temperature (^{O}C) and naphthalene (wt %) for soaking period 16Hr. The maximum apparent porosity that was achieved for a soaking period of 16Hr with increasing in sintering temperature from 1000 to 1250^{O}C and increase in naphthalene (wt %) concentration from 0-50 (wt %) was 74.75% at 1000^{O}C sintering temperature and naphthalene (50 wt %) and minimum porosity of 1.94% at 1250^{O}C and 0% naphthalene (wt %).

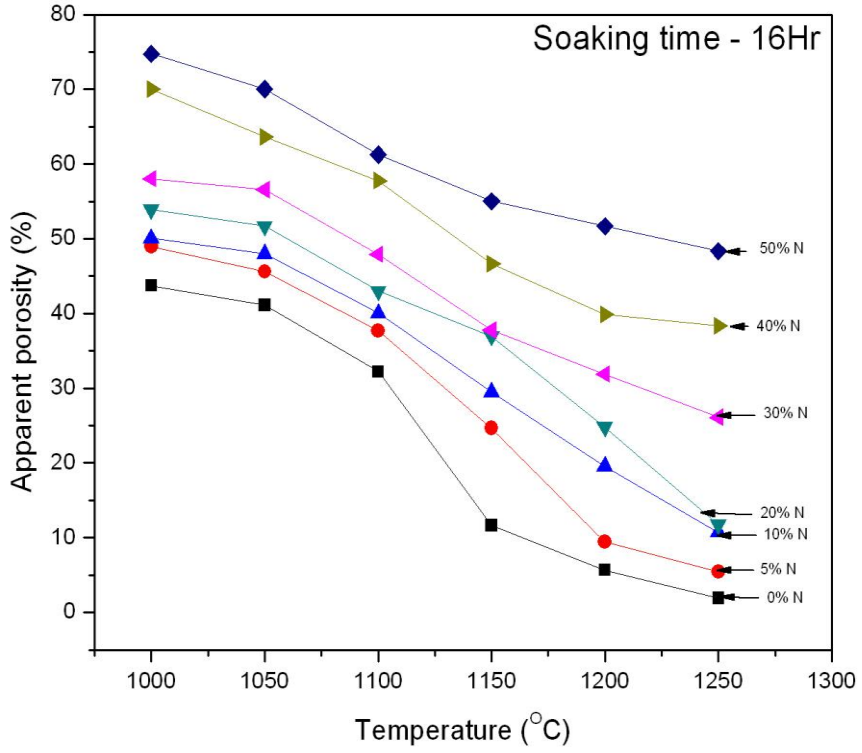

Fig.5.1.10.28 Evolution of total porosity (%) as a function of sintering temperature (^{O}C) and naphthalene (wt %) for soaking period 16Hr.

A remarkable feature to notice is that in absence of naphthalene the apparent porosity at 1250^{O}C for 16Hr is measured to be as 1.94% where as at the same condition but increasing

concentration of HAP: Naphthalene ratio by 50:50 (wt %) the apparent porosity increases to 48.34%. A possible explanation is that the porogen has a negative influence on the sintering ability of ceramic probably due to the spaces generated on the way out of the organic additive on burning. Thus, by varying concentration of naphthalene: HAP (wt %) we can control and fabricate a porous HAP with varying porosity.

Materials can be used as scaffolds for tissue engineering requires pore sizes greater than 100μm and for this highly porous ceramic body with a porosity percentage greater than 50% has been tested. The necessary temperature for the particles of the ceramic to join and form a continuous body has been investigated and the possibility of tailoring the pore size distribution by selecting the desire sintering temperature has been established.[179] Thus, by varying concentration of naphthalene: HAP (wt%) we can control and fabricate a porous HAP with high porosity and pore sizes .

5.1.10 Microstructure of Porous Hydroxyapatite.

The scanning electron microscopy of synthesized and calcined HAP from snail shell by chemical precipitation method Fig.5.1.7 showed a uniform microstructure which indicated the high degree of homogeneity of the starting powder. However, as the temperature was increased to more than 1200^{O}C considerable grain grown occurred when compared to sample at 1250^{O}C.

Fig. 5.1.10.1 represents microstructure evolution of HAP sintered at 1100^{O}C/16Hr where as Fig. 5.1.10.2 and Fig. 5.1.10.3 represents microstructure evolution of HAP sintered at 1250^{O}C/8Hr and 1250^{O}C/16Hr respectively. Porous HAP sintered at 1100^{O}C for 16hr soaking period showed pores of interconnectivity where as samples sintered to high temperature showed isolated pores of no interconnectivity.

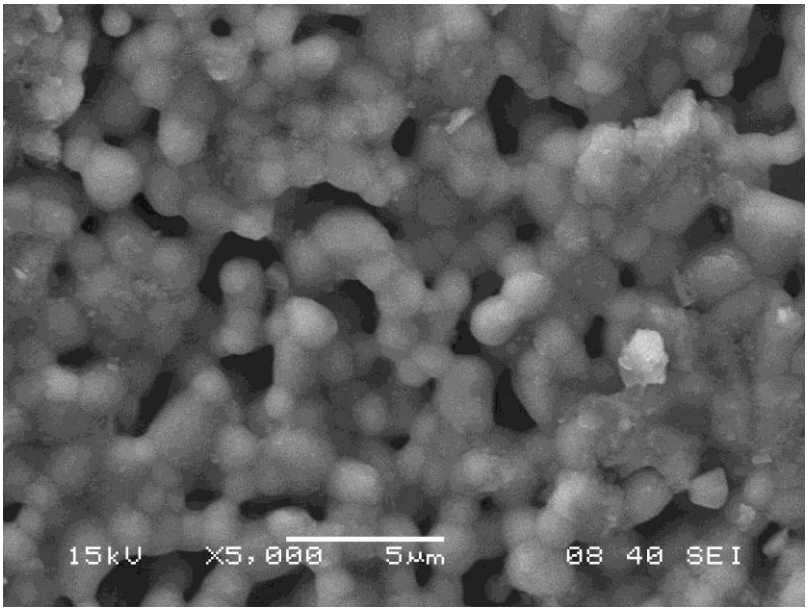

Fig. 5.1.10.1 SEM micrographs of HAP sintered at low temperature 1100^{O}C/16Hr

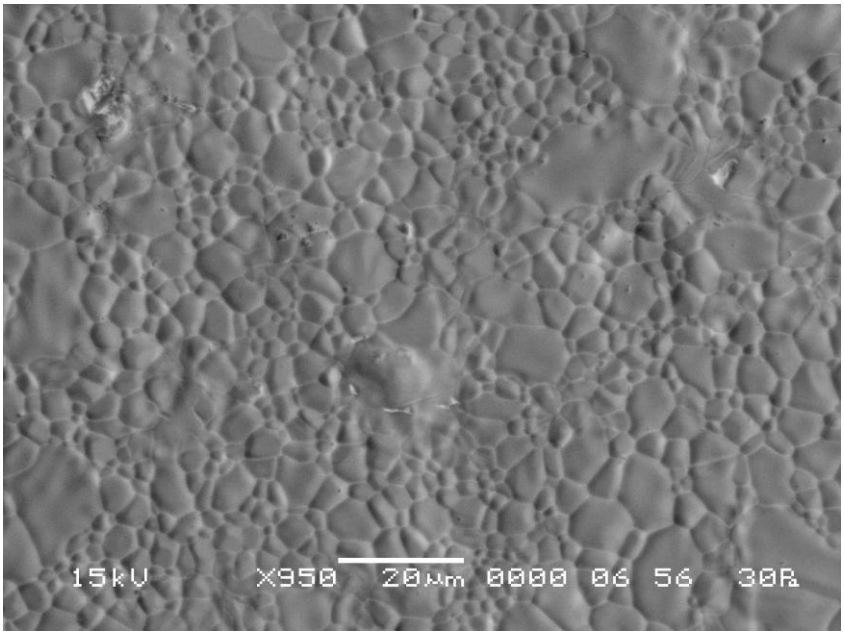

Fig. 5.1.10.2 SEM micrographs of dense HAP sintered at temperature 1200^{O}C/16Hr

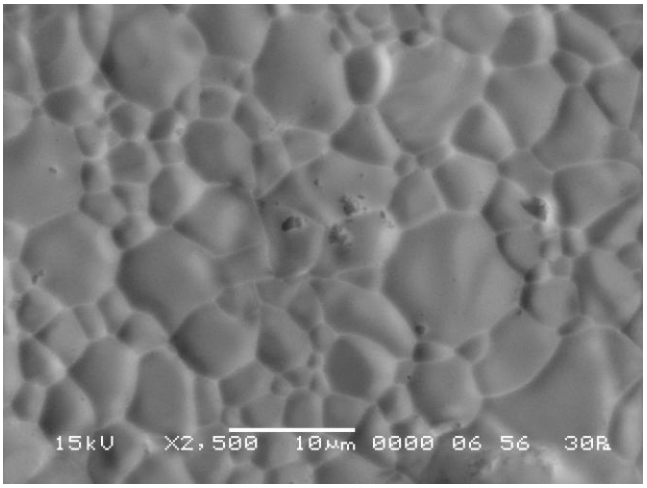

Fig. 5.1.10.3 SEM micrographs of dense HAP sintered at temperature 1250^{O}C/16Hr

Fig. 5.1.10.4 showed the change in the average grain size with increase in sintering temperature for a soaking period of 8Hr and 16hr respectively. It was found that as the sintering temperature was increased for a soaking period of 8Hr from 1100^{O}C to 1250^{O}C the average grain size also increased from 2.15µm to 8.89µm where as for a soaking period of 16Hr the grain size was 3.12 µm and 10.02 µm respectively. The graph obtained from the result depicts enhanced grain growth produced with increasing sintering temperature and sintering time. Hence, as the sintering temperature is increased this is accompanied by coalescence with occasionally exaggerated grain growth.[180]

The increase in temperature and time produces significant grain growth in material. It is to be noted that the effect of sintering temperature is more marked because diffusion is a thermally activated process.

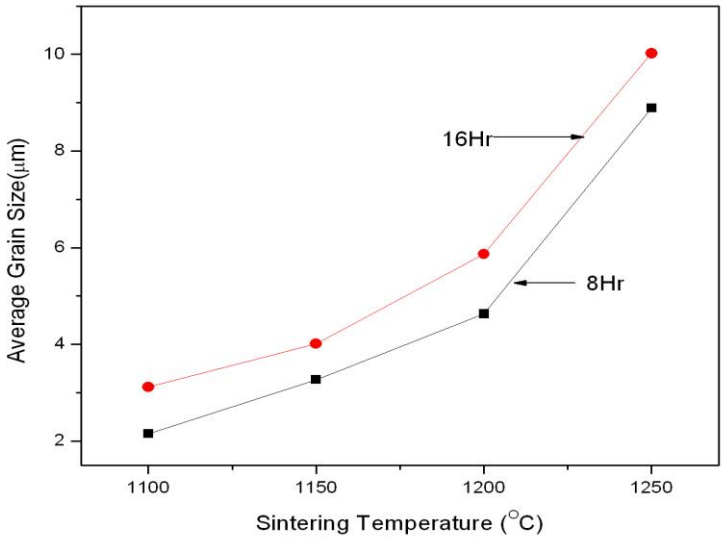

Fig. 5.1.10.4. Effect of average grain size (μm) with increasing sintering temperature (^{O}C) and soaking period for 8 Hr and 16hr

5.1.10.5 Scanning electron microscopy of porous HAP fired at 1250^{O}C/2Hr at different naphthalene (w t %)

The detail scanning electron microscopy of HAP mixed in varying concentration with naphthalene (wt %) from (5 % to 50 wt %) and fired at 1200^{O}C for a soaking period of 2hr was studied. Porous Hap with 50% porosity has the pores that are open, but they are not always connected. The addition of naphthalene at different proportion increases the porosity of the material and creates pores of interconnectivity. [181]

Fig. 5.1.10.6 shows scanning electron microscopy of porous HAP fired at 1200^{O}C/2Hr at naphthalene (5wt%). The pores obtained are interconnected to each other which are very much essential for fabricating a ceramic body is used for reconstruction or biological application. The average pore size of porous HAP with naphthalene (5 wt %) at 1200^{O}C/2Hr was found to be 2.453μm.

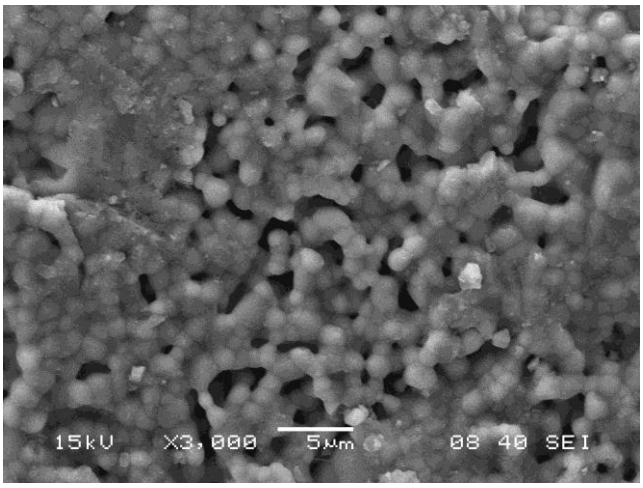

Fig. 5.1.10.6 Scanning electron microscopy of porous HAP fired at 1200^{O}C/2Hr at naphthalene (5 wt %)

Fig. 5.1.10.7 shows scanning electron microscopy of porous HAP fired at 1200^{O}C/2Hr at naphthalene (10 wt %). It is clear from the picture that the pore size increases with the increase in concentration of naphthalene (wt %). The average pore size of porous HAP with naphthalene (10 wt %) was found to be 4.257µm.

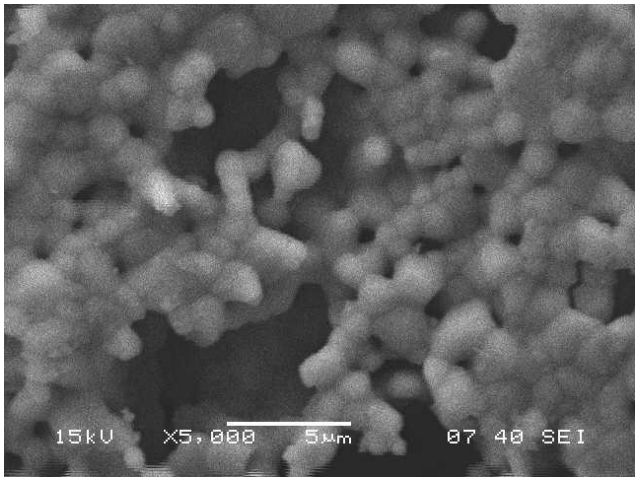

Fig. 5.1.10.7 Scanning electron microscopy of porous HAP fired at 1200^{O}C/2Hr at naphthalene (10 wt %).

Fig. 5.1.11.8 shows scanning electron microscopy of porous HAP fired at 1200^{O}C/2Hr at naphthalene (20 wt %). As the concentration of naphthalene increases the macro pores of larger size are generated. The average pore size of porous HAP with naphthalene (20 wt %) was found to be 6.49μm.

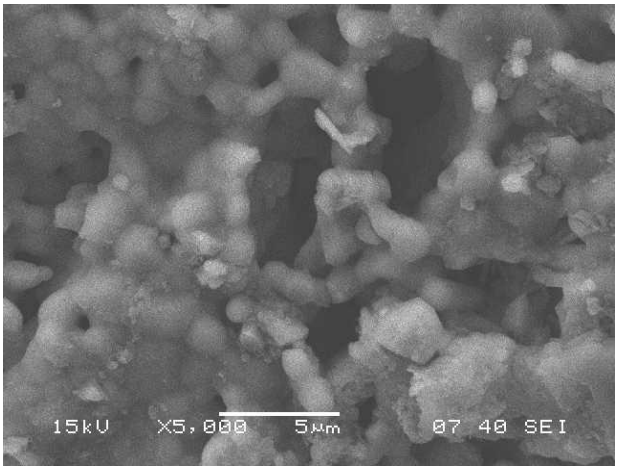

Fig. 5.1.10.8 Scanning electron microscopy of porous HAP fired at 1200^{O}C/2Hr at naphthalene (20 wt %).

Fig. 5.1.10.9 shows scanning electron microscopy of porous HAP fired at 1200^{O}C/2Hr at naphthalene (30wt%). The average pore size of porous HAP with naphthalene (30 wt %) was found to be 8.99μm.

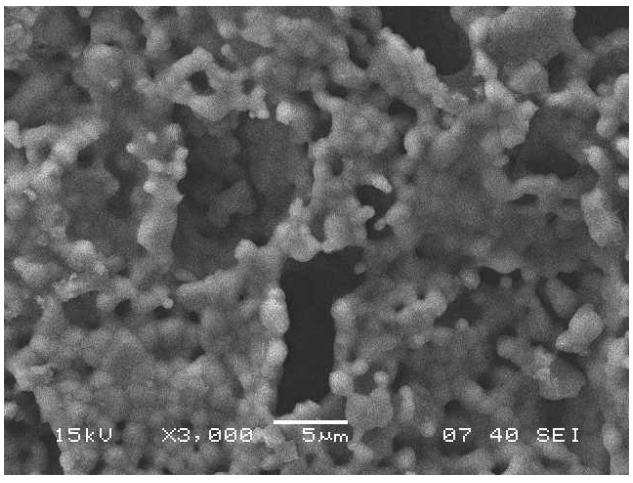

Fig. 5.1.10.9 Scanning electron microscopy of porous HAP fired at 1200^{O}C/2Hr at naphthalene (30 w %).

Fig. 5.1.10.10 shows scanning electron microscopy of porous HAP fired at 1200^{O}C/2Hr at naphthalene (40 wt %). The average pore size of porous HAP with naphthalene (40 wt %) was found to be 12.23μm.

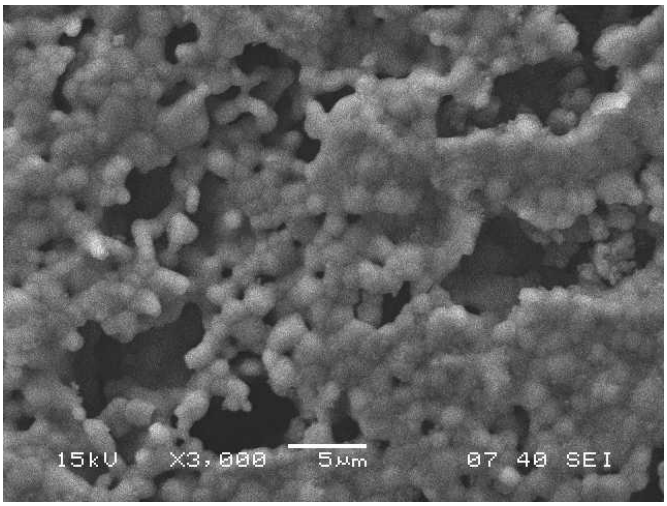

Fig. 5.1.10.10 Scanning electron microscopy of porous HAP fired at 1200^{O}C/2Hr at naphthalene (40 wt %).

Fig. 5.1.10.11 shows scanning electron microscopy of porous HAP fired at 1200^{O}C/2Hr at naphthalene (50 wt %). The higher proportion of naphthalene results in formation of highly porous structure with large macro pores. The average pore size of porous HAP with naphthalene (50 wt %) was found to be 17.67μm.

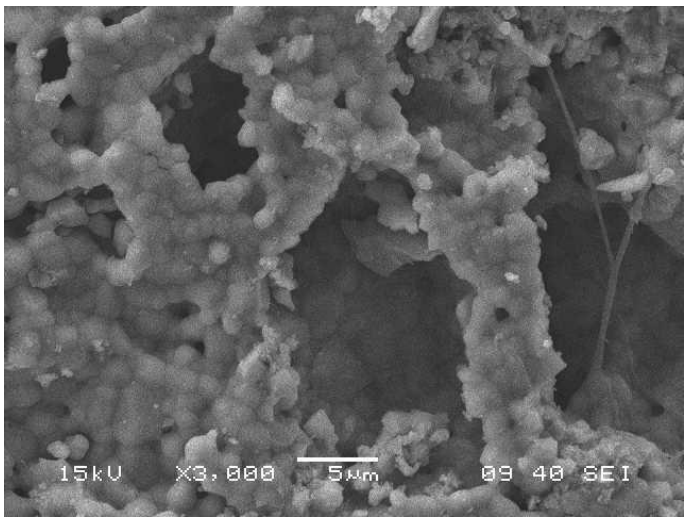

Fig. 5.1.10.11 Scanning electron microscopy of porous HAP fired at 1200^{O}C/2Hr at naphthalene (50 wt %).

Fig. 5.1.10.12 showed the graph with increase in average pore size (μm) with the increase in concentration of naphthalene (wt %). A lot of investigation to form a continuous body has been carried out and the possibility of creating the pore size distribution by selecting the desired temperature has been established. There are two possible reasons for choosing a temperature of $1200^{O}C/2Hr$:

1. The temperature of $1200^{O}C/2Hr$ is the best temperature to create the pores of interconnectivity.
2. The higher temperature results in decomposition of HAP associated with the formation of an intermediate phase, oxyapatite that forms through gradual loss of radical OH^- (dehydroxylation) in the matrix when HAP is heated in air to above $1200^{O}C$.[182]

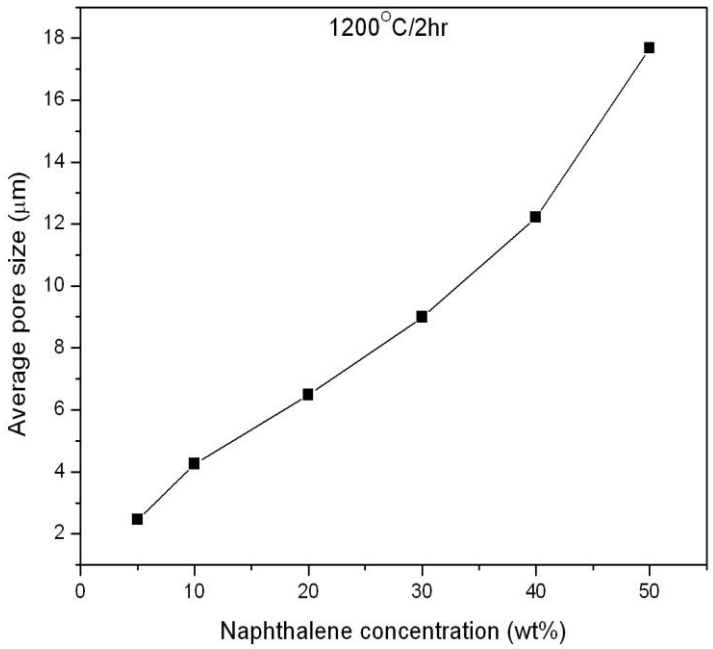

Fig. 5.1.10.12 Increase in average pore size of porous HAP with the increase in naphthalene from 0 to 50 (wt%)

5.1.10.13 Increase in pore size with more Naphthalene content

These results indicate that porous structures of calcium phosphate can be manufactured, by heating to high temperatures with convenient porosity and geometry for the growth of bone and for certain applications of bone substitutions. The majority of pores were 14-16 μm in size which implies easy in growth of fibrous tissue. Less than 10% of pores were <10% of pores were 5 μm size as a result of existence of unavoidable air bubbles. The advantage of using this method is better porosity in the material can be achieved by mixing HAP and Naphthalene in different proportion. After adding naphthalene the maximum porosity attained in HAP was 48.34%.

The function of naphthalene can be summarized below:

a) Naphthalene being volatile in nature sublimes at very low temperature >50^{O}C. It escapes out leaving pores in the material known as macro pores.
b) After sublimation of naphthalene the position of particles were left as pores
c) The porosity of HAP increased with pores of interconnectivity.
d) The reason for increase in porosity with high naphthalene content is because intentionally delivered large pores coalesce each other to become larger during the process of sintering.

5.1.11 Test of Biocompatibility for Porous HAP

The SEM micrograph of the synthesized porous HAP from Snail shell by chemical precipitation method immersed in Synthetic Body Fluid (SBF) for different soaking time is shown in Fig. 5.1.11.1 to Fig. 5.1.11.3. It is clear from the figure that tiny agglomerated bone like apatite particles are formed on the surface of HAP powder soaked for different period of time 7, 14 and 21 days respectively. Initially, the ideal body condition i.e. 37^{O}C and pH – 7.4

was maintained prior to the introduction of HAP in SBF solution. The change in pH was measured at regular time interval from 0 to 21 days by pH meter.

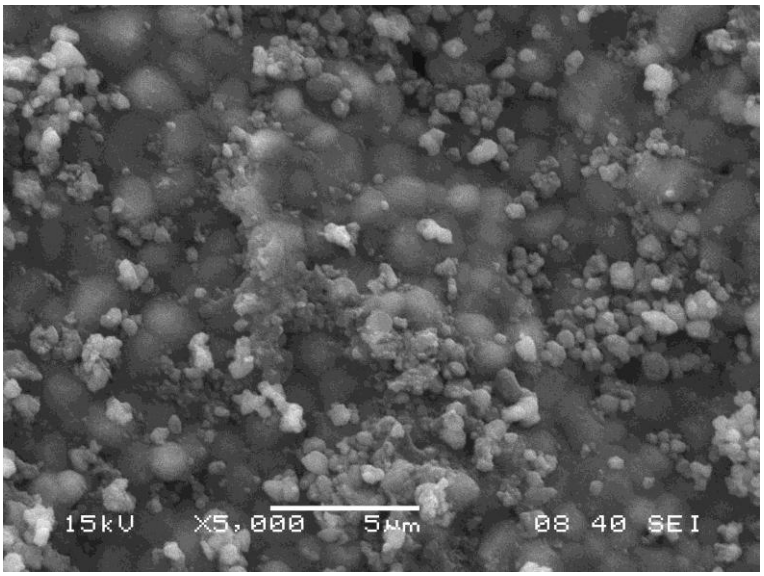

Fig. 5.1.11.1 SEM micrograph of HAP soaked in Synthetic Body Fluid (SBF) for 7 days.

Fig. 5.1.11.2 showed SEM micrograph of HAP soaked in Synthetic Body Fluid (SBF) for 14 days. As the soaking time was increased from 7 to 14 days the number and size of the agglomerated particles were also increased. The increase of agglomerated particles is evident of formation of apatite or mineralization being taking place on the surface of HAP.

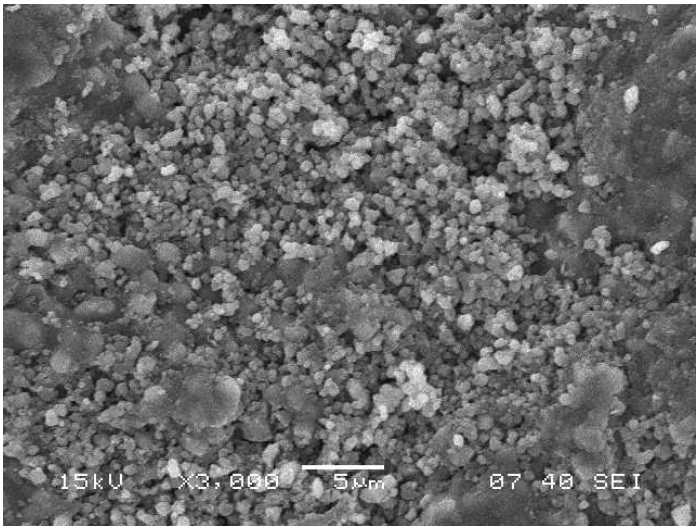

Fig. 5.1.11.2 SEM micrograph of HAP soaked in Synthetic Body Fluid (SBF) for 14 days

Fig. 5.1.12.3 shows SEM micrograph of HAP soaked in Synthetic Body Fluid (SBF) for 21 days. It is clear from the SEM analysis that with increase in soaking time there was increase in number and size of particles on the surface of HAP.

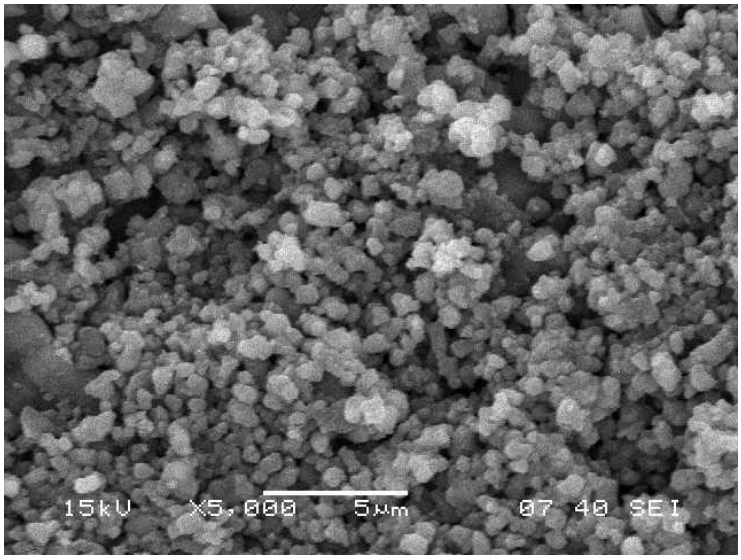

Fig. 5.1.11.3 SEM micrograph of HAP soaked in Synthetic Body Fluid (SBF) for 21 days.

The correct identification and evaluation of apatite on the surface of HAP in SBF is useful for predicting the *in vivo* bone bioactivity of the material, not only qualitatively but also quantitatively [182-185].The results indicated that the synthesized HAP powder from Garden Snail shell showed the high bioactivity in SBF solution.

The change in pH of the SBF solution was recorded and it was notice that the pH of SBF solution changes with increase in soaking time. A change in pH from 7.4 to 7.33 was recorded from 0 days to 21 days respectively.

Fig. 5.1.11.4 shows gradual change in pH value with increase in number of days. The pH value decreases with increase in number of days. The pH of the SBF initially was found to be constant as it was not resorbed in the medium which indicate its stability. The pH value depends on the solubility or resorbability of HAP. As the pH decreases the solubility increases.

The pH of prepared HAP is similar to that in biological apatite of bone.[184] The synthesized HAP has a great *in vitro* activity similar to that of biological apatite which could have great impact on implant cell interaction in a body environment. The surface of HAP exhibit dissolution couples with mineralization.

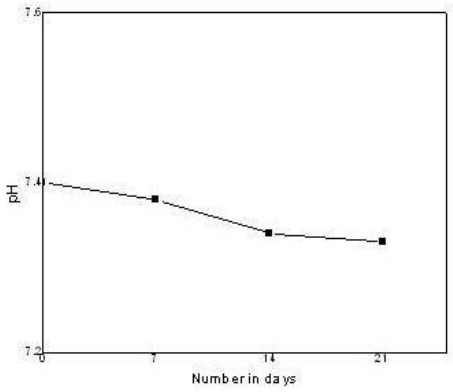

Fig. 5.1.11.4 Change in pH value with increase in number of days

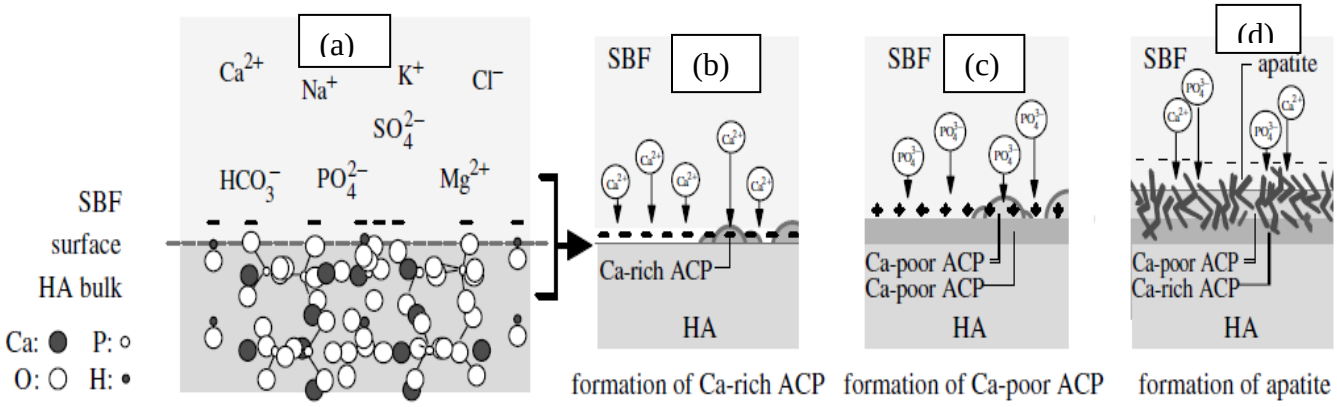

Fig. 5.1.11.5. (a) Represents negative charge on the surface of HAP, (b) Formation of Ca-rich ACP on the surface of HAP, (c) Formation of Ca-poor ACP on the surface of HAP, (d) Formation of apatite on the surface of HAP.

The possible explanation for the above can be given as the formation of apatite due to the electrostatic interaction on the HAP surface due to calcium ions and phosphate ions present in SBF. Fig. 5.1.11.5 describes the bone like apatite formation on the HAP in SBF which can be summarized as below:

1. There is formation of two precursor i.e. Ca-rich ACP Fig. 5.1.11.5(a) and Ca-poor ACP Fig. 5.1.11.5 (b) leading to the formation of apatite Fig. 5.1.11.5(c) on the surface of HAP.

2. The surface of HAP after being soaked in SBF acquires negative charge by exposing hydroxyl and phosphate ions on the surface of HAP.

3. The negative charge present on the surface of HAP attracts positive charged calcium ions from the SBF to form large number of Ca-rich ACP on the surface of HAP.

4. This positive charge Ca-rich ACP interacts with the negative charge phosphate ions present in SBF to form Ca-poor ACP. The result is the formation of apatite on the surface of HAP. [185, 186]

5. Therefore, once formed on a bioactive surface in SBF the apatite grows spontaneously, consuming the calcium and phosphate ions and incorporating sodium, magnesium and carbonate ions thereby revealing the bone mineral like compositional and structural features. [187]

5.1.11 Biodegradation of porous HAP in vitro

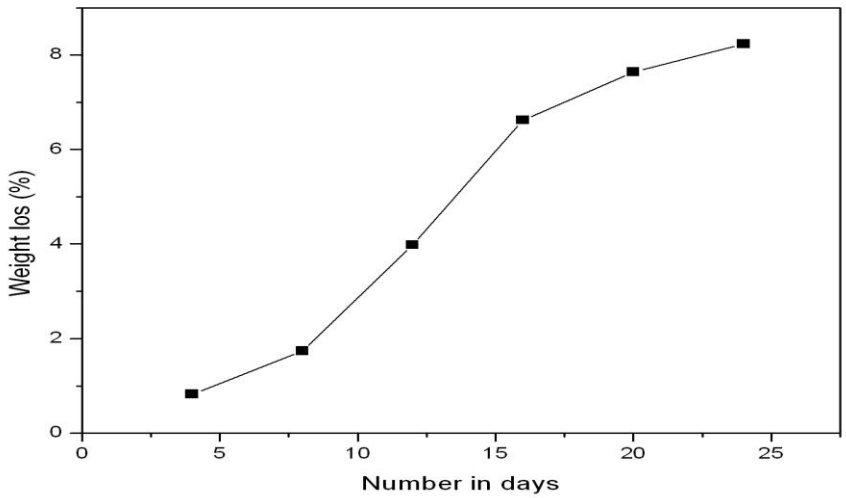

Fig. 5.1.11.6 Change in weight loss (%) in SBF with increase in number of days

Figure 5.1.11.6 showed the variation in degradation of porous HAP with increase in number of days. It is clear from the figure that there is increase in weight loss with increase in number of days and porosity. The degradability value of HAP containing naphthalene (5 wt %) for 4 days reached to 0.82%. As the number of days increased with respect to increase in naphthalene concentration (50 wt %) the degradation also increased to 8.24 % at 24 day Fig. 5.1.11.7

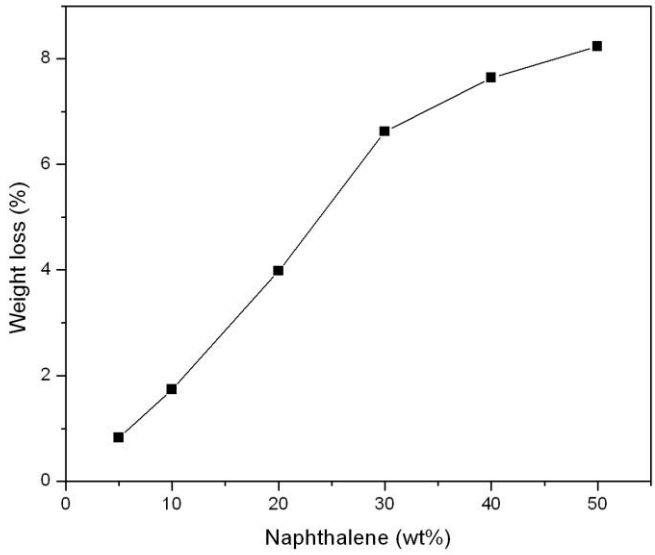

Fig. 5.1.11.7 Change in wt loss (%) with increase in porosity in HAP from Naphthalene (5-50 wt %).

The degradation rate of HAP is determined by sintering parameter, microstructure, porosity and crystallinity of ceramic [188]. However, porosity plays a dominant role in the degradation of ceramics. The *in vivo* study clearly showed that degradation rate increases with increase in porosity due to large specific area. The HAP with naphthalene (5 wt %) has smaller micropore and have lower micro porosity than those of HAP with naphthalene (50 wt %). Thus the specific surface area of pores in HAP containing naphthalene (5 wt %) is lower than that of HAP with naphthalene (50 wt %) which results in decreased degradation rate.

CHAPTER 6

6.0 Conclusions

The present work is based on the utilization of biological waste (Snail shell) to produce hydroxyapatite for the development of porosity and its study of *in vitro* bioactivity. Naphthalene in varying concentration from (0 wt %) to (50 wt %) was used as a control parameter for the fabrication of porous HAP. It was observed that with the increase in naphthalene concentration the porosity of HAP was also increased. The maximum porosity at high temperature i.e. $1250^{O}C$ for 16 Hr of soaking time was 48.24% whereas at low temperature $1000^{O}C$ for 16Hr of soaking period it was found to be 77.42%. Generally the porosity obtained at high temperature gives better mechanical strength than at low temperature. The conclusion from the above work can be summarized as follows:

1 Powder Synthesis

A stoichiometric, pure and thermally stable hydroxyapatite powder was synthesized from biological waste (Snail shell) by two different routes i.e Route 1 and Route 2. Route 1 consists of HAP prepared from $CaNO_3.4H_2O$ and $(NH_4)_2HPO_4$ and Route 2 from $Ca(OH)_2$ and H_3PO_4. HAP obtained from both the methods was pure and did not decompose to other phase even at high temperature like $1250^{O}C$ for a soaking period of 16hr. HAP synthesized in Synthetic body fluid (SBF) was pure and absence of any other calcium phosphate or tri calcium phosphate.

2 DTA/TGA of snail shell (SS) and HAP

The thermal analysis of Snail shell showed that it contains large amount of $CaCO_3$ along with small amount of $MgCO_3$ and other organic matters. The rapid decomposition of Snail

shell took place at temperature 750-850^{O}C.The thermal analysis of HAP showed weight loss at temperature < 200^{O}C and in between 300 to 800^{O}C. The spectrum obtained from FTIR studies can be divided into four regions with peaks having wave numbers around 3500, 1420, 1100 and 600cm^{-1}. Thus, the presence of PO_4^{3-} - group in HAP is almost confirm from IR studies. The surface area for synthesized HAP was found to be 76m^2/gm and for calcined HAP at 800^{O}C was 20m^2/gm. The average particle size for the synthesized HAP was found to be 2.63 μm.

3 Phase analysis by XRD

XRD analysis indicated the phase purity and crystallinity of hydroxyapatite powder. XRD patterns reveal the formation of HAP and are well resembled with the standard JCPDS file 09-432. The XRD analysis of synthesized HAP from snail shell by two different routes i.e. Route 1 and Route 2 showed the absence of any other phase like tri calcium phosphate (TCP) but the formation of TCP begins after calcined at 800^{O}C. Bone isolated from femur part of the body showed HAP peaks and was compared with the data obtained from other routes which confirm the presence of hydroxyapatite in bone.

4 Relative density

The relative density plot showed increase in measured density from 50.68% (sintered at 1000^{O}C) to 95.02% (sintered at 1300^{0}C). The powder calcined at 800^{0}C and sintered at temperature 1250^{O}C attains a maximum sintered density of 95.66 % of Theoretical Density (T.D). There is no increase in density at high temperature like 1250^{O}C because of decomposition of HAP taking place.

5 Volume shrinkage (%)

It was observed that the volume shrinkage (%) increased with the increase in temperature (^{O}C) and the maximum volume shrinkage (%) took place for HAP mixed in

naphthalene (20 wt %) fired at 1250^{O}C. The volume shrinkage (%) decreased when porous HAP heated beyond 1300^{O}C probably due to decomposition of porous HAP to other calcium phosphate.

6 Development of Porous HAP

The apparent porosity decreases with the increase of temperature and soaking time but by the help of porogen we can control the porosity in HAP. The maximum apparent porosity that was achieved for a soaking period of 2Hr with increasing in sintering temperature from 1000 to 1250^{O}C and increase in naphthalene (wt%) concentration from 0-50(wt%) was 77.56% at 1000^{O}C of sintering temperature and naphthalene (50wt%) and minimum porosity of 5.28% at 1250^{O}C and 0% naphthalene (wt%).

The maximum apparent porosity that was achieved for a soaking period of 16Hr with increasing in sintering temperature from 1000 to 1250^{O}C and increase in naphthalene (wt%) concentration from 0-50(wt%) was 74.75% at 1000^{O}C sintering temperature and naphthalene (50wt%) and minimum porosity of 1.94% at 1250^{O}C and 0% naphthalene (wt%).

HAP in absence of naphthalene the apparent porosity at 1250^{O}C for 16Hr is measured to be as 1.94% where as at the same condition but increasing concentration of HAP: Naphthalene ratio by 50:50 (wt%) the apparent porosity increases to 48.34%. A possible explanation is that the porogen has a negative influence on the sintering ability of ceramic probably due to the spaces generated on the way out of the organic additive on burning.

7 Microstructure (SEM) analysis of HAP

Scanning electron microscopy of uncalcined HAP was regular and round in shape whereas of calcined powder confirmed the presence of soft agglomerates. The microstructure

as reveals from SEM is in well- agreement with the particle size analysis and BET surface area analyzer results.

Porous HAP sintered at $1100^{O}C$ for 16hr soaking period showed pores of interconnectivity where as samples sintered at high temperature showed isolated pores of no interconnectivity. It was found that as the sintering temperature was increased for a soaking period of 8Hr from $1100^{O}C$ to $1250^{O}C$ the average grain size also increased from 2.15µm to 8.89µm where as for a soaking period of 16Hr the grain size was 3.12 µm and 10.02 µm respectively.

The higher proportion of naphthalene results in formation of highly porous structure with large macro pores. The average pore size of porous HAP with naphthalene (10 wt %) was found to be 17.67µm. Naphthalene being volatile in nature sublimes at very low temperature $>50^{O}C$. It escapes out leaving pores in the material known as macro pores.

8 Test of Biocompatibility for Porous HAP

The increase of agglomerated particles is evident of formation of apatite or mineralization being taking place on the surface of HAP. The results indicated that the synthesized HAP powder from Garden Snail shell showed the high bioactivity in SBF solution. The change in pH of the SBF solution was recorded and it was notice that the pH of SBF solution increases with increase in soaking time. A change in pH from 7.4 to 7.33 was recorded from 0 days to 21 days respectively.

The porous HAP developed from naphthalene with different concentration (5-50 wt %) soaked in Tris buffer solution at $37^{O}C$ in pH 7.4 showed weight loss from 0.82% to 8.24 %. The degradation of HAP could be adjusted by manipulating the pore size of bioceramic. The HAP with naphthalene (5 wt %) showed decrease in degradation than compared to HAP with naphthalene (50 wt %).

CHAPTER 7

7.1 Scope for future work

With the invention of new technology in the field of science bioengineering and biotechnology have emerged as a distinct discipline amid during a period of rapid globalization to meet the day to day demanding challenges. The HAP synthesized from a biological source origin can be tailored and designed for the specific purpose as given below:

1. One of the disadvantages of HAP is that it has got poor mechanical properties. There is need of improvement in mechanical property of porous HAP synthesized form Snail shell as a bone replacement material to promote bone formation.

2. Mass production of biocompatible HAP for biological application may be possible at simple and low cost through chemical precipitation method.

3. Suitable implantation of HAP synthesized from biological waste (Snail shell) in rat or rabbit as an animal model.

LIST OF REFERENCES

1. Sergey Dorozhkin V. (2010) Calcium orthophosphates as bioceramics: State of the art J. Funct. Biomater. 1:22-107.
2. K. de Groot. **(**1900) Bioceramics Consisting of Calcium Phosphate Salts. Biomaterials 1: 47-50.
3. Lee, S.J.; Oh, S.H. (2003) Fabrication of calcium phosphate bioceramics by using eggshell and phosphoric acid. Mater. Lett., 57, 4570-4574
4. Koumoulidis G C, Vaimakia T C, Sdoukos A T, Boukos N K and Trapalis C. **(**2001) Preparation of hydroxyapatite lathlike particles using high-speed dispersing equipment. J. Am. Ceram. Soc. 84: 1203-1208
5. Balazsi, C.; Weber, F.; Kover, Z.; Horvath, E.; Nemeth, C. (2007) Preparation of calcium-phosphate bioceramics from natural resources. J. Eur. Ceram. Soc., 27, 1601-1606.
6. Osaka A, Miura Y, Takeuchi K, Asada M and Takahashi K. **(**1991) Calcium apatite prepared from calcium hydroxyde and orthophosphoric acid. J. Mater. Sci. Mater. Med. 2**:**51-55.
7. Currey, J. (2002). Bones: Structure and Mechanics. Princeston University press, Princeton, NJ.
8. Cornell, C.N. and Lane, J.M (1992) Newest factors in fracture healing. Clin Orthop 277: 297-311.
9. Urist, M.R and Johnson, R.W. (1941) Calcification and ossification. IV. Healing of fracture in man under clinical conditions. J Bone Joint Surg 25: 375-426.

10. Sevitt, S., ed. (1981) Bone repair and fracture healing in man. Current problems in orthopedics. Churchill Livingstone, Edinburgh.
11. McKibbin, J. H., Fogle, J.L., Melvin, J.W., Haynes, R.R., Roberts, V.L and Alem N.M. (1970) Mechanical properties on cranial bone. J Biomech. 5: 495-511,
12. Wolff, J., ed. Das Gesstz der Transformation der Knochen. August Hirschwald Verlag, (1982) Berlin,
13. Habal, M.B. and Reddi, A.H. (1994) Bone grafts and bone induction substitutes. Clin Plast Surg 4: 525-42.
14. Ollier, L. (1858) De la production artificielle des os, an moyen de la transplantation de perioste et des greffes oseuses. C.r. Soc. Biol. 5: 145-191.
15. Phemister, D.B. (1914) The fate of transplanted bone and regenerative power of its various constituents. Surg Gyn 19: 303-33,
16. Brown, K.L., and Cruess, R.L. (1982) Bone and cartilage transplantation in orthopedic surgery. A review. J Bone Joint Surg 64A (2): 270-279.
17. Nade, S., Armstrong, L., McCartney, E. and Baggaley, B. (1983) Osteogenesis after bone and bone marrow transplantation. The ability of ceramic materials to sustain osteogenesis from transplanted bone marrow cells: preliminary studies. Clin Orthop 181:255-63.
18. Burwell, R. G. (1966)Studies in the transplantation of bone. VIII. Treated composite homograft- autografts of cancellous bone: an analysis of inductive mechanisms in bone transplantation. J Bone Joint Surg 48B (3): 532-66.
19. Banwart, J. C., Asher, M. A. and Hassanein, R. S. (1995) Iliac crest bone graft harvest donor site morbidity. A statistical evaluation. Spine 9: 1055-1060.
20. Challis, J. H., Lyttle, J. A. and Stuart, A. E. (1975) Strangulated lumbar hernia and volvulus following removal of iliac crest bone graft. Acta Orthop Scand 2: 230-233.

21. Escalas, F. and DeWald, R. L. (1977) Combined traumatic arteriovenous fistula and ureteral injury: a complication of iliac bone-grafting. J Bone Joint Surg 59A(2): 270-274.

22. Younger, E. M. and Chapman, M. W. (1989) Morbidity at bone graft donor sites. J Orthop Trauma 3: 192-195.

23. Burchardt, H. (1983) The biology of bone graft repair. Clin Orthop 174: 28-42.

24. Tessier, P. (1982) Autogenous bone grafts taken from the calvarium for facial and cranial applications. Clin Plast Surg 4: 531-538.

25. Weiland, A. J., Phillips, T. W. and Randolph, M. A. (1984) Bone grafts: a radiologic, histologic, and biomechanical model comparing autografts, allografts, and free vascularized bone grafts. Plast Reconstr Surg 3: 368-379.

26. Ritsilä, V., Alhopuro, S. and Rintala, A. (1976) Bone formation with free periosteal grafts in reconstruction of congenital maxillary clefts. Ann Chir Gynaecol 5: 342-344.

27. Baschirzev, N. J. and Petrov, N. N. (1912) Beitrage zur freien Knochenüberpflanzung. Dtcsh. Z. Chir. 113: 490-531.

28. Chase, S. W. and Herndon, C. H. (1955) The fate of autogenous and homogenous bone grafts. J Bone Joint Surg 37A: 809- 814.

29. Friedlaender, G. E., Sell, K. W. and Strong, D. M. (1978) Bone allograft antigenicity in an experimental model and in man. Acta Med Pol 19: 197-205,

30. Aho, A. J., Eskola, J., Ekfors, T., Manner, I., Kouri, T. and Hollmen, T. (1998) Immune responses and clinical outcome of massive human osteoarticular allografts. Clin Orthop 346: 196-206.

31. Tomford, W. W, Mankin, H. J., Friedlaender, G. E., Doppelt, S. H. and Gebhardt, M. C. (1987) Methods of banking bone and cartilage for allograft transplantation. Orthop Clin North Am 18: 241-247.

32. Buck, B. E. and Malinin, T. I. (1994) Human bone and tissue allografts. Preparation and safety. *Clin Orthop* 303: 8-17,

33. Khan, M. T., Stockley, I. and Ibbotson, C. (1998) Allograft bone transplantation: a Sheffield experience. Ann R Coll Surg Eng 80: 150-153.

34. Heiple, K. G., Kendrick, R. E., Herndon, C. H. and Chase, S. W. (1967) A critical evaluation of processed calf bone. J Bone Joint Surg 49A(6): 1119-1127.

35. Senn, N. (1889) On the healing of aseptic bone cavities by implatation of antiseptic decalcified bone. Amer J Med Sci 98: 219-243.

36. Urist, M. R. and McLean, F. C. Calcification and ossification. I. (1941) Calcification in the callus in healing fractures in normal rats. J Bone Joint Surg 23: 1-16.

37. Mulliken, J. B., Glowacki, J., Kaban, L. B., Folkman, J. and Murray, J. E. (1981) Use of demineralized allogeneic bone implants for the correction of maxillocraniofacial deformities. Ann Surg 3: 366-72.

38. Carter, D. R. and Hayes, W. C. (1977) The compressive behavior of bone as a two-phase porous structure. J Bone Joint Surg 59A (7): 954-962.

39. Galante, J., Rostoker, W. and Ray, R. D. (1970) Physical properties of trabecular bone. Calcif Tissue Res 3: 236-246.

40. McElhaney, J. H., Fogle, J. L., Melvin, J. W., Haynes, R. R., Roberts, V. L. and Alem, N. (1970) M. Mechanical properties on cranial bone. J Biomech 3: 495-511.

41. Wright, T. M. and Hayes, W. C. (1977) Fracture mechanics parameters for compact bone--effects of density and specimen thickness. J Biomech. 10: 419-430,

42. Lees, S. and Davidson, C. L.(1977) The role of collagen in the elastic properties of calcified tissues. J Biomech 10: 473-486

43. Mammone, J. F. and Hudson, S. M. (1993) Micromechanics of bone strength and fracture. J Biomech 26: 439-446.

44. Carter, D. R. and Spengler, D. M. (1978) Mechanical properties and composition of cortical bone. Clin Orthop 135: 192-217.

45. Swanson, S. A. and Freeman, M. A. (1966) Is bone hydraulically strengthened? Med Biol Eng 4: 433-8.

46. Crowninshield, R. D. and Pope, M. H. (1974) The response of compact bone in tension at various strain rates. Ann Biomed Eng 2: 217-225.

47. Reilly, D. T., Burstein, A. H. and Frankel, V. H. (1974) The elastic modulus for bone. J-Biomech 7: 271-275.

48. Reilly, D. T. and Burstein, A. H. (1975) The elastic and ultimate properties of compact bone tissue. J Biomech 8: 393-405.

49. Goldstein, S. A. (1987) The mechanical properties of trabecular bone: dependence on anatomic location and function. J Biomech 20: 1055-1061.

50. Manninen, J. M. (1993) Self-reinforced polyglycolide and poly-L-lactide devices in fixation of osteotomies of weight-bearing bones. p. **8**. Doctoral thesis. Yliopistopaino, Helsinki.

51. Schoenfeld, C. M., Lautenschlager, E. P. and Meyer, P. R., Jr. (1974) Mechanical properties of human cancellous bone in the femoral head. Med Biol Eng 12: 313-317.

52. Williams, D. F., Black, J. and Doherty, P. J. ed. (1992) Advances in biomaterials, Amsterdam-London-New York-Tokyo, 10: 192-196..

53. Mofid, M. M., Thompson, R. C., Pardo, C. A., Manson, P. N. and Vander Kolk, C. A. Biocompatibility of fixation materials in the brain. (1997) Plast Reconstr Surg 1: 14-20.

54. Gosain, A. K. and Persing, J. A. Biomaterials in the face: Benefits and risks. (1999) J Craniofac Surg 10: 404-414.

55. Geesink, R. G., de Groot, K. and Klein, C. P. (1988) Bonding of bone to apatite-coated implants. J Bone Joint Surg 1: 17-22.

56. Manson, P. N., Crawley, W. A. and Hoopes, J. E. (1986) Frontal cranioplasty: risk factors and choice of cranial vault reconstructive material. Plast Reconstr Surg 77: 888-904.

57. Guyuron, B. (1990) The hourglass facial deformity. J Craniomaxillofac Surg 18: 187-91.

58. Frodel, J. L. and Lee, S. (1998) The use of high-density polyethylene implants in facial deformities. Arch Otolaryngol Head Neck Surg 124: 1219-23.

59. Whear, N. M., Cousley, R. R., Liew, C. and Henderson, D. (1993) Post-operative infection of Proplast facial implants. Br J Oral Maxillofac Surg 31: 292-295.

60. Rokkanen, P. U. (1998) Bioabsorbable fixation devices in Orthopaedics and Traumatology. Ann Chir Gynaecol 87: 13-20.

61. Gombotz, W. R., Pankey, S. C., Bouchard, L. S., Phan, D. H. and Puolakkainen, P. A. (1994) Stimulation of bone healing by transforming growth factor-beta 1 released from polymeric or ceramic implants. J Appl Biomater 5: 141-150.

62. Mears, D. C., Williams & Wilkins ed. (1979), Introduction and history of joint replacement Materials and orthopaedic surgery Baltimore, 25:1-28.

63. Hench, L. L., Paschall, H. A., Allen, W. C. and Piotrowski, C. (1975) Interfacial behavior of ceramic implants. Biomaterials.34: 19-36.

64. Suominen, E. and Kinnunen, J. (1996) Bioactive glass granules and plates in the reconstruction of defects of the facial bones. Scand J Plast Reconstr Surg Hand Surg 30: 281-289.

65. Dreesman, H. Über Knochenplombierung. (1892) On bone sealing. Beitr Klin Chir 9: 804-810.

66. Calhoun, N. R., Neiders, M. E. and Greene, G. W., Jr. (1967) Effects of plaster-of-paris implants in surgical defects of mandibular alveolar processes of dogs. J Oral Surg 25: 122-128.

67. Peltier, L. F. (1961) The use of plaster of Paris to fill defects in bone. Clin Orthop 21: 1-31.

68. Yamazaki, Y., Oida, S., Akimoto, Y. and Shioda, S. (1988) Response of the mouse femoral muscle to an implant of a composite of bone morphogenetic protein and plaster of Paris. Clin Orthop 234: 240-9.

69. Jarcho, M. (1981) Calcium phosphate ceramics as hard tissue prosthetics. Clin Orthop 157: 259-278.

70. Shimazaki, K. and Mooney, V. (1985) Comparative study of porous hydroxyapatite and tricalcium phosphate as bone substitute. J Orthop Res 3: 301-310.

71. LeGeros, R. Z., Parsons, J. R., Daculsi, G., Driessens, F., Lee, D., Liu, S. T., Metsger, S., Peterson, D. and Walker, M (1988) Significance of the porosity and physical chemistry of calcium phosphate ceramics. Biodegradation-bioresorption. Ann N Y Acad Sci 523: 268-271.

72. Hulbert, S. F., Young, F. A., Mathews, R. S., Klawitter, J. J., Talbert, C. D. and Stelling, F. H. (1970) Potential of ceramic materials as permanently implantable skeletal prostheses. *J* Biomed Mater Res 4: 433-456.

73. Holmes, R. E., Wardrop, R. W. and Wolford, L. M. (1988) Hydroxylapatite as a bone graft substitute in orthognathic surgery: histologic and histometric findings. J Oral Maxillofac Surg 46: 661-671.

74. Martin, R. B., Chapman, M. W., Sharkey, N. A., Zissimos, S. L., Bay, B. and Shors, E. C. (1993) Bone ingrowth and mechanical properties of coralline hydroxyapatite 1 yr after implantation. Biomaterials 5: 341-348.

75. Rosen, H. M. and McFarland, M. M. (1990) The biologic behavior of hydroxyapatite implanted into the maxillofacial skeleton. Plast Reconstr Surg 85: 718-723.

76. Holmes, R. E. (1979) Bone regeneration within a coralline hydroxyapatite implant. *Plast* Reconstr Surg 5: 626-633.

77. Chiroff, R. T., White, E. W., Weber, K. N. and Roy, D. M. (1975) Tissue in growth of Replamineform implants. J Biomed Mater Res 4: 29-45.

78. White, E. and Shors, E. C. Biomaterial aspects of Interpore-200 porous hydroxyapatite. Dent Clin North Am 30(1): 49-67, 1986.

79. Meffert, R. M., Thomas, J. R., Hamilton, K. M. and Brownstein, C. N. (1985) Hydroxylapatite as an alloplastic graft in the treatment of human periodontal osseous defects. J Periodontol 56: 63-73.

80. Bucholz, R. W., Carlton, A. and Holmes, R. (1989) Interporous hydroxyapatite as a bone graft substitute in tibial plateau fractures. Clin Orthop 240: 53-62.

81. Salyer, K. E. and Hall, C. D. (1989) Porous hydroxyapatite as an onlay bone-graft substitute for maxillofacial surgery. Plast Reconstr Surg 84: 236-44.

82. Uchida, A., Araki, N., Shinto, Y., Yoshikawa, H., Kurisaki, E. and Ono, K. (1990) The use of calcium hydroxyapatite ceramic in bone tumour surgery. J Bone Joint Surg Br 72: 298-302.

83. Byrd, H. S., Hobar, P. C. and Shewmake, K. (1993) Augmentation of the craniofacial skeleton with porous hydroxyapatite granules. Plast Reconstr Surg 91: 15-22.

84. Kamegaya, M., Shinohara, Y., Shinada, Y., Moriya, H., Koizumi, W. and Tsuchiya, K. (1994) The use of a hydroxyapatite block for innominate osteotomy. J Bone Joint Surg Br 76: 123-126.

85. Costantino, P. D., Friedman, C. D., Jones, K., Chow, L. C. and Sisson, G. A. (1992) Experimental hydroxyapatite cement cranioplasty. Plast Reconstr Surg 90: 174-185.

86. Guillemin, G., Patat, J. L., Fournie, J. and Chetail, M. (1987) The use of coral as a bone graft substitute. J Biomed Mater Res 21: 557-567.

87. Guillemin, G., Meunier, A., Dallant, P., Christel, P., Pouliquen, J. C. and Sedel, L. (1989) Comparison of coral resorption and bone apposition with two natural corals of different porosities. J Biomed Mater Res 23: 765-779.

88. Bouchon, C., Lebrun, T., Rouvillain, J.-L. and Roudier, M. (1995) The Caribbean Scleractinian corals used for surgical implants. Bull Inst Océanogr 14: 111-122.

89. Souyris, F., Chevalier, J. P., Payrot, C., Pellequer, C., Gary-Bobo, A. and Merlier, C. (1984) Bilan après ans d'experimentation du corail au titre d'implants osseux. Ann Chir Plast Esthet 29: 256-260.

90. Patel, A., Honnart, F., Guillemin, G. and Patat, J. L. (1980) Utilisation de fragments de squelette de coraux madréporaires en chirurgie orthopédique et réparatrice. Chirurgie 106: 199-205.

91. Issahakian, S. and Ouhayoun, J. P. (1989) Evaluation clinique et histologique d'un noveau matériau de combleement: le corail naturel. J Parodontol 8: 251-259.

92. Mora, F. and Ouhayoun, J. P. (1995) Clinical evaluation of natural coral and porous hydroxyapatite implants in periodontal bone lesions: results of a 1-year follow-up. *J* Clin Periodontol 22: 877-884

93. Roux, F. X., Brasnu, D., Loty, B., George, B. and Guillemin, G. (1988) Madreporic coral: a new bone graft substitute for cranial surgery. J Neurosurg 69: 510-603.

94. Mercier, J., Piot, B., Gueguen, P., Cantaloube, D., Blanc, J. L., Boutault, F., Cariou, J. L., Devauchelle, B., Pellerin, P., Peri, G., Ricbourg, B., Stricker, M. and Wilk, A. (1996) Le plancher orbitaire en corail. Son intéret en traumatologie. Rev Stomatol Chir Maxillofac 97: 324-331.

95. Soost, F., Reisshauer, B., Herrmann, A. and Neumann, H. J. (1998) Natürliches korallines Kalziumkarbonat als alternativer Ersatz bei knöchernen Defekten des Schädels. Mund Kiefer Gesichts Chir 2: 96-100.

96. Marchac, D. and Sandor, G. (1994) Use of coral granules in the craniofacial skeleton. J Craniofac Surg 5: 213-217.

97. Kenesi, C., Voisin, M. C. and Dhem, A. (1997) Ostéotomie tibiale d'addition interne calée par un coin corail. Chirurgie 122: 379-382.

98. Rouvillain, J. L., Jouannelle, A., Delattre, O., Pascal-Mousselard, H. and Catonne, Y. (1997) A propos d'un cas fibrome chondromyxoide au niveau de l'astragale. Rev Chir Orthop 83: 372-377.

99. de Peretti, F., Trojani, C., Cambas, P., Loubiere, R. and Argenson, C. (1996) Le corail comme soutien d'un enfoncement articulaire traumatique. Rev Chir Orthop 82: 234-40.

100. Pouliquen, J. C., Noat, M., Verneret, C., Guillemin, G. and Pata,t J. L. (1989) Le corail substitué à l'apport osseux dans l'arthrodèse vertébrale postérieure chez l'enfant. Rev Chir Orthop 75: 360-369.

101. Kehr PH, Graftiaux F, Gosset K and Bencheikh K. (1995) Use of coral in cervical intersomatic grafting. Bull Inst Océanogr 14(3): 123-128.

102. Naaman, B. A. N., Patat, J. L., Guillemin, G., Issahakian, S., Forest, N. and Ouhayoun, J. P. (1994) Evaluation of the osteogenic potential of biomaterials implanted in the palatal connective tissue of miniature pigs using undecalcified sections. Biomaterials 15: 201-217.

103. Braye, F., Irigaray, J. L., Jallot, E., Oudadesse, H., Weber, G., Deschamps, N., Deschamps, C., Frayssinet, P., Tourenne, P., Tixier, H., Terver, S., Lefaivre, J. and Amirabadi, A. (1996) Resorption kinetics of osseous substitute: natural coral and synthetic hydroxyapatite. Biomaterials 17: 1345-50.

104. Chétail, M. and Fournié, J. Shell-boring mechanism of the Gastropod Purpura (Thais) lapillus: (1969) A physiological demonstration of the role of carbonic anhydrase in the dissolution of CaCO3. Am Zool 9: 983-990.

105. Gay, C. V. and Mueller, W. J. (1974) Carbonic anhydrase and osteoclasts: localization by labeled inhibitor autoradiography. *Science* **183**(123): 432-434.

106. Guillemin, G., Fournie, J., Patat, J. L. and Chetail, M. (1981) Contribution à l'étude du devènir d'un fragment de squelette de corail madrèporaire implanté dans la diaphyse des os onges chez chien. Comptes Rendus des Seances de l Academie des Sciences Serie III, Sciences de la Vie 293: 371-376.

107. Fricain, J. C., Bareille, R., Rouais, F., Basse-Cathalinat, B. and Dupuy, B. 1998(a)"In vitro" dissolution of coral in peritoneal or fibroblast cell cultures. J Dent Res 77: 406-11.

108. Fricain, J. C., Bareille, R., Ulysse, F., Dupuy, B. and Amedee, J. 1998(b) Evaluation of proliferation and protein expression of human bone marrow cells cultured on coral crystallized in the aragonite of calcite form. J Biomed Mater Res 42: 96- 102.

109. Doherty, M. J., Schlag, G., Schwartz, N., Mollan, R. A., Nolan, P. C. and Wilson, D. J. (1994) Biocompatability of xenogeneic bone, commercially available coral, a bioceramic and tissue sealant for human osteoblasts. Biomaterials 15: 601-608.

110. Burwell, R. G. (1985) The function of bone marrow in the incorporation of a bone graft. Clin Orthop, 200: 125-141.

111. Newman, M. G. and Boyne, P. J. The effect of calcified bone matrix on the osteogenic potential of hematopoietic marrow. Oral Surg Oral Med Oral Pathol 32: 506-512. 1971.

112. Lindholm, T. S. and Urist, M. R. (1980) A quantitative analysis of new bone formation by induction in compositive grafts of bone marrow and bone matrix. Clin Orthop 150: 288-300.

113. McDavid, P. T., Boone, M., Kafrawy, A. H. and Mitchell, D. F. (1979) Effect of autogenous marrow and calcitonin on reactions to a ceramic. J Dent Res 58: 1478-83.

114. Ohgushi, H., Goldberg, V. M. and Caplan, A. I. (1989) Repair of bone defects with marrow cells and porous ceramic. Experiments in rats. Acta Orthop Scand 60: 334-9.

115. Ohgushi, H., Okumura, M., Tamai, S., Shors, E. C. and Caplan, A. I. (1990) Marrow cell induced osteogenesis in porous hydroxyapatite and tricalcium phosphate: a comparative histomorphometric study of ectopic bone formation. J Biomed Mater Res 24: 1563-1570.

116. Roberts, A. B., Flanders, K. C., Kondaiah, P., Thompson, N. L., Van, O. S. E., Wakefield, L., Rossi, P., de, C. B., Heine, U. and Sporn, M. B. (1988) Transforming growth factor beta: biochemistry and roles in embryogenesis, tissue repair and remodeling, and carcinogenesis. Recent Prog Horm Res 44: 157-197.

117. Massague, J. T (1990) The transforming growth factor-beta family. Annu Rev Cell Biol 6: 597-641.

118. Assoian, R. K., Komoriya, A., Meyers, C. A., Miller, D. M. and Sporn, M. B. (1983) Transforming growth factor-beta in human platelets. Identification of a major storage site, purification, and characterization. J Biol Chem 258: 7155- 7160.

119. Derynck, R., Jarrett, J. A., Chen, E. Y., Eaton, D. H., Bell, J. R., Assoian, R. K., Roberts, A. B., Sporn, M. B. and Goeddel, D. V. (1985) Human transforming growth factor-beta complementary DNA sequence and expression in normal and transformed cells. Nature 316: 701-715.

120. Brown, P. D., Wakefield, L. M., Levinson, A. D. and Sporn, M. B. (1990) Physicochemical activation of recombinant latent transforming growth factor-beta's 1, 2, and 3. Growth Factors 3: 35-43.

121. Robey, P. G., Young, M. F., Flanders, K. C., Roche, N. S., Kondaiah, P., Reddi, A. H., Termine, J. D., Sporn, M. B. and Roberts, A. B. (1987) Osteoblasts synthesize and respond to transforming growth factor-type beta (TGF-beta) in vitro. J Cell Biol 105: 457-463.

122. Roberts, A. B. and Sporn, M. B. (1993)Physiological actions and clinical applications of transforming growth factor-beta (TGF-beta). Growth Factors 8: 1-9.

123. Beck, L. S., Ammann, A. J., Aufdemorte, T. B., Deguzman, L., Xu, Y., Lee, W. P., McFatridge, L. A. and Chen, T. L. (1991) In vivo induction of bone by recombinant human transforming growth factor beta 1. J Bone Miner Res 6: 961-968.

124. Schmitz, J. P. and Hollinger, J. O. (1986) The critical size defect as an experimental model for craniomandibulofacial nonunions. Clin Orthop 205: 299-308.

125. Bosch, C., Melsen, B., Gibbons, R. and Vargervik, K. (1996) Human recombinant transforming growth factor-beta 1 in healing of calvarial bone defects. J Craniofac Surg 7: 300-310.

126. Schmitt, J. M., Buck, D., Bennett, S., Skalla, W., Christoforou, C., Buechter, D., Gruskin, E. and Hollinger, J. (1998) Assessment of an experimental bone wax polymer plus TGF-beta 1 implanted into calvarial defects. J Biomed Mater Res 41: 584-592.

127. Lind, M., Overgaard, S., Soballe, K., Nguyen, T., Ongpipattanakul, B. and Bunger, C. (1996) Transforming growth factorbeta1 enhances bone healing to unloaded tricalcium phosphate coated implants: an experimental study in dogs. J Orthop. Res 14: 343-50.

128. McKinney, L. and Hollinger, J. O. (1996) A bone regeneration study: transforming growth factor-beta 1 and its delivery. J Craniofac Surg 7: 36-45.

129. Moxham, J. P., Kibblewhite, D. J., Bruce, A. G., Rigley, T., Gillespy, T. and Lane, J. (1996) Transforming growth factorbeta1 in a guanidine-extracted demineralized bone matrix carrier rapidly closes a rabbit critical calvarial defect. J Otolaryngol 25: 82-7.

130. Ripamonti, U., Bosch, C., van den Heever, B., Duneas, N., Melsen, B. and Ebner, R. (1996) Limited chondro-osteogenesis by recombinant human transforming growth factor-beta1 in calvarial defects of adult baboons (Papio ursinus). J Bone Miner Res 11: 938-945.

131. Wikesjö, U. M., Razi, S. S., Sigurdsson, T. J., Tatakis, D. N., Lee, M. B., Ongpipattanakul, B., Nguyen, T. and Hardwick, R. (1998) Periodontal repair in dogs: effect of recombinant human transforming growth factor-beta1 on guided tissue regeneration. *J* Clin Periodontol 25: 475-81.

132. Centrella, M., McCarthy, T. L. and Canalis, E. (1987) Transforming growth factor beta is a bifunctional regulator of replication and collagen synthesis in osteoblast-enriched cell cultures from fetal rat bone. J Biol Chem 262: 2869-2874.

133. Ripamonti, U., Duneas, N., Van Den Heever, B., Bosch, C. and Crooks, J. (1997) Recombinant transforming growth factorbeta1 induces endochondral bone in the baboon and synergizes with recombinant osteogenic protein-1 (bone morphogenetic protein-7) to initiate rapid bone formation. J Bone Miner Res 12: 1584-95.

134. Damien, C. J., Christel, P. S., Benedict, J. J., Patat, J. L. and Guillemin, G. (1993) A composite of natural coral, collagen, bone protein and basic fibroblast growth factor tested in a rat subcutaneous model. Ann Chir Gynaecol Suppl 207: 117- 128.

135. Boden, S. D., Schimandle, J. H., Hutton, W. C., Damien, C. J., Benedict, J. J., Baranowski, C. and Collier, S. (1997) In vivo evaluation of a resorbable osteoinductive composite as a graft substitute for lumbar spinal fusion. J Spinal Disord 10: 1-11.

136. Arnaud, E., Morieux, C., Wybier, M. and de Vernejoul, M. C. (1994) Potentiation of transforming growth factor (TGF-beta 1) by natural coral and fibrin in a rabbit cranioplasty model. Calcif Tissue Int 54: 493-498.

137. Dorozhkin SV. (2007) Calcium orthophosphates. J. Mater. Sci. 42: 1061-1095.

138. Kay MI, Young RA and Posner AS. (1964) Crystal Structure of Hydroxyapatite. Nature 204: 1050-1052.

139. Shi, Donglu. (2006) Introduction to Biomaterials. Tsinghua University Press. Beijing, China

140. Soballe K., (1993) Hydroxyapatite ceramics for bone implant fixation. Mechanical and histological studies in dogs. Acta Orthop. Scand. 64: 58-62.

141. Hench L.L. and Ethridge E.C., (1982) Biomaterials. An Interfacial Approach, Academic Press, New York, London.

142. Wintermantel E. and Ha, (1996) Biokompatible Werkstoffe und Bauweisen. Implantate für Medizin und Umwelt. Springer-Verlag, Berlin, Heidelberg, Tokio.

143. Kasemo B. and Lausmaa J., (1991) The biomaterial-tissue interface and its analogoues in surface science and technology, In*:* The Bone-Biomaterial Interface, J.E.Davies (ed.), University of Toronto Press, 19:32-36

144. Ohtsuki C, Kokubo T, Yamamuro T. (1992) Mechanism of HA formation of $CaO\{SiO_2\}P_2O_5$ glasses in simulated body Fluid. J Non- Cryst Solids; 143:84-92.

145. Neuman W, Neuman M. (1958) The chemical dynamics of bone mineral. Chicago: University of Chicago Press.

146. Li P, Kangasniemi I, de Groot K, Kokubo T. (1994) Bone-like hydroxyapatite induction by a gel-derived titania on a titanium substrate. J Am Ceram Soc 77:1307-1312.

147. Li P, Nakanishi K, Kokubo T, de Groot K. (1993) Induction and morphology of HA precipitated from metastable simulated body Fluids on sol gel prepared silica. Biomaterials 14:963-968.

148. Li P, Kangasniemi I, de Groot K, Kokubo T, Yli-Urpo AU. (1994) Apatite crystallization from metastable calcium phosphate solution on sol}gel prepared silica. J Non-Cryst Solids 168:281-286.

149. Cho SO, Nakanishi K, Kokubo T, Soga N, Ohtsuki C, Nakamura T, Kitsugi T, Yamamuro T. (1995) Dependence of apatite formation on silica gel on its structure: e!ect of heat treatment. J Am Ceram Soc 78:1769-1774.

150. Kokubo T, Miyaji F, Kim HM, Nakamura T. (1996) Spontaneous formation of bonelike apatite layer on chemically treated titanium metals. J Am Ceram Soc 79 :1127-1132

151. Nithyananthan thangamani, Kandasamy Chinnakali, F.D. Gnanam, (2002) Effect of powder processing of HA. Ceramic International 28: 355-362.

152. Jarcho. M, (1978) Hydroxyapatite Ceramic, U.S Patent, July, 4, 4097935.

153. S.W. Russell, K.A. Luptak, C.T.A Suchicital, T.L. Alford, V.B. Pizziconi, (1996) Chemical and Structural Evolution of Sol-Gel-Derived Hydroxyapatite Thin Films under Rapid Thermal Processing, J. Am. Ceram. Soc. 79: 843-847

154. Y. Sargin., M. Kizilyalli, C. Telli, H. Guler, (1997) A New Method for the Solid-State Synthesis of Tetracalcium Phosphate, A Dental Cement: X-ray Powder Diffraction and IR Studies**,** J. Eur. Ceram. Soc. 17: 963-967.

155. S.R. Ramanan, V. Ramannan, (2004) A Study of Hydroxyapatite Fibers Prepared via Sol–Gel Route, Material Letters 58**:** 3320-3323

156. Cuneyt Tas, (2000) Synthesis of Biomimetic Ca-Hydroxyapatite Powders at 37°C in Synthetic Body Fluids, Biomaterials 21: 1429-1438.

157. E. Caroline, E.Victoria and F.D.Gnanam, (2002) Synthesis and Characterisation of Biphasic Calcium Phosphate,Trends Biomater.Artif.Organs. 16: 12-14.

158. J. Gomez-Morales, J.Torrent-Burgues , T. Boix, J. Fraile, R. Rodriguez-Clemente, (2001) Precipitation of Stoichiometric Hydroxyapatite by a Continuous Method, Cryst. Res. Technol., 36: 15-19.

159. Sivakumar M., Sampath Kumar T.S., Shantha K.L., Panduranga Rao K. (1996) Biomaterials 17**:** 1709-1714.

160. Dean-Mo Liu, (1997) Fabrication of hydroxyapatite with controlled porosity J. Mat. Sci. 8: 227-232.

161. S. Puajindanetr , (1994) S. Best, W. Bonfield, British cer. Trans. 93: 96-99
162. Cowin SC, Vanburskirk WC and Ashaman RB (1987) Handbook of bioengineering (eds) R Skalak and S chien (New york; McGraw-Hill).
163. Sinha Amit, Ingle a, Munim K.R, Vaidya SN, Sharma BP and Bhisey AN (2001) Bull. Mater. Sci. 24: 653-657.
164. Kang, Suk-Joong L. (2005) Sintering (1st ed.), Oxford: Elsevier, Butterworth Heinemann, ISBN 0-7506-6385-5
165. Akao.M, Aoki. H, Kato. (1981) Mechanical properties of sintered hydroxyapatite for prosthetic application J, Mater. Sci. 16: 809-812.
166. Wang. P.E, Chaki. P.K, (1993) Sintering behaviour and mechanical properties of hydroxyapatite and dicalcium phosphate J. Mater. Sci. mater. In Med. 4: 150.
167. Toriyama, A. Ravaglioli, A. Krajewski, G. Celotti, A. Piancastelli, (1996) Synthesis of hydroxyapatite-based powders by mechno-chemical method and their sintering, J. Eur. Ceram. Soc. 16: 429–436.
168. Muralithran. G, ramesh. S, (2000) The effect of sintering temperature on the properties of hydroxyapatite, Ceramic International 26: 221-230
169. Rosen. H.M, (1985) Perischemic flap wash out and its effect on no reflow phenomenon Plast. Reconstr. Surg. 76:737-747.
170. Shields. CL etal, (1993) Retinoblastoma, Trans. Am. Opthalmol. Soc. 91: 177-189
171. Christmas. NJ etal, Arch. (1998) Intraorbital implants after enucleation and their complications: A 10-year review: Opthallmol 116: 1199-1203.
172. Shi Hong Li, Joost Rde Wijn, Pierre Layrolle, Klass de groot, (2003) Novel method to manufacture porous hydroxyapatite by Dual- Pha0se mixing J. Am. Ceram. Soc, 86: 65-72.

173. Rodriguez – Lorenzo. L.M, Ferreira. J.M.F, Material Research Bulletin, 39 (2004) 83-91.

174. Ramesh. S, (2001) Malaysian Grain Size-Properties Correlation in Polycrystalline Hydroxyapatite Bioceramic, Journal of Chemistry, 3: 35-40.

175. Shi. Hong Li, Joost. R. de wyes, Pierre Layrolle, Klass de Groot, (2003) Novel method to manufacture porous hydroxyapatite by dual phase mixing, J. Am. Ceram. Soc., 86: 65-72

176. Muralitharan. G, Ramesh. S, (2000) The effects of sintering temperature on the properties of hydroxyapatite, Ceramic International. 26: 221-230.

177. Williamson GK, Hall WH. (1953) Determination of size and strain, Acta Metall Sinica 1: 22-31

178. Hench LL, Wilson J. (1993) An Introduction to Bioceramics. 2nd ed. London: World Scientific Publishing Co Ltd.

179. Murugan R, Ramakrishna S. (2005) Aqueous mediated synthesis of bioresorbable nanocrystalline hydroxyapatite. J Cryst Growth 274: 209-213.

180. Kokubo T, Takadama H. (2006) How useful is SBF in predicting in vivo bone bioactivity? Biomaterials 27: 2907-3011.

181. Ebisawa T, Kokubo T, Ohura K and Yamamuro T, (1993) Bioactivity of $CaO.SiO_2$ glasses: in vitro evaluation. J. Mater. Sci.. Med, 1: 239-242

182. Ohtsuki C, Kokubo T and Yamamuro T, **(**1992) Mechanism of apatite formation on $CaO.SiO_2$-P_2O_5 glasses in a simulated body fluid. J. Non-Cryst. Solids 143**:** 84-89.

183. Kim H, Miyaji F, Kokubo T, Ohtsuki C and Nakamura T. **(**1995) Bioactivity of Na_2O-CaO-SiO_2 glasses. J. Am. Ceram. Soc. 78**:** 2405-2409

184. Takadama H, Kim H.M, Kokubo T and Nakamura T. 2001 a. (2001 a) Mechanism of biomineralization of apatite on a sodium silicate glass: TEM-EDX study *in vitro*. Chem. Mater. 13: 1108-1111.

185. Coreno J, Martinez A, Bolarin A and Sanchez F, (2001) Apatite nucleation on silica surface: a zeta- potential approach. J. Biomed. Res. 57**:** 125-129.

186. Kim H.M, Himeno T, Kawashita M, Kokubo T and Nakamura T, (2004) The mechanism of biomineralization of bone-like apatite o synthetic hydroxyapatite: an vitro assessment. J.R. Soc. Interface. 1: 17-21.

187. Lu J.X Descamps M, Dejou J, Koubi G, Hardouin P, Lemaitre J and Proust J.P. (2002) The biodegradation mechanism of calciumphosphate biomaterials in bone, J. Biomed. Mater. Res. 63: 408.
188. Klein C.P.A.T, Driessen A.A, De Groot K, (1983) Biodegradation behavior of various calcium phosphate materials in bone tissue, J. Biomed. Mater. Res. 17:769

PAPER PUBLICATION IN INTERNATIONAL JOURNALS

1. **A. Singh,** K.M Purohit**,** (2011)"Chemical Synthesis, Characterization and Bioactivity Evaluation of Hydroxyapatite Prepared from Garden snail (*Helix aspersa*)", Biotechnology and Biomaterials: 1: 1-8:
2. Neeta Raj Sharma**,** Anupama Sasankan**, Anjuvan Singh** and Giridhar Soni, (2011). Production of Polygalacturonase and Pectin Methyl Esterase from Agrowaste by using Various Isolates of *Aspergillus niger*. Insight Microbiology, 1: 1-7.
3. Neeta Raj Sharma, Prabhjot Kaur and **Anjuvan Singh.** (2011) Antifungal Potential of Achyranthes aspera Linn. Collected from Himachal Pradesh, Punjab and Haryana Region Journal of Pure and Applied Microbiology. 5 (2) 0971-0976.
4. Neeta Raj Sharma, Prabhjot Kaur and **Anjuvan Singh**, (2011) Antibacterial Potential of Achyranthus aspera Linn Procured from Himachal Pradesh, Punjab and Haryana, India, Research journal of chemical sciences, 1 (8): 1-7.
5. P. Das Mohapatra, , I. Shamnad, **A. Singh**, Study of microbial diversity of three common tropical scented flowers rose, jasmine, marigold, Journal of Pure and Applied Microbiology, 6(1):April (2012). Accepted for publication.

Conference/ Symposia participated

- ✓ **A.Singh**, P.Das.Gupta, S.KAdak, K.MPurohit, "Chemical Synthesis and characterization of Hydroxyapatite prepared from Snail shell" A **National Level** Student's Technical Symposium (Confluence 2004) during 5-7th Nov. 2004 at NIT Rourkela, Rourkela, INDIA. **Won 2nd Position**.
- ✓ **A.Singh**, P.Das.Gupta, S.KAdak, K.MPurohit, "Chemical synthesis and development of porous Hydroxyapatite prepared from mollusk shell." **International Symposium** of Research Students on Materials Science and Engineering (ISRS-2004) during 20-22 Dec 2004 at IIT Madras, Chennai, INDIA.
- ✓ **A.Singh**, P.Das.Gupta, S.KAdak, K.MPurohit, "Chemical Synthesis and characterization of Hydroxyapatite prepared from Snail shell as a biological waste material" All INDIA **National seminar** on utililisation of waste material, 2004 held at N.I.T Rourkela, Orissa, INDIA
- ✓ **A.Singh,** P.Das.Gupta, S.KAdak, D.Sarkar and K.MPurohit,'Development of porous hydroxyapatite synthesized from snail shell by chemical precipitation method' **Indo-Singapore Symposium** on Advance Functional Materials AFMS-06, February 24-26, 2006 at I.I.T Bombay, India.
- ✓ **A.Singh**, S.KAdak, and K.MPurohit,**'Synthesis of hydroxyapatite by Chemical Route from snail shell and its study of biocompatibility' An International Symposium on Molecular Pathology and Applied Genomics' ISMPAG-09** on **November 06-07, 2009** at Delhi, India.

Papers Communicated in International journal

1. A.Singh, M.Das Gupta Adak, S.KAdak, and K.Mpurohit "**Chemical Synthesis of Hydroxyapatite Prepared From Garden Snail Shell and its Characterization**". **Ceramic International**. Under review.

2. A.Singh, S.K Adak, M. Das Gupta Adak and K.Mpurohit "Chemical **Synthesis and Development of Porous Hydroxyapatite Prepared From Garden Snail Shell and its study of bioactivity**". Biomaterials. Under Review.

3. A.Singh, M. |Das Gupta Adak, S.KAdak, A. Basak, D.Sarkar and K.Mpurohit "**Chemical synthesis, characterization and bioactivity evaluation of hydroxyapatite prepared from garden snail (*Helix aspersa)*.** Bulletin of Material Sciences. Under Review.

ANJUVAN SINGH

CONTACT ADRESS:

C/O – Bijay Kumar Singh

Plot N0- 386/1046,

Near Radio Station, Jagda,

Rourkela, Orissa. 769048

Phone no. +91-7837651937

Email anjuvan@gmail.com

EDUCATIONAL QUALIFICATION

Degree	Year	Result
Ph.D (National Institute of Technology, Rourkela)	Joined in 2004	
M.Sc (Biotechnology)	2003	First Class

PROFESSIONAL EXPERIENCE :

2010-2011

- ✓ Presently working as faculty in Department of Biotechnology at Lovely Professional University, Phagwara, Punjab, INDIA.

2006-2010:

- ✓ Worked as H.O.D (In charge) of Biotechnology at Neelachal Institute of Medical science affiliated to Utkal University, Vanivihar, Orissa, INDIA.

2004 – 2006:

- ✓ As a Part time resource person in Biotechnology as (Lecturer) in Government College, Rourkela, Panposh, Orissa, INDIA.